The regulation of VPS34 and WNK1 kinase in the proximal tubule of the kidney in health and disease

Dissertation

zur Erlangung des Doktorgrades

der Mathematisch-Naturwissenschaftlichen Fakultät

der Christian-Albrechts-Universität zu Kiel

vorgelegt von

Luis Zanon Rodriguez

Kiel, April 2023

Referees:

Prof. Dr. Franziska Theilig

Prof. Dr. Thomas Roeder

Day of examination: 02.06.2023

Year of publication: 2023

SUMMARY

The proximal tubule (PT) is a high metabolic segment of the kidney. It possesses a reduced glycolytic activity and relies on oxidative mitochondrial metabolism to satisfy its energy demands. This peculiar characteristic makes the PT especially vulnerable to ischemic, hypoxic and metabolic injuries. The function of the PT after glomerular filtration is to reabsorb the number of solutes to avoid excessive loss of vital metabolites but dysfunctions of the proximal tubule can cause excessive excretion of glucose, amino acids and low-molecular weight proteins. The class III phosphoinositide 3-kinase VPS34 and the with-no-lysine [K] (WNK) kinases, have a wide range of functions and are both related to a disease context. The aim of this thesis was to analyze changes in the proximal tubule epithelial cell morphology, function and gene expression using two distinct animal models with conditional knockout of *Vps34* and *Vhl* respectively in the proximal tubule.

In a first approach, we elaborated a comprehensive analysis to study the function of VPS34 in vivo as well as the antiviral host response by VPS34 inhibition in vitro. By using a new conditional knockout mice model with specific knockout of VPS34 in the PT we could analyse the effect of VPS34 on proximal tubule cell homeostasis. We found that VPS34 depletion induced membrane exocytosis, caused a reduction of the retromer complex leading to a loss of fuel and biomass and abrogated SARS-CoV-2 infection.

The second approach was to study the role of hypoxia in the PT using a genetic method targeting the PT-specific deletion of *Vhl* in diabetic and non-diabetic mice. Alignment of *Vhl*-deletion related genes of diabetic mice in heat maps revealed that HIF-1 stabilization preconditions the animals against diabetic kidney disease as a result of a reset of gene expression responsible for the PT dysfunction. Among the genes altered between both diabetic groups we found *Slc12a1*, *Nr3c1*, *Klotho*, *Zbtb16* and *Wnk1*. Hypoxia also controls the expression of L-wnk1. As L-wnk1 modulates angiogenesis, proliferation and autophagy, this evidence underlines the participation of dysregulation of WNK signalling in the pathophysiology of diabetic kidney disease.

Our results provide new insights in the regulation of VPS34 in the proximal tubule and show that HIF-1α Stabilization can prevent the onset of DKD.

ZUSAMMENFASSUNG

Der proximale Tubulus ist ein metabolisch hochaktives Segment der Niere. Er besitzt aber eine eingeschränkte glykolytische Aktivität und deckt seinen Energiebedarf vorwiegend durch oxidativen mitochondrialen Metabolismus. Dieses besondere Merkmal macht den proximalen Tubulus besonders anfällig für ischämischen, hypoxischen und metabolischen Schaden.

Die Funktion des proximalen Tubulus, die der glomerulären Filtration nachgeschaltet ist, besteht in der Rückresorption von gelösten Stoffen, um einen gravierenden Verlust von wichtigen Metaboliten zu vermeiden. Daher führen Funktionsstörungen des proximalen Tubulus zu einer pathologischen Ausscheidung von Glukose, Aminosäuren und niedermolekularen Proteinen. Die Klasse III Phosphatidylinositol 3-Kinase VPS34 und die With-no-lysine [K] (WNK) Kinasen üben eine Vielzahl an Funktionen aus und stehen beide in Zusammenhang mit deren respektiven Pathologien. Ziel dieser Arbeit war die Analyse von epithelialer Zellmorphologie, Funktion und Genexpression im proximalen Tubulus anhand zweier unterschiedlicher Tiermodelle mit einem konditionellen Knockout von *Vps34* bzw. *Vhl* im proximalen Tubulus.

In einem ersten Ansatz wurde sowohl die Funktion von VPS34 in vivo analysiert als auch der Effekt der antiviralen Reaktion des Wirtes nach VPS34 Hemmung in vitro bestimmt. Mithilfe eines neuen konditionellen Mausmodells, das durch einen konditionellen Knockout von Vps34 im proximalen Tubulus gekennzeichnet ist, konnten wir den Effekt von VPS34 auf die Zellhomöostase untersuchen. Wir konnten zeigen, dass der Knockout von VPS34 zu einer Membran-Exozytose und zu einer Reduktion der Funktion des Retromerkomplexes führte, was mit einem Verlust an Brennstoff und Biomasse gekoppelt war. Des Weiteren zeigte sich, dass VPS34-Hemmung zur Verhinderung einer SARS-CoV-2-Infektion in vitro führte.

Der zweite Ansatz umfasst die Untersuchung der Rolle von Hypoxie im PT mithilfe genetischer Methoden, mit dem Ziel eines PT- spezifischen Knockouts von *Vhl* in diabetischen und nicht-diabetischen Mäusen. Analyse der signifikant veränderten Genexpression zwischen den Mausgruppen anhand von Heatmaps deutete auf eine Präkonditionierung nach HIF-1α Stabilisierung gegen eine diabetische Nephropathie als Folge einer Gen-Reprogrammierung hin. Unter den Genen, die in beiden diabetischen Gruppen verändert waren, fanden wir *Scl12a1*, *Nr3c1*, *Klotho*, *Zbtb16* und *Wnk1*. Hypoxie führt im PT zu einer Heraufregulation der Genexpression von L-wnk1. Da L-wnk1 die Angiogenese, Proliferation und Autophagie beeinflusst, unterstreichen diese Resultate die Beteiligung von den Wnk1-Signalwegen in der Pathologie der diabetischen Nephropathie.

Unsere Ergebnisse geben neue Einblicke in der Regulation von VPS34 im proximalen Tubulus und zeigen, dass HIF-1α Stabilisierung die Entstehung von diabetischer Nephropathie vermeiden kann.

Table of contents

List of figures

List of tables

List of abbreviations

ACE	Angiotensin-converting enzyme
AGE	Advanced glycation end product
AMN	Amnionless
AMPK	Adenosine monophosphate-activated protein kinase
AQP1	Aquaporin channel 1
AQP2	Aquaporin channel 2
ARH	Autosomal recessive hypercholesterolemia
ATP	Adenosine triphosphate
BBM	Brush-border-membrane
cAMP	Cyclic adenosine monophosphate
CCP	Clathrin-coated-pits
CD	Collecting duct
CKD	Chronic kidney disease
CMA	Chaperone-mediated autophagy
CME	Clathrin-mediated endocytosis
Dab-2	Disabled homolog 2
DCT	Distal convoluted tubule
DEPTOR	DEP domain-containing mTOR-interacting protein
DKD	Diabetic kidney disease
DM	Diabetes mellitus
DT	Distal tubule
ECM	Extracellular matrix
EE	Early endosome
EEA1	Early endosome antigen 1

EGF	Epidermal growth factor
ENaC	Epithelial sodium channel
ERC	Endosomal recycling compartment
ESCRT	Endosomal sorting complex required for transport
ESRD	End-stage renal disease
G6Pase	Glucose-6-phosphatase
GBM	Glomerular basal membrane
GFR	Glomerular filtration rate
GLUT1/2	Glucose transporter 1/2
GR	Glucocorticoid receptor
HRE	Hypoxia-response element
IGF-2	Insulin-like growth factor 2
IGS	Imerslund-Grasbeck syndrome
KS-WNK1	Kidney-specific with no lysine kinase 1
L-WNK1	Long with no lysine kinase 1
MMP2	Matrix metalloproteinase 2
mTORC1	Mammalian target of rapamycin complex 1
mTORC2	Mammalian target of rapamycin complex 2
MVB	Multivesicular body
NAPiII	Sodium phosphate cotransporter type 2
NBCe1-A	Sodium Bicarbonate cotransporter type 1A
NHE3	Sodium/Hydrogen-exchanger isoform 3
NCC	Sodium-chloride symporter
NKCC2	Sodium-potassium-2 chloride cotransporter
NOS1	Nitric oxide synthase 1

OK	*Opossum kidney*
PEPCK	Phosphoenolpyruvat carboxykinase
PKA	Protein kinase A
PIP2	Phosphatidylinositol (4,5)-bisphosphate
PIP3	Phosphatidylinositol (3,4,5)-trisphosphate
PI3K	Phosphatidylinositol 3-kinase
PLD1	Phospholipase D1
PLZF	Promyelocytic leukemia zinc finger
PRAS40	Proline-rich AKT substrate 40 kD
PT	Proximal tubule
PTC	Proximal tubule cells
PTH	Parathyroid hormone
RAAS	Renin-Angiotensin-Aldosterone-System
Rheb	Ras homolog enriched in brain
RICTOR	Rapamycin-insensitive companion of mTOR
ROS	Reactive oxigen species
S6K1	Ribosomal protein S6 kinase beta-1
SARS-CoV-2	Severe acute respiratory syndrome-coronavirus 2
SGLT2	Sodium glucose cotransporter 2
SNX	Sorting nexin
TAL	Thick ascending limb (of Henle´s loop)
TF	Transcription factor
TGF	Tubuloglomerular feedback
TGF-β	Transforming growth factor β
TGN	Trans-Golgi network

TSC1	Tuberous sclerosis complex 1
TSC2	Tuberous sclerosis complex 2
ULK1	Unc-51 like autophagy activating kinase 1
UVRAG	Ultraviolet radiation resistance associated gene
VCAM-1	Vascular cell adhesion molecule 1
VEGF	Vascular endothelial growth factor
VHL	Von Hippel-Lindau
VPS15	Vacuolar protein sorting 15
VPS26	Vacuolar protein sorting 26
VPS29	Vacuolar protein sorting 29
VPS30	Vacuolar protein sorting 30
VPS34	Vacuolar protein sorting 34
VPS35	Vacuolar protein sorting 35
VPS38	Vacuolar protein sorting 38
WT	Wild-type
WNK1	With no lysine kinase 1
WNK4	With no lysine kinase 4
ZBTB16	Zinc finger and BTB domain containing 16

1. Materials and Methods

1.1 Materials

1.1.1 Kits

Kit	Company
BCA protein assay kit	Pierce
DeadEnd™Fluorometric Tunel System	Promega

1.1.2 Mammalian cell lines

1.1.2.1 OK (Opossum Kidney) cells

The OK cell line was derived from the kidney of an adult female North American opossum (Didelphis marsupialis virginiana) and display many characteristics of kidney proximal tubular epithelial cells. The OK cell line is an adherent epithelial cell line suitable for transfection. 2 OK cell lines expressing the target genes *EmGfp* and *Zbtb16* after doxycycline induction, termed OK LV +Ind +GFP and OK LV +Ind +ZBTB16 respectively, were used for the luciferase experiments.

1.1.2.2 TAL (Thick Ascending Limb) cells

The thick ascending limb cell line, has been established from freshly isolated rat medullary thick ascending limb tubules. TAL cells exhibit a polygonal morphology characteristic of epithelial cells.

1.1.2.3 MpkCCD (c14) (murine principal kidney cortical collecting duct) cells

The mpkCCD (c14) cell line is a murine principal kidney cortical collecting duct cell line isolated from 1-mo-old SV-PK/Tag male mouse. This cell line express typical electrophysiological features of tight epithelium.

1.1.3 Cell culture media

Opossum Kidney cell medium

Ham´s F-12 (PAN Biotech; P04-15500)	250 ml Ham´s F-12
DMEM high glucose (PAN Biotech; P04-03590)	250 ml DMEM high glucose
	2 mM glutamine

	100 U/ml penicilin
	100 µg/ml streptomycin
	5 mM HEPES
	1,5 g NA2CO3
	5% FCS

TAL cell medium

Ham´s F-12 (PAN Biotech; P04-15500)	250 ml Ham´s F-12
DMEM high glucose (PAN Biotech; P04-03590)	250 ml DMEM high glucose
	2 mM glutamine
	100 U/ml penicillin
	100 µg/ml streptomycin
	20 ng/µL EGF
	5% FCS

mpkCCD (c14) cell medium

Ham´s F-12 (PAN Biotech; P04-15500)	250 ml Ham´s F-12
DMEM high glucose (PAN Biotech; P04-03590)	250 ml DMEM high glucose
	5 µg/ml Insulin
	5 x10^{-8} M Dexamethasone
	60 nM Selenium
	5 µg/ml transferrin
	10^{-9} M triiodothyronine
	10 ng/ml EGF
	20 mM HEPES
	2 mM glutamine
	5% FCS

100 U/ml penicilin

100 µg/ml streptomycin

1.1.4 Laboratory equipment

Item	Company
HybEZ II Oven	Advance Cell Diagnostics
Analytical balance BP 61	Sartorius
Balance 440-33N	Kern
Centrifuge Mega Star 1.6 R	VWR
Centrifuge 5415 R	Eppendorf
Centrifuge 15 RE	VWR
Compact fluorescence microscope Keyence BZ-x800e	Keyence Deutschland GmbH
Facility line STED microscope	Abberior Instruments GmbH
Gene Amp PCR System 2400	Perkin Elmer
Incubator Shaker innova 4200	New Brunswick
Inverse light microscope Axiovert 200M	Carl Zeiss Göttingen
Inverted fluorescence microscope Axiovert 200M	Carl Zeiss Göttingen
Leica TCS SP5 confocal microscope	Leica
Microwave 1100 W	Panasonic
Microscope Illuminator Hal Axiovert 135	Carl Zeiss Göttingen
Mini-Centrifuge	Carl Roth
Reax Top Shaker	Heidolph
Spectrophotometer NanoDrop ND-1000	Peqlab
ThermoMixer C	Eppendorf
Ultrasonic Processor 200S	Hierlscher
Vortex Mixer VF2	Janke & Kunkel IKA

Wide Mini Sub Cell GT	Bio-Rad

1.1.5 Laboratory materials

Item	**Manufacturer**
MicroAmp®Optical 96-Well Reaction Plate	Sarstedt
MicroAmp™Optical Adhesive Film	Sarstedt
Multiply®-µ-Strip Pro 8-strip	Sarstedt
Nitrocellulose membrane, Whatman Protran, 0,2 µm	Bio-Rad
Nitrocellulose membrane, plain, white pore size 0,45 µm	SERVA
Parafilm®M	Laboratory Film
Pipette tips, 10 µl, 200 µl and 1000 µl	Sarstedt
Pipette tip 5 ml, Eppend type	Sarstedt
Plastic tubes, 10 ml, 15 ml and 50 ml	Sarstedt
Rotilabo® Blotting papers, thick 0,35 mm	Carl Roth
Serological pipette 2 ml, 5ml, 10 ml and 25 ml	Sarstedt
Syringe 20 ml	BD
Syringe filters	Sarstedt
TC Flask T75, Stand.,Vent. Cap	Sarstedt
TC Flask T25, Stand.,Vent. Cap	Sarstedt
24 well microtiter plates, flat bottom, transparent	Sarstedt
96 well microtiter plates, flat bottom, transparent	Sarstedt
96 well microtiter plates, flat bottom, white	Greiner-Bio-One
Whatman filter paper	GE Healthcare Life Sciences

1.1.6 Chemicals and reagents

Agarose	Carl Roth
Albumin from BSA, Alexa Fluor™ 555	Thermo Scientific

APS	Carl Roth
Milk powder, non-fat	Carl Roth
Poly-D-Lysine	Sigma Aldrich
Collagen IV	Santa Cruz
Chloroform	Carl Roth
Ethanol	VWR
Isopropanol	Carl Roth
Methanol	Carl Roth
Page Ruler	Thermo Scientific
Rotiphorese 40% acrylamide solution	Carl Roth
Sodium docecyl sulfate (SDS)	Carl Roth
Tris Puffer	Carl Roth
Triton X®-100	Carl Roth
TRIzol reagent	Ambion
Trypsin/EDTA	Carl Roth
Tween®20	Carl Roth
TEMED	Carl Roth
Xylol	Carl Roth
Immersion oil type-F for microscopy	Olympus
1 kb DNA ladder	Solis BioDyne

1.1.7 Buffers and solutions

Buffer/solution	**Composition**
Laemmli buffer (5x)	0,5 M Tris-Base pH 6,8
	20 % Glycerol
	20 % SDS

	1 % Bromophenol Blue
	1 % β-mercaptoethanol
PBS (10x)	80 g NaCl
	2,4 g KH2PO4
	17,8 g Na2HPO4
	4 g KCl
	pH adjusted to 7,4
	1000 ml H_2O
TBS (10x)	9 g Tris-Base
	69 g Tris-HCl
	88 g NaCl
	1000 ml H_2O
	pH adjusted to 7,4
TBS-T	0,1 % Tween-20 in TBS (1x)
1,5 M separating gel buffer	36,4 g Tris-Base
	pH adjusted to 8,8
	200 ml H_2O
0,5 M stacking gel buffer	6,1 g Tris-Base
	pH adjusted to 6,8
	100 ml H_2O

SDS-PAGE running buffer (10x)	30 g Tris-Base 144 g Glycine 10 g SDS 1000 ml H_2O pH adjusted to 8,3
SDS-PAGE transfer buffer (10x)	30 g Tris-Base 144 g Glycine 1000 ml H_2O
SDS-PAGE transfer buffer (1x)	100 ml 10x transfer buffer 100 ml MetOH 800 ml H_2O
Citrate buffer	21 g citrate acid monohydrate 500 ml H_2O pH adjusted to 6,0
Sucrose Buffer	8,56 g Sucrose (Saccharose) 133 µl TEA (Triethanolamine) pH adjusted to 7,5
Phosphatase inhibitors	90 mg Na Pyrophosphate 3,68 mg Na Orthovanadate 84 mg Na Fluoride

Proteases Inhibitors	1 ml 20x PI Roche
Paraformaldehyde	30 g PFA 100 ml H_2O
Ponceau S	0,5 g Ponceau S (tetrasodium salt) 10 % acetic acid (glacial)

1.1.8 Plasmids

Plasmid name	Size	Resistance	Company
pGL3-human L-WNK1 Promoter	6003 bp	ampicillin	VectorBuilder
pGL3-human KS-WNK1 Promoter	5994 bp	ampicillin	VectorBuilder
pRL TK	4045 bp	ampicillin	Promega
pGL3-Basic Vector	4818 bp	ampicillin	Promega
pcDNA-GATA3	6739 bp	ampicillin	Addgene
MAFB pcDNA 3.1	5428 bp	ampicillin	Dr. Celio Pouponnot

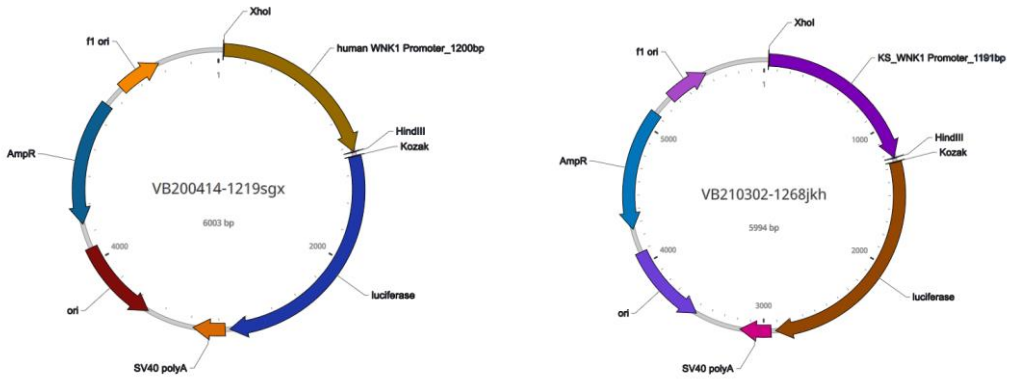

Fig. 1. Vector maps of L-wnk1 and Ks-wnk1 reporter plasmids.

The pGL3-based human L-wnk1 and Ks-wnk1 promoter-luciferase reporter plasmids, contain 1200-bp of the human L-wnk1 promoter sequence and 1191-bp of the human Ks-wnk1

promoter sequence respectively and a firefly luciferase gene sequence coding for the 61 kDa firefly luciferase protein.

1.1.9 Antibodies

1.1.9.1 Primary antibodies

Antibody	Stock	Cat. Number	Company
Rabbit anti-mouse NBC1	0,8 mg/ml	ANT-075	Alomone labs
Rabbit anti-mouse Ezrin	0,8 mg/ml	ab40839	Abcam
Rabbit anti-mouse P-Ezrin	1 mg/ml	ab47293	Abcam
Mouse anti-mouse β-actin	200 µg/ml	sc-47778	Santa Cruz
Rabbit anti-RAB11A	1 mg/ml	71-5300	Invitrogen
Goat anti-VPS35	0,5 mg/ml	1397SS	Novus Biologicals
Goat anti-Galectin3	1 µg/ml	AF1197-SP	R&D Systems
Rabbit anti-Alix	200 µg/ml	sc-49267	Santa Cruz
Rabbit anti-mouse WNK1	2 mg/ml		Self made
Guinea Pig anti-mouse WNK1	2 mg/ml		Self made
Rabbit anti-mouse B0AT1			F.Verrey, Zurich
Goat anti-mouse 4F2hc			F.Verrey, Zürich
Rabbit anti-mouse SGLT2			H.Koepsell, Würzburg
Rabbit anti-mouse γ^+LAT1			F.Verrey, Zürich
Rabbit anti-mouse γ^+LAT2			F.Verrey, Zürich
Rabbit anti-Megalin			Self made

1.1.9.2 Secondary antibodies

Antibody	Stock	Cat. Number	Company
Alexa 488	1,5 mg/ml		Dianova
Cy2	1,5 mg/ml		Dianova
Cy3	1,5 mg/ml		Dianova
Alexa 647	1,5 mg/ml		Dianova
Star 580	1 mg/ml		Abberior
Star Red	1 mg/ml		Abberior
Alexa 647 Phalloidin	5 mg/ml		Thermo Scientific
Acti-Stain 488 Phalloidin	14 µM		Cytoskeleton, Inc.
Peroxidase-conjugated	0,8 mg/ml		Dianova

1.1.10 Enzymes

Enzyme	Activity	Company
DNAse I	1000 UN	Sigma Aldrich
RT RNase	50000 U	Promega
XhoI	10 u/ml	Thermo Scientific
BamHI	10 u/µl	Fermentas
BglII	10000 u/µl	New England Biolabs

1.1.11 Statistical analysis

Data are presented as mean ± SD. Testing of statistical significance between two groups was done by Mann-Whitney U test or unpaired Student's t test with Welch correction. A P value < 0.05 was regarded as significant.

1.1.12 Software and online tools

Software	Company
ApE 2.0.49	Bio-Soft.Net

Fusion	Vilber Lourmat
GraphPad Prism 5.0	GraphPad Software, Inc
ImageJ	Public domain
Imspector	Abberior Instruments
Leica Application Suite X	Leica
MS Office 2010	Microsoft
MatInspector	Genomatix
Online tools	**Website**
NCBI	http://www.ncbi.nlm.nih.gov/
PubMed	http://www.ncbi.nlm.nih.gov/pubmed/

1.2 Methods

1.2.1 Animal experiments

All animal experiments were conducted according to the NIH Guide for the care and use of laboratory animals, as well as the German and Swiss law for the welfare of animals. All animal experiments were approved by local authorities (G-11/51 and M-9/11) and (FR25959,2014_55_FR) respectively. Mice were housed in a SPF facility with free access to chow and water and a 12h day/night cycle. Breeding and genotyping was done according to standard procedures. Vps34 *fl/fl* have been described previously [140] and were crossed to *Pax8rtTA* and *TetOCre* animals [1]. At 5 weeks of age, inducible animals and respective controls (lacking either *TetoCre* or *Pax8rtTA*) received doxycycline hydrochloride (Fagron, Barsbuettel Germany) via drinking water (2 mg/ml with 5% sucrose, protected from light) for a total of 14 days. *Vhl fl/fl* mice have been described previously [2] and were crossed to $\mathrm{SGLT2}^{Cre}$ mice (Jackson laboratories). Diabetes mellitus was induced in the mice groups *Vhl fl/fl* and *Vhl fl/fl/*$\mathrm{SGLT2}^{Cre}$ at 12 weeks of age by injection of streptozotocin (100 mg/kg) intraperitoneal for two consecutive days. All mice presenting a blood glucose level higher than 300 mg/dl were considered diabetic.

1.2.2 Cell culture methods

1.2.2.1 General cell culture conditions

All cell lines used in this thesis were grown in sterile cell culture flasks at 37°C under 5 % CO2 atmosphere with a 95 % humidity. Passage of cells was done after reaching confluence. Therefore, the cells were incubated with trypsin/EDTA in PBS until cells detached from the surface of the flask and then were resuspended in cell culture medium and centrifuged at 1000 rpm for 5 min. Pellets were resuspended in cell culture medium and the cell suspension was transferred to a new T175 flask in a ratio 1:4.

1.2.2.2 Coating of cell culture flasks and plates

1.2.2.2.1 Coating with Poly-D-Lysine (PDL)

Poly-D-Lysine promotes the adhesion of culture cells on plastic ware. The cell culture surface of cell culture flasks or 6 well plates were coated with 1 ml 0,002 % Poly-D-Lysine per 25 cm^2 culture surface, incubated for 30 min and rinsed twice with dH_2O. Subsequently, the cell culture surfaces were left to dry for one hour, protected from light and kept at room temperature.

1.2.2.3 Counting of cells

Cells were counted before seeding by using a Neubauer improved counting chamber in order to guaranty similar conditions between the experiments. To asses cell number, cell suspension was stained with trypan blue in 1:1 ratio. A reduction in the membrane integrity allows trypan blue to penetrate dead cells. Therefore, 10 µl of cell suspension were mixed with 10 µl of trypan blue solution. Same amount was pipetted into the Neubauer improved chamber and four corner squares were counted using a 10 x PH objective. The average result of four squares was calculated and the cell number was determined per milliliter of cell suspension according to the following formula:

average number per corner square * dilution factor from trypan blue $*10^4$ cells / ml

1.2.2.4 Cryopreservation of mammalian cells

Cells were freezed for longtime storage and to avoid aging and transformation. Cells were grown to confluency in a T175 cell culture flask, trypsinized and centrifuged for 5 min at 1000 rpm. Cells were resuspended in 2 ml cell culture medium containing 10 % DMSO and 1 ml was transferred to a sterile cryo tube. A gradual freezing process was established to avoid damages

in cell membranes due to the formation of crystals. Cryo tubes were then kept for 2-4 hours at -20°C, then were kept 24 hours at -80°C and finally transferred to a -140°C freezer for long storage.

1.2.2.5 Transfection of cells

1.2.2.5.1 Transfection of cells using jetOPTIMUS®

Cells were seeded in a 24-well culture vessel filled with 0,5 ml medium in each well at a confluence around 50 - 60 %. 0,5 µg of DNA were diluted in a microcentrifuge tube with jetOPTIMUS buffer to a final volume of 50 µl. The mix was vortexed for 5 seconds at high speed and 0,5 µl of jetOPTIMUS reagent were added to the diluted DNA and mixed well for 10 seconds at high speed. The mix was incubated at room temperature for 10 minutes in order to create a nanoparticle complex solution. After incubation, the nanoparticle complex solution was spun down for 10 seconds in a microcentrifuge. Cells were washed with 1x PBS and replaced with 1 ml fresh medium. 0,5 µg of DNA Plasmid was added dropwise to each well of the 24-well plate. At the end, the plate was shaken up and down and side to side gently in order to spread the nanoparticle complex solution evenly. The plate was incubated overnight at 37°C. Next day, the cells were washed with 1x PBS in order to remove all left nanoparticle complexes and replaced with 1 ml of fresh medium.

1.2.3 Gene expression analysis

1.2.3.1 Plasmid DNA purification

1.2.3.1.1 Plasmid DNA purification with Miniprep Kit

Selected single *E. coli* clones from the bacterial colony plate, were cultivated overnight in LB media at 37°C. The bacterial culture was harvested by centrifugation at 8000 rpm in a microcentrifuge for 5 min at room temperature. Plasmid DNA was purified according to the Thermo Scientific GeneJET Plasmid Miniprep Kit #K0502. Pelleted cells were carefully resuspended and after completed cell lysis, DNA was washed and transferred to a new column. DNA was eluted with 50 µl of elution buffer and centrifuged two times for 2 min. Quantification of the DNA probes was made using NanoDrop ND-1000 and stored at -20°C.

1.2.3.1.2 Plasmid DNA purification with Midiprep Kit

A single colony from an overnight *E. coli* culture was picked and inoculated in 5 ml of LB medium with the correspondent antibiotic and incubated overnight at 37°C. The cells were

harvested by centrifugation for 10 min at 5.000 x g. Plasmid DNA was purified according to the Thermo Scientific GeneJET Plasmid Midiprep Kit #K0481. Pelleted cells were carefully resuspended and after completed cell lysis, DNA was washed and transferred to a new column. DNA was eluted with 350 µl of elution buffer and centrifuged for 5 min at 3000 g. Quantification of the DNA amount of plasmid was made using NanoDrop ND-1000 spectrophotometer and stored at -20°C.

1.2.3.2 Restriction enzyme digests

For the Dual Luciferase Reporter Assay System, all the DNA plasmids were confirmed for the presence of the insert and for the insert size by restriction enzyme digestion.

Analytical Restriction digest:

200 ng plasmid DNA

1 µl 10x NEF buffer

1 µl enzyme

up to 10 µl dH_2O

The reaction was incubated for 2 hours at 37°C and analysed by agarose gel electrophoresis.

1.2.3.3 Agarose gel electrophoresis

Gel electrophoresis was used to separate DNA samples according to their size. To achieve optimal results gels were made with an agarose concentration of 1 % (w/v) dissolved in 1x TAE buffer. For gel preparation, 1 gram of agarose was weighted and dissolved in 100 µl TAE buffer using a microwave oven. To the agarose were added 12 µl of peqGreen to allow visualize the DNA under ultraviolet light. The agarose was cooled down for 5 min at room temperature and poured into a gel tray provided with a well comb. After 20-30 min at room temperature, the agarose was completely solidified and was placed in a gel chamber and filled with 1 x TAE buffer. Before loading, 2 µl of 6x DNA loading buffer was added to the DNA samples and 3 µl of DNA ladder were loaded for identification of the size of the DNA fragments. Gel electrophoresis was performed at 100 V for one hour and the gel visualized with ultraviolet light on FUSION detector and photographed for documentation.

1.2.3.4 Isolation and purification of RNA from kidney tissue

1.2.3.4.1 Total RNA isolation

50-100 mg tissue samples were lysed in 500 µl trizol and then homogenized in a Poyltron homogenizer. 100 µl Chloroform was added to the homogenized tissue and incubated for 3 min at room temperature. The lysate was centrifuged by 12.000 g for 15 min at 4 °C. The aequous phase was taken and placed in a new tube. The same amount of isopropanol was added to the aequous phase, incubated for 10 min at room temperature and centrifuged at 12.000 g for 10 min at 4 °C. The supernatant was removed and the pellet was washed with 500 µl of 75% Ethanol. The sample was centrifuged by 7500 g for 5 min at 4°C. Ethanol was completely removed and the pellet was left to dry at room temperature. Once dried, the pellet was diluted in 25 µl R-nase free water and dissolved by shaking at 60°C for 10 min. The amount and purity of isolated RNA was measured with NanoDrop ND-1000. RNA was considered as pure when the ratio of absorbance at 260 nm versus 280 nm in the range between 1.8 to 2.0 lay. RNA samples were kept at -80°C until further analysis.

1.2.3.4.2 Treatment of RNA with DNAse I

In order to remove genomic DNA from the RNA templates, DNAse digest was performed using DNAse I (Sigma Aldrich). RNA samples were mixed with 10x DNase Buffer and 1,5 µl DNAse I (1 U/µl) and digested for 20 min at 37°C. After digestion, 1,5 µl Stop Solution (EDTA 20 mM) was added to the mix to stop the reaction and incubated for 10 min at 37°C.

1.2.3.5 Generation of first-strand cDNA from total RNA

Template RNA extracted from kidney tissue as describe above (1.2.3.4.1) was synthesized into cDNA according to the manufacturer´s instructions (Promega).

Table 1-1: Pipetting scheme for cDNA synthesis from total RNA

Component	Volume
RNA	15 µl
5x M-MLV Reverse Transcriptase-reaction buffer	6,0 µl
10 mM dNTP-Mix	1,5 µl
Random hexamer primer	1,5 µl
M-MLV Reverse Transcriptase	1,6 µl
ddH_2O	4,4 µl

RNA templates (1 µg/µl) were mixed with 1,5 µl reverse-transcriptase (Promega), reaction buffer and nuclease free water in a total reaction volume of 30 µl. The reaction was incubated for 10 min at 25°C, 50 min at 42°C and 15 min at 70°C. The cDNA was kept at -20°C.

1.2.3.6 Real-time quantitative PCR analysis

The gene expression of WNK1 kinase in mouse kidney tissue was analysed by reverse-transcription polymerase chain reaction (RT-PCR). 10 µl of Applied Biosystems™ TaqMan®Mastermix was mixed with 1 µl cDNA template followed by 1 µl of Tbp Probe VIC and 1 µl of WNK1 probe FAM. The reaction was filled with dH_2O to an end volume of 20 µl per Well of the 96 well plate. All assays were performed in duplicates. PCR reactions were performed according to the manufacturer´s instructions (7500 Fast Real Time PCR from Applied Biosystems™). The running method for the Real-Time PCR reaction was set according to following steps, first a 95°C step for 10 min followed by 40 cycles with 15 seconds at 95°C and 1 min at 60°C, corresponding to denaturation of cDNA and alignment. Real time PCR experiments were performed using the Taqman probes WNK1 catalogue number: 4448892 Assay ID: mM 01184002_m1 and TBP catalogue number: 0046973.

Table 1-2: Pipetting scheme for Real-Time PCR

Component	Volume
cDNA template	1 µl
Taqman Mastermix	10 µl
Tbp Probe VIC	1 µl
WNK1 probe FAM	1 µl
dH_2O	7 µl

1.2.4 Biochemical methods

1.2.4.1 BaseScope

To deparaffinize the sections, slides were submerged in a dish containing 200 ml fresh Xylene and incubated two times for 5 min at room temperature. Immediately the slides were submerged in a dish containing 200 ml of fresh 100 % alcohol and incubated two times for 1 min at room temperature. Slides were removed from the rack and left to dry for 5 min at room temperature. Next, 5 drops of RNAscope Hydrogen Peroxide were added to the deparaffinized sections and were incubated for 10 min at room temperature. To remove the RNAscope Hydrogen Peroxide solution, slides were washed three times in distilled water. In order to equilibrate the slides, they were added to a container, filled with distilled water previously

heated to 95°C. For target retrieval, the slides were put in a slide holder filled with 400 ml target retrieval buffer and was placed in a pot. The pot was covered with a lid and slides were heated for 15 min at 95°C. Afterwards, the slides were removed from the pot and transferred quickly to a container filled with 400 ml of distilled water. The slides were submerged in 100 % alcohol for 3 min and left to dry for 60 minutes in a 60°C incubator. Using a hydrophobic barrier pen, a barrier was drawn around each section by surrounding the slide two times with the pen. Slides were incubated overnight at room temperature. The next day, the slides were placed on the HybEZ Slide Rack and 5 drops of RNAscope Protease IV were added to each section. After adding the Protease IV, the lid of the slide rack was closed and inserted in a tray. The tray was put in the oven and incubated for 15 min at 40°C. The Protease IV excess liquid was removed and the slides were washed three times with distilled water. In order to hybridize the probe, 15 µl of L-wnk1 was added to each section and incubated in the oven for two hours at 40°C. The hybridize L-wnk1 excess liquid was removed and the Slides were placed in a container filled with 1x wash buffer. Slides were washed twice for 2 min at room temperature by shaking the slides shortly in the container. Next, 15 µl of AMP1 were added to each section and incubated in the oven for 30 min at 40°C. The AMP1 excess liquid was removed and the Slides were placed in a container filled with 1x wash buffer. Slides were washed twice for 2 minutes at room temperature by shaking the slides shortly in the container. After washing the slides 15 µl of AMP2 were added to each section and incubated in the oven for 30 min at 40°C. Next, 15 µl of AMP3 were added to each section and incubated in the oven for 15 min at 40°C. After washing the slides for 2 min, 15 µl of AMP4 were added to each section and incubated in the oven for 30 min at 40°C. The same was applied to AMP 5 probe. After washing the slides for 2 min, 15 µl of AMP6 were added to the slides and incubated in the oven at 40°C for 15 min. After washing the slides for 2 min, 15 µl of AMP7 were added to the slides and incubated at room temperature for 30 min. 15 µl of AMP8 were added to the slides and incubated at room temperature for 15 min. To detect the signal of the L-WNK1 probe, a solution consisting in Fast RED-B and Fast RED-A was prepared in a ratio 1:60. 15 µl of the RED working solution was added to each slide and incubated in the dark for 10 min at room temperature. After incubation, the slides were submerged in a container filled with tap water and rinsed three times with fresh tap water. To mount the samples, 12 µl of Glycerine/PBS was placed on the slide after removal of the excess water and immediately placed a 24 mm x 50 mm coverslip over the tissue section.

1.2.4.2 Dual-Luciferase Reporter Assay

The Dual-Luciferase Reporter Assay System is a genetic reporter system that allows to study gene expression through bioluminescent reactions. Firefly luciferase (61 kDa) and Renilla luciferase (36 kDa) have different enzyme structures and substrate requirements that makes possible to separate their bioluminescent reactions. For the glucose stimulation assays and the assays under hypoxic conditions, ok cells were incubated with DMEM (GIBCO, A14430-01) without fetal bovine serum and supplemented with 5 mM or 25 mM glucose, 2 mM glutamine, 100 U/ml penicillin, 100 µg/ml streptomycin, 5 mM HEPES and 3 g/L Na2CO3 for 24 h. MpkCCD (c14) cells were incubated with DMEM (GIBCO, A14430-01) without fetal bovine serum and supplemented with 5 mM or 25 mM glucose, 2 mM glutamine, 5 mM HEPES, 100 U/ml penicillin, 100 µg/ml streptomycin and 50 nM dexamethasone for 24 h. Cells were transfected with 1 µg of L-wnk1, Ks-wnk1 luciferase reporter construct or pGL3-Basic and co-transfected with 0,2 µg of pRL-TK (Promega, Madison USA) expressing *Renilla* luciferase as a control for transfection efficiency. 15 hours after transfection, transfection medium was removed and replaced by medium containing 5 mM glucose or 25 mM glucose. After stimulation, cells were prepared for the measure of the luciferase activity. The firefly luciferase reporter is measured first after adding its substrate luciferase assay reagent (LAR II) to generate a luminescent signal. After quantifying this luminescence, the reaction is quenched and the Renilla reaction is initiated by adding its substrate Stop & Glo reagent and quantified. For preparation of cell lysates, cells were washed three times with 1x PBS and replaced with 100 µl of passive lysis buffer. Cultured cells were incubated with passive lysis buffer for 15 min on a shaker at room temperature. To ensure that all cells are detached from the surface of the culture vessel, cells were scraped with a cell scraper and well resuspended until homogeneity was reached. 25 µl of the cell lysate were transferred to a 96 well plate (Greiner) in triplicates. Before starting the measurement of the plate, injector 1 of TriStar²S LB 942 was primed with 50 µl of firefly substrate (LAR II) per well and injector 2 was primed with 50 µl of Renilla substrate (Stop & Glo) per well. Measurement was carried out according to Promega´s manual parameters. The firefly luciferase activity was performed with one second elapsed time. The quantification of the firefly luciferase activity was accomplished within 12 seconds. The quenching of the firefly luciferase activity was done within one second, and the quantification of the Renilla luciferase activity was performed within 12 seconds. The total elapsed time for the DLR™ Assay was 30 seconds.

1.2.4.3 Endocytosis Assay

OK cells were seeded into 10 cm² dishes to a 60-80% confluency. OK cells were incubated with OK medium without FCS overnight. For the endocytosis assay, OK cells were incubated with 0,3 mg/ml Albumin Alexa Fluor 555 for 15 min at 37°C. Cells were washed three times with cold PBS on ice. Subsequently, the cells were fixed with 4% PFA for 15 min at room temperature and washed again three times with PBS. After 15 min incubation in 0,5 % Triton, cells were incubated with 5% milk in PBS for one hour. After blocking with blocking solution (5% milk in 1x PBS) cells were incubated with ZO1 antibody overnight at 4°C. After incubation with Alexa 488 secondary antibody, cells were washed and incubated with Alexa 647 antibody for one hour and DAPI for 30 min. Cells were mounted and analysed under confocal microscopy.

1.2.4.4 TUNEL Assay

Kidney tissue sections were deparaffinised according to the section 2.2.7.3. Samples were incubated with 85 % NaCl for 5 min at room temperature and fixed in 4% formaldehyde solution in PBS for 15 min at room temperature. For permeabilization, the tissue sections were incubated with 20 µg/ml Proteinase K solution in PBS for 10 min at room temperature. After washing three times with PBS, the tissue sections were fixed in 4% formaldehyde solution in PBS for 5 min at room temperature. Tissue sections were equilibrated for 10 min and labelled with 51 µl of rTdT reaction mix for 60 min at 37°C protected from light. To stop the reaction, the tissue sections were washed twice with 2 x SSC for 15 min and incubated with DAPI for 10 min. Slides were mounted with glycerol/PBS solution. Samples were analysed under a fluorescence microscope using a green fluorescence filter at 520 ± 20 nm and a blue filter at 460 nm.

1.2.5 Protein biochemistry methods

1.2.5.1 Membrane fractions

Extraction of membrane fractions from kidney lysates was done using a porcelain morter and a pestle that were initially precooled at -20°C. The morter was filled with liquid nitrogen. Half of a frozen kidney was placed inside the morter and pressed with the pestle until all liquid nitrogen was evaporated and the kidney was pulverized. 500 µl of sucrose buffer were added to the pulverized kidney. The kidney was homogenized with a pestle until it was defrozen and then transferred into a 1,5 ml Eppendorf tube and kept on ice. The morter was rinsed with another 500 µl of sucrose buffer to take the rest of the homogenized kidney and added to the

1,5 ml Eppendorf tube. To sonicate the probes, the sonotrode of the sonicator was put inside the tube containing the homogenized tissue kept on ice during the process to cool down. The tissue was sonicated 3 times for 3 seconds and centrifuged at 4°C for 5 min by 3500 rpm. The supernatant was transferred to a new tube and centrifuged for 30 min by 15.000 rpm. The pellet was resuspended in 200 µl of sucrose buffer, sonicated 2 times for 3 seconds while kept on ice and frozen into liquid nitrogen. Probes were stored at -20°C.

1.2.5.2 Quantification of protein concentration

Quantification of protein concentration was done according to the Thermo Scientific™ Pierce™ BCA Protein Assay Kit. Albumin standards were diluted to a final BSA concentration of 2000, 1000, 500, 250, 125 and 0 µg/ml. Protein samples were diluted in dH_2O in a 1:10 ratio. 10 µl of each standard and protein sample were pipetted into a microplate well. 200 µl of BCA reagent A and reagent B in a 50:1 ratio were added to each well. The microplate was protected from light and incubated for 30 min at 37°C. Absorbance was measured at 540 nm wavelength on a plate reader.

1.2.5.3 SDS polyacrylamide gel electrophoresis (SDS PAGE)

SDS-PAGE is an analytical technique that allows separation of proteins based on their molecular weight. SDS is an anionic detergent that unfolds proteins into linear chains with a negative charge that is proportional to the polypeptide chain length. Unfolded proteins migrate from cathode side (-) to anode side (+) at different rate depending on the concentration of the separating gel. The gel for the SDS-PAGE was made in two steps, first a separating gel and second a stacking gel. Glass plates and spacers were cleaned with 70% EtOH and assembled according to the Bio-Rad manual of instructions. Reagents listed in table number 2-3 were well mixed to form the separating gel and poured immediately into the glass plate. Isopropanol was added on top of the separating gel in order to smooth the surface and eliminate bubbles. After polymerization of the separating gel, the isopropanol was completely removed. Subsequently, the reagents listed in table number 2-1 were well mixed to form the stacking gel and poured in top of the separating gel. To form the pockets of the gel, a comb was inserted inside of the stacking gel. After one hour at room temperature, the comb was removed and the pockets rinsed with dH_2O. The gel was assembled into a Mini-Protean II apparatus and filled with 1x running buffer. For sample preparation, probes were dissolved in 5 x laemli buffer to a final concentration of 1x and heated at 95°C in a thermomixer at 300 rpm for 5 min. Before loading the probes, 3 µl of protein molecular marker PageRuler were added in the first pocket of the gel as a reference for the protein size. After loading the samples

into the rest of the wells, the gel was run at 100 V for 15 min until the dye front reached the separating gel and then increased to 120 V for 100 min.

Table 1-3: Composition for SDS-PAGE-Gels for 10 ml polyacrylamide

	Separating gel					Stacking gel
	6%	**8%**	**10%**	**12%**	**15%**	**4%**
H2O	5,8 ml	5,3 ml	4,8 ml	4,3 ml	3,55 ml	7,5 ml
40% APP	1,5 ml	2 ml	2,5 ml	3 ml	3,75 ml	1 ml
TRIS 1,5 M	2,5 ml	2,5 ml	2,5 ml	2,5 ml	2,5 ml	-
TRIS 0,5 M	-	-	-	-	-	1,3 ml
10% SDS	100 µl	100 µl	100 µl	100 µl	100 µl	100 µl
10% APS	100 µl	100 µl	100 µl	10 µl	100 µl	100 µl
TEMED	10 µl	10 µl	10 µl	10 µl	10 µl	10 µl

1.2.5.4 Western Blot

An open transfer cassette plate was submerged onto a tray filled with 1x transfer buffer. A sponge was placed onto the cassette and air bubbles were removed with a 15 ml tube. On top of the sponge, two pieces of blotting paper were placed. A nitrocellulose membrane, previously incubated in transfer buffer was placed over the blotting paper. The gel was removed from the electrophoresis plate and the part of the gel belonging to the wells was cut off. The gel was carefully laid flat against the membrane eliminating all air bubbles. Another two pieces of blotting paper were added to the gel and another sponge was added onto the blotting paper. Air bubbles were removed and the cassette was closed gently and placed into a transfer tank. The transfer tank was filled up with 1x transfer buffer and closed. Transfer was done at constant 100 V and approx. 400 mA for two hours at 4°C. After transfer was completed, the nitrocellulose membrane was removed from the cassette and washed shortly in 1x TBS.

1.2.5.5 Ponceau S staining

Ponceau S staining solution was made by mixing 0,5 g Ponceau S with 10 % acetic acid and bringing the mix to a total volume of 50 ml with dH_2O. Nitrocellulose membrane was washed with 1 x TBS and stained with Ponceau S solution in shaker for 5-10 min. Finally, the membrane was washed with dH_2O and scanned for documentation.

1.2.5.6 Blocking, antibody incubation and detection

The nitrocellulose membrane was incubated in 5% milk in TBS for one hour at room temperature on a shaker. The membrane was cut by the corresponding marker size and incubated with primary antibody in 5% milk overnight at 4°C. The membrane was washed three times in TBST for 15 min on a shaker and incubated with secondary antibody in 5 % milk for 2 hours at room temperature. For detection, the membrane was incubated for 5 min with Immobilon Western Chemiluminescent HRP solution and exposed to detection on a chemiluminescence imaging system (Fusion).

1.2.6 Immunohistochemical methods

1.2.6.1 Cryosectioning of frozen tissue

For preparation of cryosectioning, the cryostat was set to -20°C and a new blade was inserted. To allow frozen kidneys to equilibrate reaching the cryostat temperature, they were left for 20 minutes inside the cryostat. Kidneys were fixed with embedded medium to a small plate. 5 µm sections were cut and transferred to a room temperature slide by touching the slide to the cryosections and rubbing the underside of the slide with the finger to facilitate adhesion. Cut sections were then transferred to -20°C until further use.

1.2.6.2 Sectioning of paraffin tissue

Kidney paraffin blocks were chilled at 4°C to make sectioning easier. 5 µm paraffin sections were cut with a microtome and transferred to a 43-45°C water bath. Paraffin cuts were given time in water to expand in order to eliminate wrinkles. When the sections were lying flat, they were transferred to a slide and kept overnight in a 60°C incubator.

1.2.6.3 Deparaffinization and rehydration of paraffin sections

The kidney sections that had been incubated at 60°C overnight in order to allow a good adhesion of the section to the slide had to be deparaffinised and rehydrated before proceeding with the IHC staining protocol.

The tissue sections were then deparaffinized in Xylene (3 x 10 min), rehydrated in graded alcohol and washed in 1 x PBS to rinse off the remained ethanol in order to achieve posteriorly a good staining of the sections. The 5 µm paraffin kidney sections were deparaffinised and rehydrated according to the procedure described in table 1-4.

Table 1-4: Conventional procedure for deparaffinise and rehydrate paraffin sections

Reagent	Time
Xylene I	10 min
Xylene II	10 min
Xylene III	10 min
100% Ethanol	5 min
96% Ethanol	5 min
90% Ethanol	5 min
70% Ethanol	5 min
PBS	5 min

1.2.6.4 Antigen retrieval

For heat induced antigen retrieval, slides were brought to a small, heat-resistant basket filled with 1x sodium citrate buffer (pH 6.0) and placed into a pressure cooker filled with water (200-500 ml). The cooker was brought to 95°C on a hot plate and then maintained at a sub-boiling temperature for 6 min. Afterwards, kidney sections were cooled down for 20 min and quickly transferred into 1 x PBS.

1.2.6.5 Immunofluorescence staining

Immunofluorescence is a technique to visualize proteins of interest in fixed cells or tissue using a fluorescence microscope. This method is based on antigen binding of a primary antibody followed by binding of a fluorophore-conjugated secondary antibody. Slides were washed with 1 x PBS three times and permeabilized with Triton X 0,5% in PBS for 30 min at room temperature and washed three times with 1x PBS afterwards. Subsequently slides were incubated with blocking buffer (5% milk in 1x PBS) for one hour at room temperature. Primary antibody diluted in blocking buffer was added to the slides and incubated overnight at 4°C in a wet chamber protected from light. The next day, slides were washed three times with 1x PBS and incubated with secondary antibody at room temperature for 2 hours protected from light. Slides were washed three times with 1x PBS and stained with DAPI for 10 min at room temperature. Slides were finally mounted with Glycerine/PBS solution and imaged with the compact fluorescence microscope Keyence BZ-x800e or with the facility line STED microscope (Abberior Instruments).

2. Chapter 1: VPS34-dependent control of apical membrane function of proximal tubule cells and nutrient recovery by the kidney

2.1 Abstract

Kidney proximal tubular cells contribute to electrolyte and nutrient homeostasis by reabsorption of proteins and nutrients from the ultrafiltrate. Endocytosis is a cellular process used for receptor signalling, nutrient uptake, transport of proteins, membrane remodelling and pathogen entry. VPS34 (vacuolar protein sorting 34) is the sole member of the class III phosphoinositide 3-kinase in mammals and plays a key role in the control of cell homeostasis and vesicular trafficking including endosomal dynamics, macroautophagy and lysosomal function. Although there are not complete Vps34 knockout mice studies due to early embryonic lethality, a great progress in the information of the structure of Vps34, regulation of its enzyme activity and its functions has been made in the last decade.

Here, a conditional knockout of Vps34 in proximal tubule cells of adult mice was induced to perform an exhaustive analysis of the function of VPS34 in vivo via assessment of proteomic profiling, phosphoproteomics, metabolome analysis and endocytosis assays. Conditional deletion of VPS34 in proximal tubule cells, resulted in impaired pinocytosis, defective intracellular trafficking, altered basal membrane differentiation and inhibition of autophagy.

Disruption of glucose and amino acid transporters led to glucosuria and amino aciduria. Alterations in exosomal galectin-3 and galectin-9 concentration, resulted in increased intracellular recruitment of galectins into intraluminal vesicles and reduced exocytosis. Phosphorylation of retromer complex components led to a reduced retromer complex activity necessary for protein transport and membrane recycling leading to a loss of biomass. Integration of urinary and tissue proteo-metabolome revealed an increased abundance of beta oxidation, reduced gluconeogenesis and usage of glutamine for energy consumption. All omics dataset demonstrated multi-layered aspects of antiviral cytokine response such as induction of antiviral protein IFITs and reduction and shedding of the ACE2 receptor. Pharmacological inhibition of VPS34 in a proximal tubule cell line strongly reduced SARS-CoV-2 infection, a process relying on sufficient glutamine supply. This broad multivariate map of VPS34 functions in the proximal tubule, sketches the advantages and disadvantages of systemic VPS34 inhibition as a part of therapeutic measures in several diseases with special emphasis in cancer, metabolic and neurodegenerative diseases.

2.2 Introduction

2.2.1 Structure of the kidney

2.2.1.1 The nephron

The nephron represents the structural and functional unit of the kidney. Each human kidney contains around one million nephrons. Nephrons show a substantial heterogeneity from a functional and anatomic perspective that allows to differentiate them in three groups depending on the location of their renal corpuscle in the cortex. Superficial cortical nephrons have glomeruli located within one millimetre of the capsular surface and have short loops of Henle. Mid-cortical nephrons have glomeruli located in mid-cortex and may have short or long loops of Henle. Juxtamedullary nephrons have glomeruli located in the cortex just above the cortex medulla junction and have long loops of Henle which descend deep into the medulla.

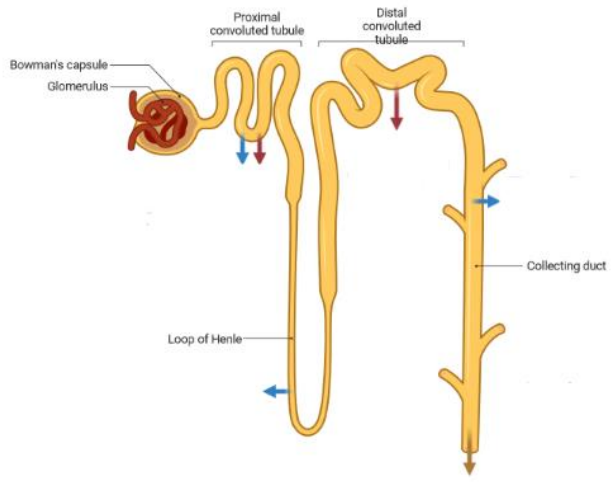

Fig. 2.1. Renal corpuscle, tubules of the nephron and collecting tubules/ducts. *After leaving the renal corpuscle, the filtrate passes through the proximal tubule where water, solutes, glucose, amino acids, vitamins and proteins are reabsorbed. In the loop of Henle, composed of a thick descending limb (pars recta), a thin descending limb and a thick ascending limb takes place further reabsorption of water (descending limb) and sodium and chloride ions (ascending limb). In the distal convoluted tubule, the variable reabsorption of water and sodium ions is regulated under hormonal control. In the connecting tubules and collecting duct, takes place variable reabsorption of water (blue arrows) and reabsorption or secretion of sodium, potassium, hydrogen and bicarbonate ions (red arrows). Self-created diagram by biorender.com.*

Each nephron consists of a renal corpuscle (Corpuscula renalis) and a renal tubule (Tubulus renalis). The renal corpuscle consists of a capillary network called glomerulus and an epithelial capsule that surrounds the glomerulus called Bowman´s capsule. Fluid flows from the lumen

of the capillaries through the basement membrane into the Bowman´s capsule as a result of the difference of the hydrostatic and colloid osmotic pressure. The luminal aspect of the glomerular capillaries is characterized by a fenestrated endothelium which permits blood filtration. The glomerular basement membrane represents the fusion of the endothelial cell and the podocyte basal lamina. The podocytes form the distal layer of the glomerular filter. They are characterized by prominent food processes called *pedicels* that enwrap the glomerular capillaries. This foot processes are separated by small gaps, known as filtration slit, slit diaphragm or slit pore. The filtration barrier formed by the podocytes, the layer of the fenestrated endothelium and the glomerular basement membrane, allows the filtration of cationic molecules, electrolytes depending on their size and electric charge. Large macromolecules such as serum albumin, gamma globulin and plasma proteins do not enter the barrier filter and remain in the bloodstream. The mesangial cells are situated between the capillary loops and embedded in their own mesangial matrix. They play a role in production of basement membrane proteins, uptake of macromolecules as contractile properties for the regulation of the blood flow.

2.2.1.2 The proximal tubule

The proximal tubule of the kidney is composed of two sections, a convoluted part (Pars convoluta) and a straight part (Pars recta). Besides the structural subdivision of the proximal tubule in a convoluted and a straight section, there is also a classification of the proximal tubule according to the morphology of the cell in three segments S1, S2 and S3. The segments S1 and S2 belong to the convoluted part and the segment S3 belongs to the straight part.

Characteristic for all proximal tubule cells is the cuboidal form of the cell and a membrane polarity defined by an apical membrane facing the lumen of the proximal tubule and a basolateral membrane oriented to the basement membrane. This cell surface membrane polarity is essential for the movements of ions, water and macromolecules between the different cell compartments. Proximal tubule cells possess a brush border with millions of microvilli on the luminal surface that increase the surface area and the tubular reabsorption.

2.2.2 Functions of the proximal tubule

2.2.2.1 Acid-base balance

One of the most important functions of the proximal tubule is the secretion of H^+ into the tubule lumen and the reabsorption of filtered HCO_3^-. Through this mechanism, the proximal tubule represents a regulatory system that can adjust changes in the acid-base balance caused

by physiological and pathophysiological alterations of the acid-base homeostasis. The proximal tubule reabsorbs approximately 80% of the filtered HCO_3^-, the rest is reabsorbed by the thick ascending limb and the distal nephron so that practically no HCO_3^- is eliminated with the urine. The proximal tubule cell, secretes H^+ from the cytosol through the brush border membrane into the lumen via NHE3 and the vacuolar-type H^+-ATPase [3, 4]. The majority of the H^+ that the proximal tubule cell secretes into the lumen combines with filtered HCO_3^- that is not able to cross the apical membrane of the proximal tubule cell to form H_2CO_3.

Then, the carbonic anhydrase IV, which is a luminal membrane-associated enzyme converts H_2CO_3 to CO_2 and H_2O. At this point, CO_2 enters the cell by diffusion and H_2O by the aquaporin 1 channel (AQP1). In the cytosol, both CO_2 and H_2O are converted back into HCO_3^- and H^+ by the carbonic anhydrase II and the new created HCO_3^- exits the cell with Na^+ across the basolateral membrane via the electrogenic Na^+/HCO_3^- cotransporter (NBCe1-A) first into the interstitial space and subsequently into the blood stream. The second contribution of the proximal tubule cells to the acid-base balance is the production of ammonium. Ammonium (NH_4^+) is formed in the proximal tubule cell by biochemical reactions that origin from glutamine. The first step in ammoniagenesis is made by the enzyme glutaminase although the production of an additional NH_4^+ molecule is mediated by the glutamate dehydrogenase. The result is a net of two molecules of bicarbonate and ammonia per glutamine. Ammonia is secreted into the luminal fluid as NH_4^+ through a mechanism involving transport via the apical Na^+/H^+ exchanger NHE-3 [5].

2.2.2.2 Parathyroid hormone (PTH)

PTH is secreted by the chief cells of the parathyroid glands. It is synthetized as a 115 amino acid long prepro-PTH composed of a precursor peptide extended by a leader signal and a prohormone sequence. The leader signal and the prosequence are cleaved in the endoplasmatic reticulum and Golgi resulting in an active (1-84) PTH which is the circulating form of the hormone [6].

In the proximal tubule, PTH exerts its effects through apical and basolateral PTH-receptor (PTHR1). The activation of PTHR1 on the apical BBM, leads to PLC-PKC stimulation mediated by NHERF, whereas activation of PTHR1 at the basolateral membrane, leads to activation of cyclic adenosine monophosphate (cAMP)/protein kinase A (PKA) pathway [7]. The result of the activation of the PTHR1 is a reduction in the uptake of P_i via downregulation of NaPi-IIa and NaPi-IIc at the BBM of proximal tubule epithelia. These two Na^+-coupled transporters mediate the uptake of P_i from the glomerular filtrate, NaPi-IIa drives a secondary active

electrogenic transport whereas the NaPi-IIc mediated P_i transport is electroneutral. The mechanism underlying the downregulation of NaPi-IIa from the BBM has been reported to involve clathrin-mediated endocytosis of the receptor and transport to the lysosomes for degradation [8].

2.2.2.3 Gluconeogenesis

Gluconeogenesis is the regulatory pathway for the production of glucose from non-hexose precursors such as lactate, pyruvate, glycerol and amino acids. Initially, the synthesis of glucose was attributed exclusively to the liver and the kidney was considered a producer of glucose only during acidosis and prolonged fasting. However, later studies have revealed that the kidney accounts for approximately 40% of all glucose released into circulation in postabsorptive healthy humans [9]. Renal gluconeogenesis takes place in the proximal tubule, as this is the only part that is provided with the appropriate enzymes for *de novo* synthesis of glucose and differs from hepatic gluconeogenesis in its substrate affinity and physiological stimuli. In the kidney there are four gluconeogenic precursors: lactate, glutamine, glycerol and alanine. Lactate is the main precursor for hepatic gluconeogenesis. In renal gluconeogenesis, lactate, which is fully filtered by the glomerulus and reabsorbed by proximal tubule cells, has been reported to be 3.5, 2.5 and 9.6-fold higher than that from glycerol, glutamine and alanine respectively [10].

The production of glucose in the proximal tubule is regulated by stress hormones such as hydrocortisone and epinephrine [11, 12]. Insulin is a negative regulator of renal gluconeogenesis and its inhibitory effect has been demonstrated in rodent models. Studies in mice with targeted deletion of the insulin receptor (IR) in the proximal tubule, revealed high blood glucose and higher mRNA expression of glucose-6-phosphatase (G6Pase) which is the enzyme that regulates the final step of glucose production by dephosphorylating glucose-6-phosphate [13, 14]. Metabolic acidosis can also regulate glucose metabolism. During acidosis, the PEPCK mRNA expression in the proximal tubule cell is increased resulting in higher glucose production [15].

2.2.2.4 Endocytosis

2.2.2.4.1 Clathrin-mediated endocytosis (CME)

Internalization of protein-receptor complex by CME involves the formation of clathrin-coated-pits (CCP) composed of three clathrin heavy chains associated with clathrin light chains and

the adaptor protein-2 (AP-2). CME can be divided in four stages: initiation, stabilization, maturation and fission [16]. The steps of CME are regulated by multiple inputs and molecules.

The initiation of the clathrin complex formation requires accumulation of phosphatidylinositol-4,5-bisphosphate (PIP2) and several adaptor proteins whereas the scission involves BAR domain proteins, dynamin and dephosphorylation of PIP2 [17]. After detachment of the clathrin coated vesicle from the plasma membrane, the chaperone adenosine triphosphatase Hsc70 and the J domain protein auxilin, dissociate clathrin and release the vesicle for fusion with other vesicles or with early endosomes. Early endosomes (EEs) sort endocytosed material for recycling and degradation. Essential mediators of early endosome function and maturation are the small GTPase Rab5, PI3P, which is the product of the phosphatidylinositol 3-kinase (PI3K) and endosomal acidification. An acidic pH is required for uncoupling the internalized ligand-receptor complex as well as for MVB formation and activation of degradative enzymes. EEs have a pH of 6.0-6.5, which decreases to 5,0-5,5 in late endosomes and to 4,5 in the lysosomes.

Internalized cargo from the plasma membrane is sorted in EEs and either is destined for degradation in lysosomes or returns to the plasma membrane via recycling pathways. The mechanism that regulates cargo transport along the degradative pathway is well known whereas the sorting and recycling process is more complex and less characterized. During the sorting process, the cargo destined for recycling is organized into tubular domains and sent back to the plasma membrane or to recycling endosomes via fast and slow recycling signalling [18]. The fast-recycling pathway describes a route from EEs to the plasma membrane via Rab4-positive recycling endosomes. Slow recycling consists in transport of cargo from the EEs to a distinct subpopulation of recycling endosomes, known as endosomal recycling compartment (ERC), defined by the presence of Rab11 and from the ERC to the plasma membrane [19].

2.2.2.4.2 Macropinocytosis

Macropinocytosis is a type of endocytosis that involves the nonspecific uptake of large volumes of extracellular fluid such as soluble molecules, nutrients and antigens to form macropinosomes at the base of cell membrane ruffles. In contrast to other forms of endocytosis, macropinocytosis does not require coat and scission proteins as in the case of clathrin-and caveolin mediated endocytosis. In epithelial cells, one of the main characteristics of macropinocytosis is that is induced by growth factors [20]. Upon growth factor stimulation, the signal transduction cascade that initiates macropinosome formation is mediated by the small GTPase Ras and the class I phosphatidylinositol 3-kinase which are activated by receptor

tyrosine kinases such as epidermal growth factor receptor and platelet-derived growth factor receptor. Other effector proteins such as Rac1, a GTPase that regulates the actin cytoskeleton, Rab5 and PAK1 have been reported to contribute to macropinosome formation and closure [21]. Macropinocytosis may be essential for cell growth. The delivery of extracellular proteins and amino acids to the lysosomes by macropinocytosis has been suggested to activate mTORC1. The nutrient transfer from macropinosomes to the lysosomes is mediated by the activation of Rag GTPases and subsequently mTORC1 recruitment onto the lysosomal membranes where is activated by Rheb. This theory has been supported by in vitro experiments in macrophages and fibroblasts [22].

2.2.2.4.3 Albumin endocytosis in the proximal tubule

Albumin is an anionic single chain protein of approximately 65 kDa that accounts for over 60% of the total plasma protein content. The most important functions of albumin are the maintenance of oncotic pressure and blood volume, antioxidant functions and the transport of fatty acids, bilirubin, calcium, magnesium and vitamins. The amount of albumin filtered in the glomeruli has been determined from micropuncture studies in rats and mice, being estimated in a concentration between 1 and 50 μg/ml [23]. Albumin is reabsorbed in the proximal tubule by the multiligand receptors megalin and cubilin, responsible also for the uptake of a wide variety of plasma proteins.

2.2.2.4.3.1 Megalin

Megalin is a large glycosylated receptor of approximately 600 kDa that belongs to the low-density lipoprotein receptor family and it was originally identified as the antigen in Heymann nephritis, a rat model of membranous glomerulonephritis [24]. Megalin contains a large extracellular domain, a single transmembrane domain and a short carboxy-terminal cytoplasmatic domain. The extracellular domain is composed of four cysteine-rich clusters of low-density lipoprotein receptor type A repeats which represent ligand binding regions. These ligand binding domains are separated by a total of 17 epidermal growth factor (EGF)-type repeats and eight spacer regions containing the amino acids YWTD. The transmembrane domain of megalin is composed of 23 amino acids and is the site of the regulated intramembrane proteolysis mediated by the γ-secretase complex [25]. The cytoplasmatic domain of megalin contains two NPXY motifs, the first binds to the phosphotyrosine-binding domain of the autosomal recessive hypercholesterolemia (ARH) protein and the second motif interacts with the PTB domain of Dab-2. ARH is involved in the trafficking of megalin from the plasma membrane to the endocytic recycling compartments. It has been demonstrated that

ARH directs megalin from the plasma membrane to the early endosomes. Through interaction with subunits of the dynein protein, ARH can facilitate the transport of megalin from the early endosome to the endocytic recycling compartment along microtubules [26]. Dab-2 interacts with the second NPXY motif of megalin and this interaction has been suggested to mediate megalin internalization [27, 28]. Dab-2 interacts with the protein myosin VI which is responsible for trafficking of vesicles through the cortical actin network in the plasma membrane [28]. Conditionally mutant *Dab-2* mice showed reduced clathrin-coated pits and excretion of plasma proteins in the urine that are specific ligands for megalin, indicating reduced transport by megalin in the proximal tubule cells [29].

In proximal tubule cells, megalin is expressed in the brush-border membrane and in apical endocytic compartments [30]. Recent proteomic analysis from proximal tubules of the rat revealed that the S2 segment of the proximal tubule contain the highest concentration of megalin whereas S1 and S3 tubules have lower concentration [31]. Megalin has a broad ligand specificity that accounts for the reabsorption of a vast number of filtered plasma molecules including vitamins such as vitamin-D binding protein and retinol binding protein, carrier proteins such as albumin, myoglobin, lactoferrin. Moreover, megalin has high affinity to hormones and signal proteins such as parathyroid hormone, insulin, thyroglobulin and to enzymes such as plasminogen and cathepsin B [32].

2.2.2.4.3.2 Cubilin

Cubilin is a glycosylated extracellular protein with a molecular weight of 460 kDa and is coexpressed with megalin in the brush-border membrane and in the apical cytoplasmatic compartments of proximal tubule cells. The importance of cubilin for the uptake of proteins was manifested in patients with Imerslund-Grasbeck syndrome (I-GS), a genetic disease caused by cubilin or amnionless (AMN) gene defects. Analysis of urinary protein excretion in I-GS patients, revealed an increase in the excretion of transferrin, apoA-I, vitamin D-binding protein and albumin [33]. Because cubilin lacks both, a transmembrane domain and a cytoplasmatic domain, interacts with other membrane proteins for its localization at the plasma membrane and for endocytosis. The function of cubilin depends on AMN, which colocalizes with cubilin and is important for its trafficking to the apical membrane of the tubule cell [34]. Cubilin also interacts with megalin forming a co-receptor complex that binds to ligands such as vitamin-D protein, albumin, transferrin and high-density lipoprotein. Thus, the two-receptor-ligand complex requires megalin to be internalized and transferred to the lysosomes for degradation [35].

2.2.3 Galectins in intracellular and extracellular vesicle trafficking

The galectin family comprises 15 small molecular weight soluble non glycosylated lectins with a carbohydrate recognition domain. Galectins are synthetized in the cytoplasm and are involved in multiple cellular functions such as cell cycle, cell differentiation and vesicular trafficking. Galectin-3 (GAL-3) been identified in the cytoplasm, in exosomes or microvesicles but also in the extracellular space [36], what suggest it has a biological role via exosomal secretion in intercellular communication. The multiple effects of galectin-3 are mediated through a large number of GAL-3 binding proteins. GAL-3 interacts with the ESCRT component Tsg101, with Bcl-2, CD95 and Alix as well as with a variety of extracellular matrix ligands, such as laminin, fibronectin, mucin and macrophage surface antigens [37]. The increased expression of galectins has been associated with human pathologies such as atherosclerosis, neural degeneration and diabetes [38]. Specially, the expression of GAL-1 and GAL-3 is frequently altered in most cancers [39].

2.2.4 The PI 3-Kinase family

The phosphoinositide-3 kinase (PI3K) family comprises three classes of kinases that are essential for the regulation of cellular processes such as metabolism, cell growth and cell survival and are features in common human pathologies like diabetes or cancer [40]. The class I and II are only present in eukaryotes whereas class III PI3K is conserved from yeast to mammalians. A common characteristic of all the PI3Ks is that they phosphorylate the 3´position hydroxyl of the inositol head group to generate phosphoinositide forms. The Class I PI3Ks are further divided into class IA and class IB which are activated by receptor tyrosine kinases and G-protein-coupled receptors respectively. Notably, AKT is a downstream target of class I PI3K. PtdIns (3,4,5) P3 leads to the membrane recruitment of AKT to regulate cell growth, proliferation, survival and metabolism [41]. Class II PI3Ks have been less studied than class I PI3Ks and its role has been attributed to cell processes such as migration, glucose transport, endocytosis and exocytosis [42]. For many years, it was understood that the main production of PtdIns3P was generated by the class III PI3Ks, but new evidence has shown that in basal conditions, class II PI3Ks are also involved in this process [43]. Increased lines of evidence have centred the role of class II PI3Ks in cell migration showing that lysophosphatidic acid (LPA) can activate class II PI3K to produce a pool of the lipid second messenger PtdIns-3-P to regulate signalling pathways leading to cell migration [3]. The class III PI3K is solely represented by VPS34. The lipid kinase VPS34 is conserved from yeast to human and through

association with cellular multiprotein complexes and by production of PI(3)P regulates endosomal sorting, macropinocytosis and phagocytosis [44].

2.2.4.1 The class III PI 3-Kinase VPS34

VPS34 is an enzyme that represents class III phosphatidylinositol 3-kinases, which are involved in cell signaling and membrane trafficking. The most important function of VPS34 until now is the regulation of endocytosis and the process of autophagy. VPS34 is evolutionary conserved and it was first identified in *Saccharomyces cerevisiae* [45]. In yeast and mammalian cells, VPS34 forms two complexes which separately regulate vacuolar protein sorting and autophagy. Complex I is involved in autophagy, while complex II regulates endosomal fusion, sorting and trafficking from endosomes to lysosomes [46, 47].

2.2.4.1.1 The VPS34 core complexes

In Yeast, complex I is required for autophagy, a process that is initiated after nutrient deprivation and consists in a core component formed by Vps34-Vps15-Vps30 together with Atg14 and the homodimer Atg38. Complex II is required for vacuolar protein sorting and comprises to the core component Vps34-Vps30-Vps15 the protein Vps38 [48]. In a similar manner to yeast, the mammalian complex I of Vps34 regulates the early stages of autophagy to provide enough amount of nutrients and amino acids in a metabolic stress situation. The mammalian Vps34 complex II contains Vps34, Vps15, Beclin1 and UVRAG and is involved in endocytosis, pinocytosis and internalization of cell surface receptors [49].

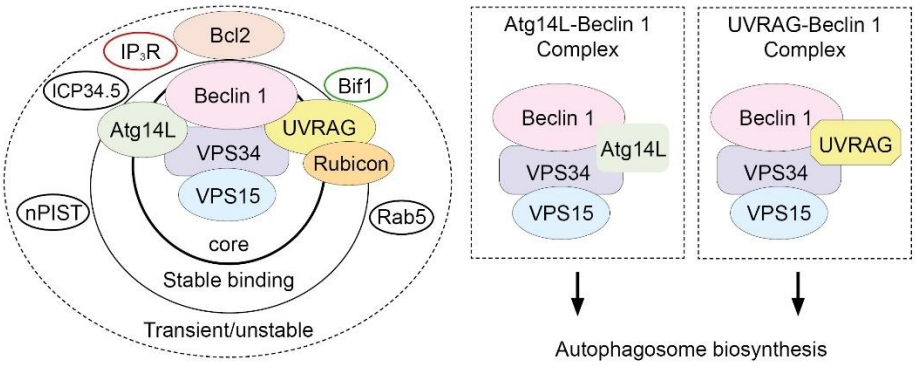

Fig. 2.2. Multiple Beclin 1-VPS34 complexes in yeast and mammals. *Illustration of Beclin 1 protein complexes shows Atg14L, UVRAG and rubicon as stable binding partners of the complex. Unstable binding partners comprise Bcl-2, Rab5, Bif-1. In yeast two Atg6-Vps34 complexes I and II regulate autophagy and vacular protein sorting. In mammals, multiple Beclin 1 complexes act to regulate*

different stages of autophagy and endocytic trafficking. Self-created diagram based on Funderburk et al. 2010 [50].

2.2.4.2 Physiological functions of VPS34

Until now, the best characterized function of VPS34 is the phosphorylation of phosphoinositol lipid targets but the role of VPS34 in the cytosolic structure organization, substrate specificity and in pathophysiological conditions is not completely understood. VPS34 regulates different cell processes such as endocytic sorting, glucose and lipid metabolism, autophagy, cell growth and differentiation. The activity of VPS34 in the cell depends on several parameters and conditions, for instance membrane electrostatics, curvature and membrane lipid composition [51].

2.2.4.2.1 Regulation of glucose metabolism

VPS34 influences a variety of cellular functions and is implicated in signal transduction pathways of a variety of peptide hormones such as angiotensin II and insulin. VPS34 activation is an important step in insulin-mediated control of cell metabolism. Insulin is synthetised and released by beta cells in pancreas and exerts its effects by binding the transmembrane insulin receptor. The activated insulin receptor (IR) binds and phosphorylates adaptor proteins of the insulin receptor substrates family leading to stimulation of PI3K activity. A direct action of IR on the UVRAG-containing class III PI3K complex (VPS34 complex II) leading to its activation, has been shown to represent negative feedback on hepatic insulin signalling [52]. In hepatocytes and muscle cells, the inhibition of VPS34 alters energy metabolism by activating AMPK signalling pathway. In the liver, Vps34 inactivation limits substrate availability for mitochondrial respiration and reduces hepatic glucose production whereas in muscle cells, inactivation of Vps34 increases glucose uptake by switching oxidative phosphorylation towards glycolysis [53].

2.2.4.2.2 Regulation of vesicle trafficking

Endocytosis is a process that allows cells the acquisition of nutrients and proteins and modulation of the composition of the plasma membrane. Pinocytosis, is a particular way of endocytosis responsible for the uptake of fluid and solutes and intracellular trafficking and comprises four different mechanisms: macropinocytosis, clathrin-mediated endocytosis (CME), caveolae-mediated endocytosis and clathrin-and caveolae-independent endocytosis.

VPS34 has been recently shown to be an essential player in pinocytosis with a predominant role in apical vesicular trafficking [54]. The first evidence of the involvement of VPS34 in

endocytic trafficking was observed in *in vitro* assays, where the recruitment of EEA1 to the endosome was dependent on the presence of Rab5 and PI(3)P [55]. This is a key step in the endocytic process as EEA1 is an early endosomal Rab5 effector protein that is important for the docking of endocytic vesicles before fusion with early endosomes. The role of VPS34 in the endocytic pathway was understood with the use of inhibitory antibodies. Blocking the activity of VPS34 resulted in inhibition of the recruitment of EEA1 to early endosomes. Inhibition of VPS34 also relented the internalization and recycling of certain membrane receptors and suppressed the formation of vesicles in multivesicular bodies [56, 57].

The cargo sorting into intraluminal vesicles is mediated by the ESCRT complex. ESCRT is another effector protein that belongs to the endocytosis machinery and was identified years later. ESCRT binds to the endosomal membrane and enables the sorting of endosomes into multivesicular bodies. The maturation of endosomes depends on Rab5-Rab7 conversion, which is the specific step of early endosome to late endosome transition. Interestingly, the displacement of Rab5 by Rab7 and the cargo sorting by the ESCRT complex are processes that are dependent on PI(3)P [58, 59]. As mentioned in the previous section, PI(3)P is of vital importance for the endosome regulation. At the endosomal membrane, PI(3)P interacts with FYVE (Fab1, YOTB, Vac1 and EEA1) and PX (Phox homology) domain-containing proteins like EEA1, Rab5 and Rab4 [60]. The production of PI(3)P by VPS34 is limited to the location of its different complexes. While complex I produces PI(3)P at the phagophores promoting the formation of the autophagosomes, complex II produces PI(3)P on endosomal membranes facilitating endosomal sorting [61]. *In vitro* experiments have shown that the transition from early endosomes to late endosomes is a process that is dependent on Rab GTPases [62]. Rab GTPases cooperate with VPS34 to regulate endosome trafficking. The Rab5 GTPase which is fundamental for early endosome maturation, has been identified as an interactor protein of VPS34 and VPS15 [63]. Rab7 also interacts with the p150 subunit of the mammalian VPS34 complex in late endosomes, showing that the recruitment of FYVE-domain proteins and the synthesis of PI(3)P are correlated [64]. Recent findings have shown that also Rab5a recruits and activates VPS34 complex II on endosomal membranes [65].

2.2.4.2.3 Regulation of autophagy

Autophagy is the process of degradation of cellular structures in the lysosomes after being engrossed in vesicles. There are several forms of autophagy: macroautophagy, microautophagy and chaperone-mediated autophagy (CMA). Microautophagy consists in the direct engulfment of cytoplasmic cargo by autophagic tubes by mediating invagination and

vesicle formation and scission [66]. CMA is the degradation of tagged proteins with a specific motive that binds to the HSC70 chaperon complex facilitating internalization in the lysosomes [67]. Macroautophagy is a physiological response to nutrient and growth deprivation, ER stress and hypoxia and is characterized by intracellular degradation of cytosolic content by the formation of double walled vesicles called autophagosomes.

VPS34 complex I is involved in the early stages of autophagosome formation. The mechanism of VPS34 regulation during the induction of autophagy was provided by a series of studies that demonstrated that autophagosome initiation required the formation of PI3P by a VPS34-Beclin-1 complex and the recruitment of key proteins with PI3P-binding domains [68, 69]. The VPS34 complex I specific activity in the autophagy process, involves the participation of three kinases: mTORC1, AMPK and ULK1 and it has been shown that all these three kinases interact with VPS34 (MUNSON 2015) [70]. Upon nutrient deprivation, AMPK can regulate autophagy by phosphorylating Raptor, a member of the mTORC1 complex and ULK1. Once activated, ULK1 translocates from the cytoplasm to the omegasome, which is a subdomain of the ER and the initial step in the formation of the autophagosome. At the omegasome, ULK1 can recruit and phosphorylate members of the VPS34 complex I such as ATG14L and Beclin1. ATG14L is the mammalian homologue of yeast ATG14 and has been recently shown that ULK1 O-GlcNAcylation is crucial for binding and phosphorylation of ATG14L at S29 [71].

2.2.4.2.4 Regulation of the retromer complex function

The retrograde membrane trafficking between endosomes and *trans*-Golgi network (TGN) is essential to transfer newly synthetized proteins to the endosomes and to the plasma membrane [72]. One of the most studies protein complexes that play an important role in this process is the retromer complex which recognizes specific membrane proteins, known as cargo, that are concentrated at the endosomal membrane. The classical retromer complex consists of a membrane-bound coat formed by the sorting nexins SNX1-SNX2 and SNX5-SNX6 which are referred as SNX-BAR sorting nexins and a cargo-selective sub-complex formed by VPS26, VPS29 and VPS35 [73]. However, the VPS26-VPS29-VPS35 evolutionarily conserved retromer complex can form alternative sorting complexes with different SNX members. For example, SNX3 associates with the sub-complex through direct binding to VPS35 but independently of the SNX-BAR proteins. The SNX3-retromer complex is involved in the retrograde transport of cargo receptors such as the Wnt sorting receptor Wntless [74].

One of the theories how the retromer complex is recruited to the endosome membranes is by binding of two of its subunits to PI(3)P [75]. In mammalian cells, other proteins that might

contribute to the recruitment of the Vps sub-complex to the endosomal membrane are Rab5 and Rab7 GTP-ases [76]. The retromer also interacts with a number of adapter proteins to facilitate the transport of receptors in polarized epithelial cells, like for example the immunoglobulin receptor [77]. Studies in *Saccharomyces cerevisiae*, have demonstrated that Vps34 regulates the function of the retromer complex through its subunits Vps5p and Vps17p to guarantee an efficient endosome to Golgi retrograde transport [78]. In C. elegans, it has been demonstrated that BEC-1, the mammalian ortholog of Atg6/Vps30/Beclin-1, was required for retrograde transport of proteins [79]. Although many studies of the retromer complex are centered in the transport of acid hydrolases [80] new investigations have uncovered a role of the retromer complex in multiple physiological processes. The retromer complex has a role in the trafficking and metabolism of proteins related to the Alzheimer´s Disease such as amyloid-beta peptides. In this context, a retromer deficiency facilitates the accumulation of toxic amyloid-beta oligomers in endosomal compartments of neurons leading to abnormal endosomal enlargement and subsequently cell death [81].

2.2.4.2.5 VPS34 and mTOR Complex I signaling

The mammalian target of rapamycin (mTOR) is a serine/threonine kinase that belongs to the family of the phosphoinositide 3-kinase (PI3-K)-related kinase family and regulates cell growth, metabolism, survival and cell proliferation [82]. mTOR consist of two complexes mTOR complex I (mTORC1) and mTOR complex II (mTORC2) [83]. mTORC1 consist of five components: mTOR, regulatory associated protein of mTOR (RAPTOR), mammalian lethal with Sec13 protein 8 (mLST8), proline-rich AKT substrate 40 kD (PRAS40) and DEP domain-containing mTOR-interacting protein (DEPTOR) [84]. mTORC2 consist of mTOR, mLST8, Deptor, rapamycin-insensitive companion of mTOR (RICTOR), mammalian stress-activated protein kinase-interacting protein 1 (mSIN1) and protein associated with rictor 1 or 2 (PROTOR1/2) [85]. Until now, there are no studies that show that VPS34 directly regulates mTOR kinase activity. Though, it has been suggested that VPS34 contributes to mTOR regulation. At the plasma membrane, VPS34 regulate mTOR/S6K1 by creating a complex with TSC1 that downregulates TSC2 and activates RheB. Besides its role in endocytosis and autophagy, VPS34 has been implicated in regulating nutrient signaling. In this context, it has been demonstrated that VPS34 mediates nutrient signaling to mTORC1 resulting in activation of S6K1 [86]. A role of VPS34 in cell growth and cellular transformation has also been reported in the context of oncogenic transformation. New mechanisms have been unveiled in which

VPS34 mediates RheB and mTORC1 activation via TSC2 downregulation leading to an increase in cell size [87].

However, mTOR is regulated by VPS34 in multiple pathways like for example Ca2+/Calmodulin (CaM) which binds to VPS34 and increases mTORC1 signaling and Phospholipase D1 (PLD1) which is activated by the VPS34 product PI(3)P, leading to its translocation to the lysosomes [88, 89]. The interaction of VPS34 and mTORC1 at the lysosomes is controversial. While VPS34 and PI(3)P play a concomitant role on lysosomal function, mTOR activity has been shown to regulate lysosomal tubulation. One study has discovered two mTOR specific phosphorylation sites in VPS34 complex II-member UVRAG, which are important for VPS34 activation and scission of lysosomal tubulation [90]. Another proposal for mTORC1 activation by VPS34, links the activation of mTORC1 to its positioning in the lysosomes. In the presence of nutrients, it comes through binding of PI(3)P to FYCO1, to a translocation of lysosomes along microtubules towards the plasma membrane, where mTORC1 activity is enhanced [91]. Given that VPS34 stimulates autophagy and also activates mTOR which inhibits autophagy, the existence of an interplay between VPS34 and mTOR might respond to the need of a switch into the cellular network, regulated by different complexes and in different cellular compartments.

2.2.5 Pharmacological inhibition of VPS34

Most of the initial studies to uncover the functions of VPS34 were done using Wortmannin and LY294002. Wortmannin is a fungal metabolite that had been shown to act as a selective inhibitor of phosphoinositide 3-kinase [92]. Thus, the Wortmannin and LY294002 concentrations that were needed to inhibit the activity of VPS34, also suppressed class I PI3K, mTOR and many other protein and lipid kinases compromising the understanding of VPS34 signaling caused by redundancies with other signaling pathways.

IN1 was the first highly selective cell permeable VPS34 Inhibitor to be reported. Evidence of the selectivity of IN1 to VPS34 was provided by profiling VPS34-IN1 against 340 different kinases including members of the class II PI3K. Verification of suppression of the activity of VPS34 was confirmed by the observation of a reduced pool of PtdIns(3)P and reduced activity and phosphorylation of SGK3 [93]. SAR405 is one of the first used selective inhibitors of VPS34. The effectivity of SAR405 was confirmed as VPS34 inhibition affected vesicle trafficking between late endosomes to lysosomes as well as impaired autophagy and lysosomal function [94].

2.2.6 SARS-CoV-2 infection of epithelial cells

SARS-CoV-2 is a positive-sense single-stranded RNA virus that belongs to the family of *Coronaviridae*. SARS-CoV-2 is responsible for the COVID-19 pandemia, which has caused more than 510 million infections worldwide and over 6 million deaths (WHO-2022). SARS-CoV-2 is able to enter the cell through the angiotensin converting enzyme receptor 2 (ACE2) and the transmembrane protease TMPRSS2 [95]. The infection of the airway tract by SARS-CoV-2 has been the cause of flu-like symptoms that occasionally have progressed to pneumonia, acute respiratory distress syndrome (ARDS) and death [96]. TMPRSS2 is an alveolar protease that colocalizes in the lungs on cell surfaces with ACE2 and activates and enhances the virus entry in the cell [97]. ACE2 receptors are also expressed by epithelial cells and are present in several organs like heart, kidney and intestine. In particular mRNA expression levels of ACE2 are high in proximal tubule cells whereas TMPRSS2 mRNA levels are highly expressed in distal tubular cells and less in the proximal tubule cells [98, 99].

Recent studies have discovered that, after the coronavirus entry in the cell has taken place through binding to the ACE2 receptor at the plasma membrane, the internalization and fusion with endosomes and lysosomes causes viral RNA to be released into the cytoplasm for replication [100]. Implications of SARS-CoV-2 have been observed not only in the activation of the ULK-1-Atg14 and VPS34-VPS15-Beclin1 complex but in the regulation of autophagy. Recent studies have also confirmed the participation of SARS-CoV-2 in the signaling that induces autophagosome formation [101].

2.2.7 Aim of the study

Signal transduction mechanisms are crucial for cellular processes such as development, cell growth, differentiation and apoptosis and provide the coordination required for the functionality of multicellular organisms. Phosphoinositide 3-kinases are responsible for the phosphorylation of the D3 position of phosphoinositides which are acidic phospholipids that regulate membrane identity and vesicular trafficking. PI3K are divided into three classes depending on their activity and substrate specificity. Class I PI3K represents so far, the most characterized type whereas roles for classes II and III PI3K have been initially discovered in vesicular trafficking. The class III PI3K VPS34 (vacuolar protein sorting 34) plays important roles in endocytic trafficking, autophagy and nutrient sensing.

The aim of this study was to develop a comprehensive molecular landscape of the functions of VPS34 in the kidney proximal tubule cells *in vivo*. To analyze the effects of Vps34 deletion

on the proximal tubule function, a novel adult mouse model with a doxycycline inducible *Pax8* promotor driven tubular deletion of Vps34 was generated. For the molecular characterization of VPS34, focus was set in intracellular compartments as well as extracellular compartments (urine) analysis from Vps34 deficient mice compared to wildtype mice. Kidney proximal tubular cells mediate efficient reabsorption of water, solutes and proteins from the ultrafiltrate. To directly link proximal tubule receptor-mediated endocytosis with the PI3-kinase VPS34, micropinocytosis was analyzed through uptake of fluorescent labeled lactoglobulin. Apical markers of the endocytosis process were localized using specific antibodies and visualized with high-resolution microscopy. VPS34 dependent functions, were further analyzed with proteomic analysis and phosphoproteomic analysis to unveil distinct phosphorylation processes in cell organelles and compartments of Vps34 deficient mice. SARS-CoV-2 was responsible for the biggest pandemic of this century with severe consequences for human health and global economy. Coronaviruses interact with the host cell membrane and with the membrane machinery at different stages of their life cycle. In this study, we aim to determine the susceptibility of SARS-CoV-2 to inhibitors of the VPS34 kinase activity *in vitro*.

2.3 Results

2.3.1 Vps34 deletion alters proximal tubule cell function

The novel adult mouse model used in this thesis to analyze the effects of VPS34 in the kidney proximal tubule cells, was generated with a doxycycline inducible Pax8 promotor driven tubular deletion of Vps34 (Vps34fl/fl*Pax8rtTA*TetOCre) formally termed as Vps34 $^{\Delta PT}$. As a result of an incomplete recombination in some proximal tubule cells that are Pax8 positive, a mosaic expression pattern was observed along this segment of the nephron. The result is that some proximal tubule cells show features of wild type cells, having an apical membrane expression of VPS34 while other cells lack expression of VPS34.

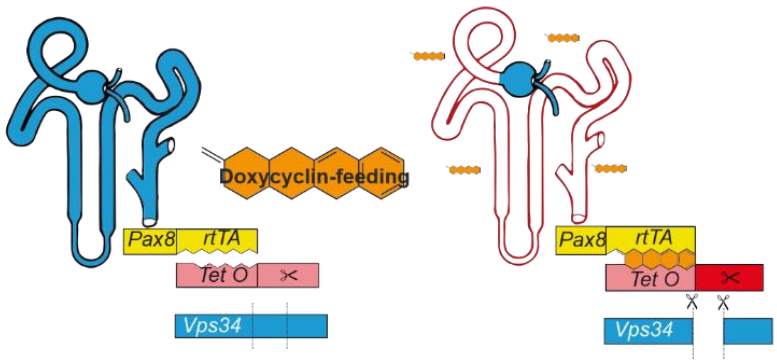

Fig. 2.3. Graphic representation of generation of the mouse models control and Vps34 $^{\Delta PT}$. *Schematic representation of control mice showing full expression of Vps34 along the nephron. After docycycline treatment, Vps34 deficient mice, show no expression of Vps34 in some cells of the tubule system.*

The knockout grade of Vps34 deficient mice was first determined by micropinocytosis through injection of fluorescent labeled lactoglobulin 5 minutes prior to perfusion. Lactoglobulin is filtered through the kidney and taken up by proximal tubule cells through receptor-mediated endocytosis (micropinocytosis). Inhibition of lactoglobulin uptake was observed in some proximal tubule cells of kidneys of Vps34 $^{\Delta PT}$ mice (Figure 2.4; right) compared to control mice (Figure 2.4; left).

This mosaic expression pattern was verified also by immunohistochemistry for VPS34. Examination of mosaic tubular cells revealed that VPS34 is localized to the apical membrane of proximal tubule cells, which showed uptake of lactoglobulin (Figure 2.5; left). On the contrary, Vps34 $^{\Delta PT}$ cells were characterized by lack of lactoglobulin and showed no presence of VPS34 on their apical side (Figure 2.5; right).

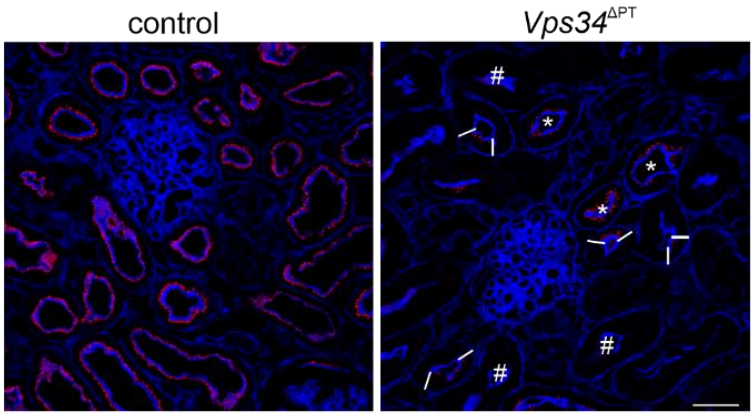

Fig. 2.4. Micropinocytosis as assessed by Alexa Fluor 555-labeled lactoglobulin uptake. *Representative confocal image of the cortex of the kidney of control mice, shows uniform Alexa Fluor 555-labeled lactoglobulin uptake in proximal tubules (red). In Vps34 $^{\Delta PT}$ mice, wild-type cells are marked by an asterisk and Vps34 $^{\Delta PT}$ cells are indicated by a hash. Alexa Fluor®647-Phalloidin was used as a marker for proximal tubules (blue). Images are representative of five mice per group. Scale bar: 50 µm.*

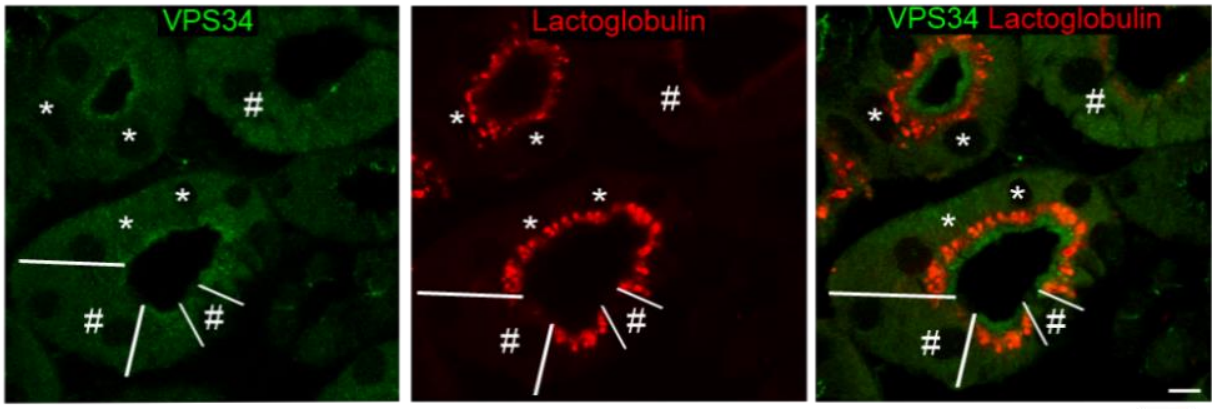

Fig. 2.5. Representative confocal images of the cortex of Vps34 deficient mice. *VPS34 (green) is located at the apical membrane of the proximal tubule cells. Wild-type cells are marked by an asterisk and Vps34 $^{\Delta PT}$ cells are marked by a hash. White stripes show borders of wild-type cells with Vps34 $^{\Delta PT}$ cells. Lactoglobulin signal (red) can be observed in proximal tubule cells marked with an asterisk representing wild-type cells. Vps34 deficient cells, represented by a hash, show no uptake of lactoglobulin and also show no signal of VPS34 (green) compared to wild-type cells. Scale bar: 10 µm.*

2.3.2 Disruption of endosomal markers in Vps34 $^{\Delta PT}$ mice

According to the results of proteomic data, the protein expression of markers of the endocytic uptake machinery in Vps34 $^{\Delta PT}$ was analyzed by western blot and immunofluorescence. Megalin is a transmembrane protein highly expressed in the apical membrane of the proximal tubule and inolved in clathrin mediated endocytosis. The expression of megalin in the proximal tubule is concentrated mainly in coated pits and also in the microvilli of segment 1 and 2.

Figure 2.6; A shows the expression of the megalin receptor in wild-type cells of the segment 1 located in a subapical layer under the brush border membrane of the cell. In Vps34 $^{\Delta PT}$ cells, the expression of the megalin receptor loses its systematic appearance and shows up redistributed and mislocalized into deep cytoplasm.

Clathrin is a protein that is involved in the formation of the clathrin-coated vesicles and plays a role in the receptor mediated endocytosis. Clathrin is located in the plasma membrane and in intracelular vesicles. In wild-type cells of Vps34 $^{\Delta PT}$ mice , the expression of clathrin is visible at the apical side of the proximal tubule cell under the brush border membrane. In Vps34 deficient cells, a disruption of clathrin can be observed at the apical compartments (Figure 2.6; B).

EEA1 is a protein located at the membrane of early endosomes. In the proximal tubule, the expression of EEA1 is localized in subapical compartments. The expression of EEA1 in wild-type cells of Vps34 $^{\Delta PT}$ mice can be observed in figure 2.6; C in subapical compartments. In contrast, in Vps34 deficient cells, which are marked by a hash and bordered by white lines, there is a down-regulation of EEA1 in the subapical membrane (Figure 2.6;C).

Because RAB11 is a marker for the recycling pathway of receptors and transporters, the expression of RAB11 was also analyzed to elucidate the effect of Vps34 deficiency on the endocytotic and recycling pathway. RAB11 expression is localized at the apical compartment of the proximal tubule cell. In wild-type cells of Vps34 $^{\Delta PT}$ mice, RAB11 signal appears as dense punctate under the brush border membrane.

In Vps34 deficient cells, RAB11 expression is strongly reduced (Figure 2.6; D). As late endosomes belong to the endocytic machinery, LAMP-2 immunolabeling was analyzed next. LAMP-2 expression is located at the membrane of lysosomes and late endosomes in subcellular compartments. In wild-type cells, the expression of LAMP-2 is observed in cluster in late endosomes and lysosomes. In Vps34 deficient cells, LAMP-2 signal appears mislocated and extends until the basal cytoplasm (Figure 2.6; E; AG Theilig).

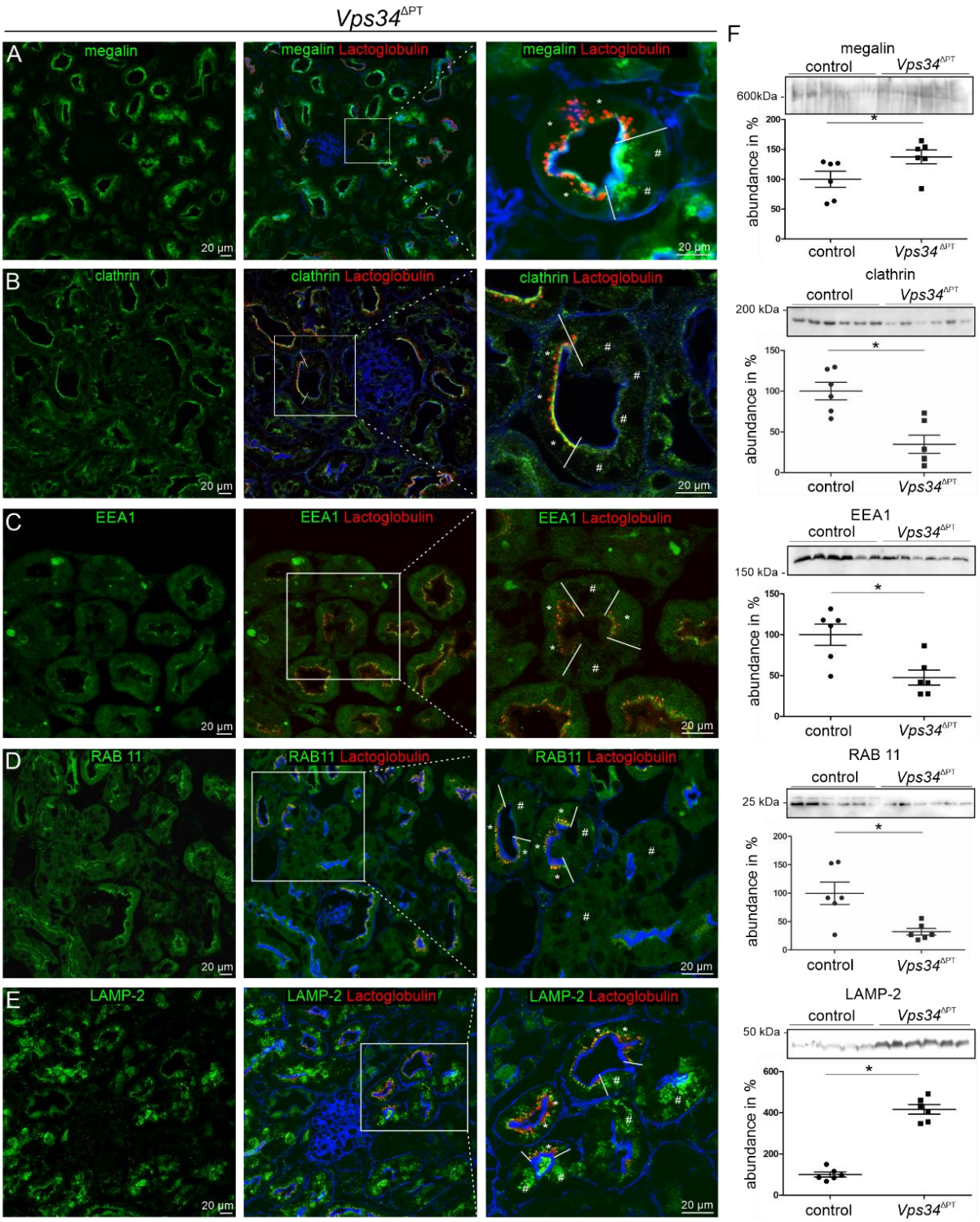

Fig. 2.6. Cellular localization of megalin receptor and proteins involved in endocytosis process in Vps34 $^{\Delta PT}$ mice. *Confocal imaging of kidney sections of Vps34 $^{\Delta PT}$ mice. (A) Megalin as endocytic receptor (green). (B) Clathrin as marker of clathrin vesicles (green). (C) EEA1 as marker of early endosomes (green). (D) RAB11 as marker of recycling endosomes (green). (E) LAMP-2 as membrane marker of lysosomes (green). Lactoglobulin as indicator of mosaicism (red). Mosaicism is indicated by two white lines. Vps34 wild-type proximal tubule cells are indicated by * and by the presence of Alexa Fluor®555-lactoglobulin. Vps34 $^{\Delta PT}$ cells are indicated by #. Alexa Fluor®647-Phalloidin (blue) was used as marker of actin filaments of the brush border membrane for indentification of proximal tubules. (F)*

Effect of Vps34 deletion on megalin, clathrin, EEA1, RAB11 and LAMP-2 protein expression with corresponding analysis of protein abundance (p < 0,05 vs. control, n=6). Mann-Whitney test (AG-Theilig).

2.3.3 Proteomic analysis of Vps34 $^{\Delta PT}$ mice show reduction of membrane transporters and channels and atypical tubular proteinuria

Proteomic analysis of kidney cortex from Vps34 $^{\Delta PT}$ and control mice was performed at a depth of 5800 identified proteins in order to determine pathways altered by conditional deletion of Vps34 in proximal tubule cells. Results showed a reduction in proteins of the endocytic uptake machinery like the scavenger receptor protein cubilin, amnionless, clathrin and EEA1. Proteomic analysis showed increases formation of multivesicular bodies, which was associated with increased abundance of ALIX, a marker for multivesicular bodies that give rise to exosomes. The proteomic dataset highlighted also an increased formation of late endosomes/lysosomes in Vps34 $^{\Delta PT}$ kidney cortex but reduced abundance of V1-adenosine triphosphatase and lysosomal hydrolases, indicating loss of lysosomal function.

Proteomic data revealed also a reduction of proteins of the retromer complex consisting of VPS35-29-26. Interestingly galectin-3 (GAL-3) and galectin-9, two proteins that control trafficking and cell polarization were strongly increased. On the basis of this proteomic mapping of the kidney of Vps34 $^{\Delta PT}$ mice, the urine of Vps34 $^{\Delta PT}$ was compared with the urine of control mice. Low molecular weight proteins and membrane proteins of exosomal or vesicular origin were increased in the urine of Vps34 $^{\Delta PT}$ mice. In order to investigate whether proteins enriched in the urine of Vps34 $^{\Delta PT}$ mice, originated from tubulear epithelial cells, the proteomes from urine and cortical kidney tissue from Vps34 $^{\Delta PT}$ mice were compared. The result showed that lysosomal proteins such as NPC intracellular cholesterol transporter 2 (NPC2); neuraminidase 1 (NEU1), lysosomal alpha-mannosidase (MAN2b), cathepsin Z (CTSZ), cathepsin H (CTSH) and N-acetylgalactosamine-6-sulfatase (GALNS) were increased in the urine of Vps34 $^{\Delta PT}$ mice and decreased in Vps34 $^{\Delta PT}$ kidney cortices.

A **B**

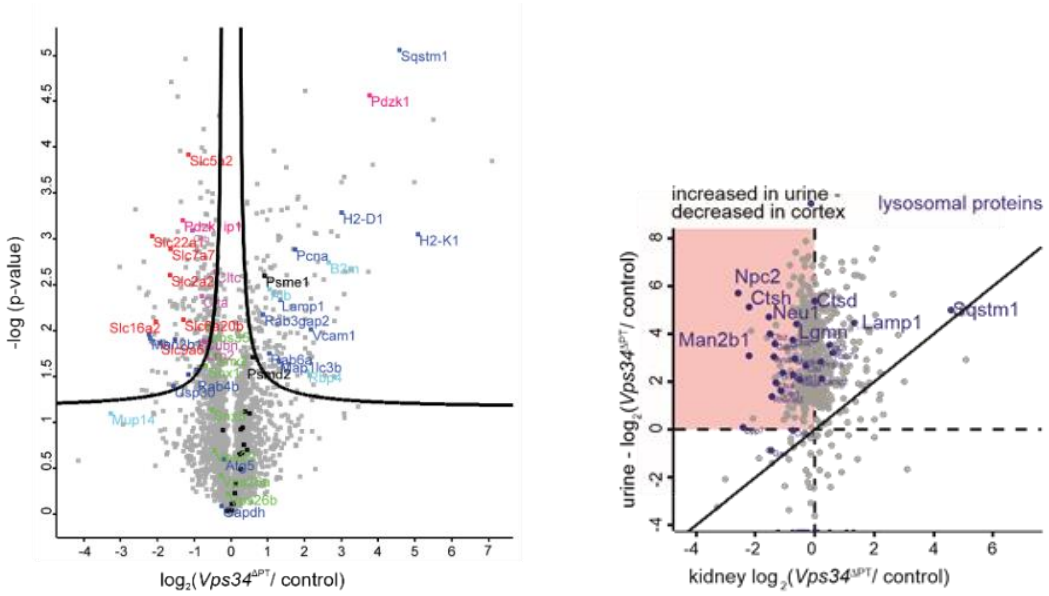

Fig. 2.7. Alterations in protein profile in mice with Vps34 deletion show reduced abundance of membrane transporters and channels and atpypical tubular proteinuria. *A) Volcano plot analysis of protein abundance in kidney cortex from Vps34 $^{\Delta PT}$ and control mice. The log P value of a two-tailed t test is plotted against the log2 ratio of Vps34 $^{\Delta PT}$/control. The proteins beyond the lines indicate significance after correction for multiple testing. Proteins are related to retromer complex (green), endocytic proteins (pink), autophagy (blue), proteasome (black), and others (red). B) Integrated presentation of fold changes between Vps34 $^{\Delta PT}$ mice urine and proteins. Lysosomal proteins are represented in blue. The pink quadrant marks proteins that were increased in urine and decreased in the kidney cortex of Vps34 $^{\Delta PT}$ mice. (AG Theilig).*

2.3.4 Cell surface reduction of sodium glucose cotransporter 2 (SGLT2) and amino acid transporters in Vps34 $^{\Delta PT}$ mice

The uptake of glucose and filtered amino acids from the ultrafiltrate is an important function of proximal tubule cells. Because the proteomic data revealed a decrease in several nutrient transporter and channels in Vps34 $^{\Delta PT}$ mice, the protein expression of SGLT2 and some relevant amino acid transporters in proximal tubule cells were analyzed via immunofluorescence and westen blot in Vps34 $^{\Delta PT}$ mice. SGLT2 is encoded by the gene *Slc5a2* and is expressed along the apical membrane of the S1-S3 segment of the proximal tubule of the kidney. In wild-type cells of Vps34 $^{\Delta PT}$ mice, SGLT2 can be detected in the apical brush border membrane of the early proximal convoluted tubule. In contrast, in Vps34 depleted cells the expression of SLGT2 is strongly down-regulated (Figure 2.8; A). The sodium bicarbonate cotransporter 1 (NBC1) expression in the kidney is located to the basolateral membrane of the proximal tubule cell. Figure 2.8; B shows the protein expression of the amino acid transporter

NBC1 in proximal tubule cells of Vps34 $^{\Delta PT}$ mice. In wild-type cells, NBC1 can be detected at the basolateral membrane of the proximal tubule cell of the S1 segment. In contrast, Vps34 deletion in proximal tubule cells results in a down-regulation of the expression of the basolateral transporter NBC1.

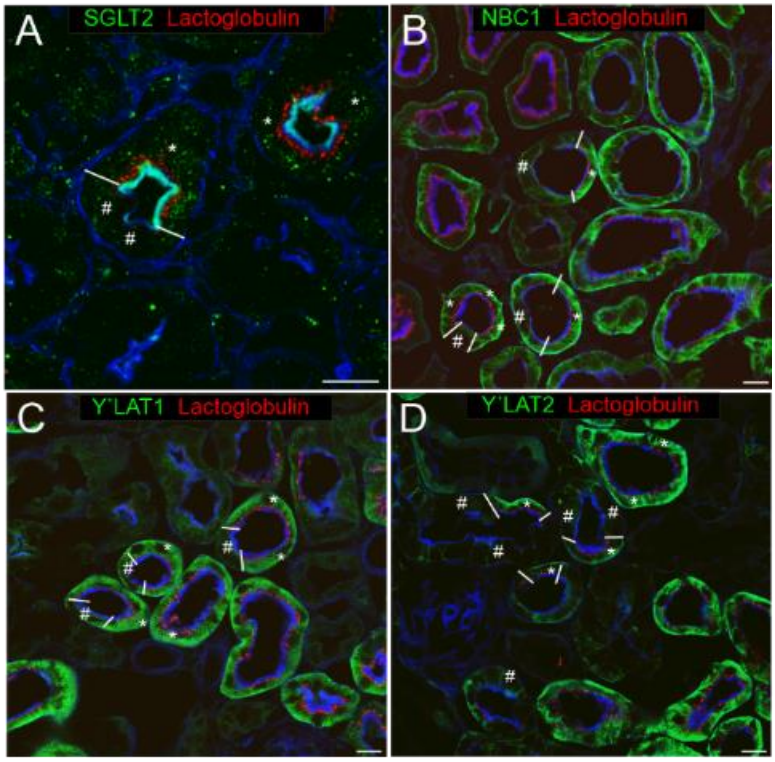

Fig. 2.8. Down-regulation of SGLT2, NBC1 and amino acid transporters in proximal tubule cells of Vps34 $^{\Delta PT}$. Confocal imaging of SGLT2 and amino acid transporters in kidney sections from wild-type and Vps34 $^{\Delta PT}$ mice. Mosaic expression pattern is indicated by two white lines. Wild-type proximal tubule cells are indicated by * and by the presence of Alexa Fluor® 555-lactoglobulin (red). Vps34 $^{\Delta PT}$ proximal tubule cells are indicated by #. (A) SGLT2 (green) colocalizes with brush border membrane at the apical side of the proximal tubule cell stained with Alexa Fluor®647-Phalloidin (blue) and is down-regulated in Vps34 $^{\Delta PT}$. (B-D) NBC1 transporter (green) γ^+LAT1 transporter (green) and γ^+ LAT2 transporter (green) are down-regulated at the basolateral membrane of proximal tubule cells of Vps34 $^{\Delta PT}$ mice. Alexa Fluor®647-Phalloidin was used as marker of brush border membrane for identification of proximal tubules (blue). Scale bar: 20 µm.

γ^+LAT1 encoded by the gene *Slc7a7* is a light subunit composing the heterodimeric transport system for cationic and neutral amino acids and its expression is found along the kidney proximal tubule. Figure 2.8; C shows the protein expression of γ^+LAT1 in proximal tubule cells of Vps34 $^{\Delta PT}$ mice. In wild-type cells, the expression of γ^+LAT1 is located at the basolateral membrane of the proximal tubule cells. On the contrary, in Vps34 deleted cells the expression of γ^+LAT1 at the basolateral side of the cell is strongly down-regulated. γ^+LAT2 encoded by

the gene *Slc7a6* is also a heterodimeric amino acid exchanger expressed along the kidney proximal tubule. Figure 2.8; D shows the expression of γ^+LAT2 in Vps34 $^{\Delta PT}$ mice. In wild-type cells, γ^+LAT2 is also located at the basolateral membrane of the proximal tubule cells. Vps34 deficient cells, show a down-regulation in the protein expression of γ^+LAT2 at the basolateral membrane. The protein expression of SGLT2, NBC1, γ^+LAT1 and γ^+LAT2, B^0AT1 and 4F2hc was analyzed by western blotting to confirm the results of the immunofluorescence assays. Western blot analysis of SGLT2, NBC1, γ^+LAT1 and γ^+LAT2 confirmed the significant decrease in protein expression of SGLT2, NBC1, γ^+LAT1 and γ^+LAT2 in Vps34 $^{\Delta PT}$ mice compared to control animals (Figure 2.9; A). The amino acid transporters B^0AT1 and 4F2hc showed also a significant decrease in protein abundance in Vps34 $^{\Delta PT}$ mice compared to control mice (figure 2.9; A).

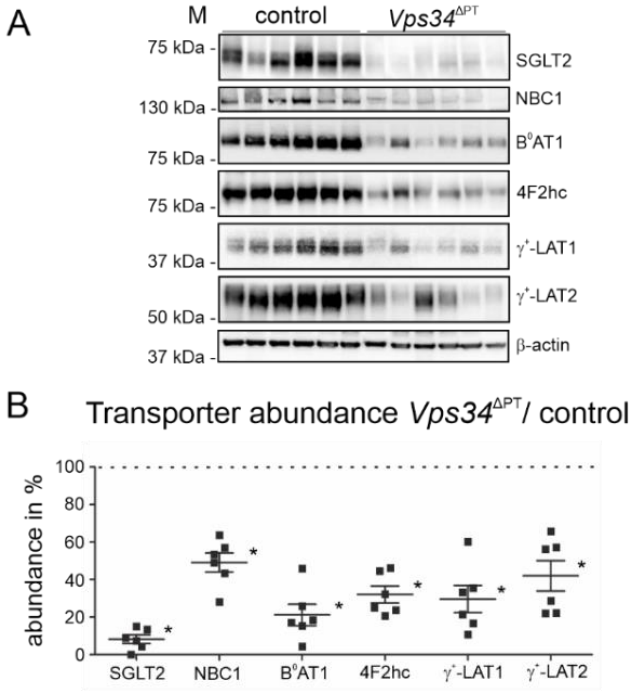

Fig. 2.9. Representative Western blots of SGLT2, NBC1 and amino acid transporters in kidneys of Vps34 $^{\Delta PT}$ mice. *(A) Effect of Vps34 deletion on SGLT2, NBC1 and amino acid transporters B^0AT1, 4F2hc, γ^+LAT1 and γ^+LAT2.* β-actin *served as loading control. (B) Corresponding analysis of protein abundance of SLGT2, NBC1, B^0AT1, 4F2hc, γ^+LAT1 and γ^+LAT2 in Vps34 $^{\Delta PT}$ mice normalized to control mice (p < 0,05 vs. control, n=6). Mann-Whitney test.*

2.3.5 Vps34 deficiency alters epithelial polarity markers

Further investigation of proteomic data revealed also a reduction of membrane proteins related to cell polarity like sodium-potassium ATPase (Na/K-ATPase) and proteins related to the secretory pathway like the retromer complex and the interacting sorting nexings 3, 12 and

27.VPS35 is a component of the retromer protein complex wich plays a role in endosomal protein sorting. The retromer complex is responsible for the recovery of proteins from the endosomes to the golgi apparatus. In figure 2.10; A, the expression of VPS35 in wild-type cells appears ubiquitous in the proximal tubule cell, but strongly concentrated in subapical compartments. In Vps34 deficient cells, a disruption of VPS35 can be observed specially in the subapical zone, where the endocytotic machinery is located, as well as a redistribution of VPS35 throughout the cell. Western blot analysis of VPS35 (Figure 2.11; A) showed a significant decrease in the intensity of the band of VPS35 in Vps34 knockout mice compared to control mice.

In the proximal tubule, the expression of the sodium-potassium ATPase (Na/K-ATPase) is localized at the basolateral membrane. In wild-type cells, the expression of the Na/K-ATPase is visible on the basolateral membrane infolding and invaginations. Vps34 deficient cells showed reduced basolateral infoldings. The Na/K-ATPase was only detected at the cell borders (Figure 2.10; B). Western blot analysis of Na/K-ATPase (Figure 2.11; B) showed a significant decrease in the intensity of the band of Na/K-ATPase in Vps34 $^{\Delta PT}$ mice compared to control mice.

Moreover, proteomic analysis also revealed an increase of proteins that control trafficking and cell polarization like galectin-3 and galecting-9 and proteins involved in the formation of multivesicular bodies like alix. Galectin-3 is mostly localized in the nucleus, cytoplasm, cell surface but also in the extracellular space as a result of secretion mechanisms. Figure 2.10; C shows the expression of galectin-3 in wild-type cells mainly localized outside the cell at the apical and basolateral side. On the contrary, in Vps34 deficient cells, the expression of galectin-3 appears redistributed in cytosol. The effect of galectin-3 in Vps34 knockout mice was examined by Western blot (Figure 2.11; C). The quantification of the intensity of the molecular weight band representing galectin-3 after normalization with control mice, showed a significant increase in the intensity of the band of galectin-3 in Vps34 $^{\Delta PT}$ mice compared to control mice. Alix is mainly localized in multivesicular bodies and is involved in lysosomal trafficking. The effect of alix in Vps34 $^{\Delta PT}$ mice was examined by immunoblotting. The quantification of the intensity of the molecular weight band representing alix after normalization with control mice, showed a significant increase in the intensity of the band of alix in Vps34 $^{\Delta PT}$ mice (Figure 2.11; D).

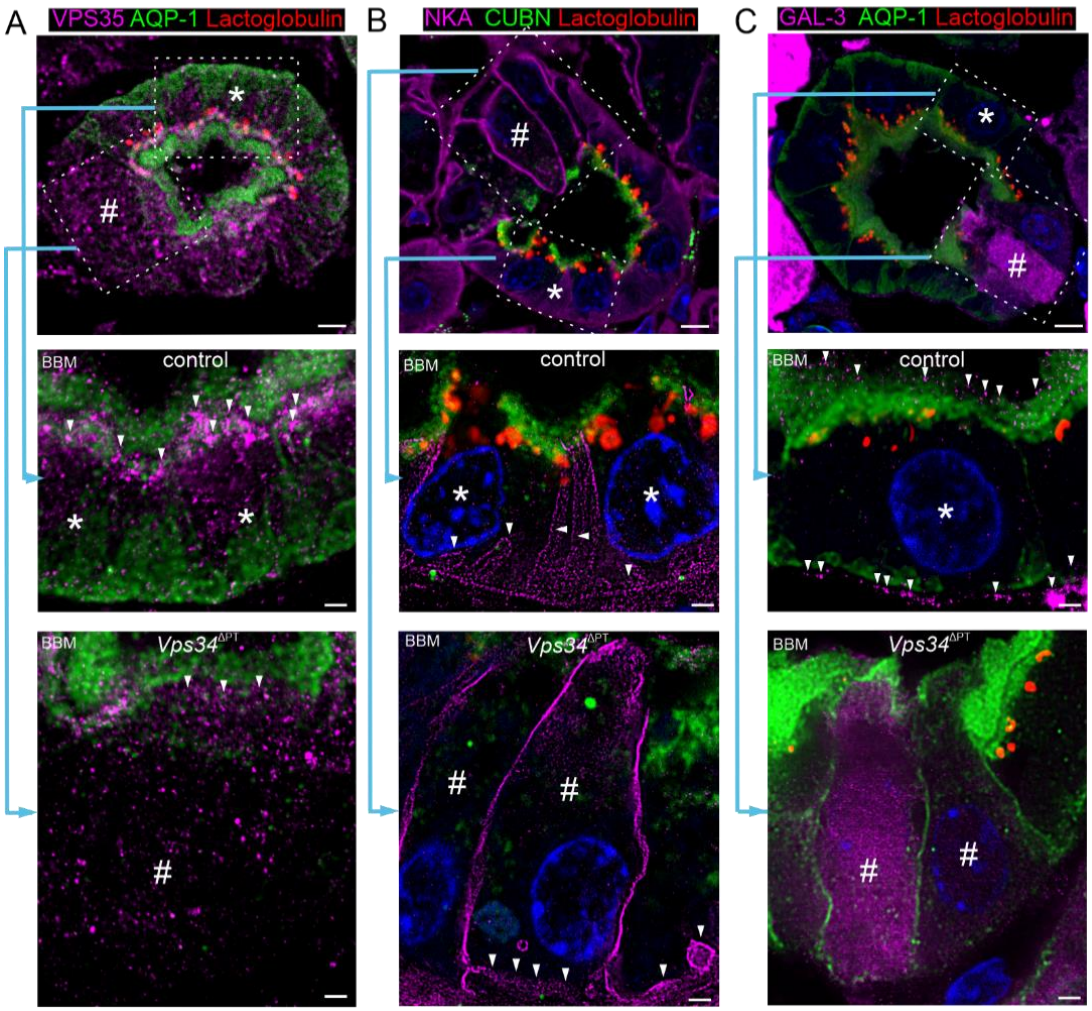

Fig. 2.10. Cellular localization of epithelial polarity markers and proteins of the secretory pathway in Vps34 $^{\Delta PT}$ mice*. (A) VPS35 as marker of retromer complex (magenta). AQP-1 as marker for brush border membrane (green) and lactoglobulin (red). (B) NKA as marker of basal membrane (magenta) and cubillin as marker of brush border membrane (green). (C) GAL-3 as marker of cell trafficking (magenta) and AQP-1 as marker of brush border membrane (green). Cell nuclei stained with DAPI (blue). Vps34 wild-type proximal tubule cells are indicated by * and by the presence of Alexa Fluor®555-lactoglobulin. Vps34 $^{\Delta PT}$ proximal tubule cells are indicated by #. Scale bars: 20 µm (AG-Theilig).*

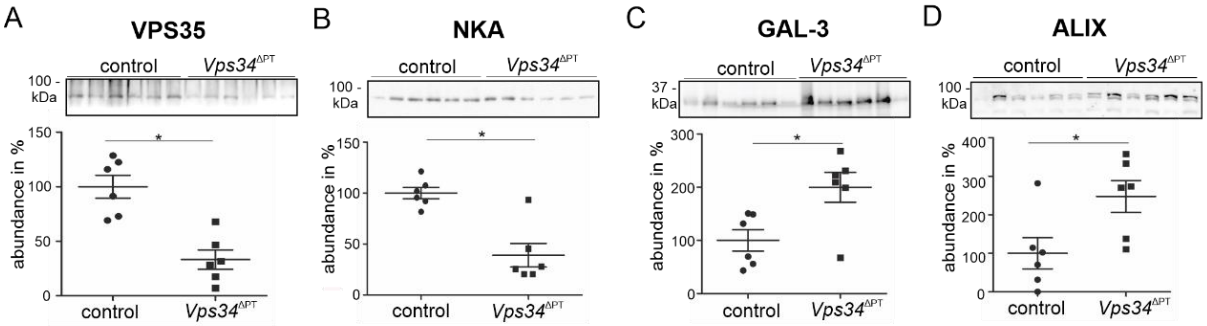

Fig. 2.11. Representative Western blots of epithelial polarity markers in kidneys of Vps34 $^{\Delta PT}$ mice. *(A) Effect of Vps34 deletion on (A) VPS35 (B) NKA, (C) GAL-3 and (D) ALIX with corresponding analysis*

of protein abundance in Vps34 $^{\Delta PT}$ mice normalized to control mice (p < 0,05 vs. control, n=6). Mann-Whitney test.

2.3.6 Vps34 deficiency leads to TUNEL-positive cells in proximal tubule cells

A common characteristic of apoptosis is DNA fragmentation. This special condition allows the differentiation of apoptotic cells from healthy cells and from cells dead by necrosis. TUNEL assay makes possible the identification of TUNEL-positive cells through the incorporation of flurorescein-12-dUTP at 3´-OH DNA ends using the terminal deoxynucleotidyl transferase recombinant enzyme (rTdT). To account if Vps34 knockout has an apoptotic effect on proximal tubule cells, kidney slices of control and Vps34 deficient mice were analyzed using TUNEL assay. Proximal tubule cells of control mice showed no DNA-fragmentation and therefore no staining of TUNEL-positive nuclei. In contrast, in Vps34 deficient mice, a moderate number of TUNEL-positive cells in proximal tubules were observed. The nuclei of this cells was TUNEL positive and showed a green fluorescence staining.

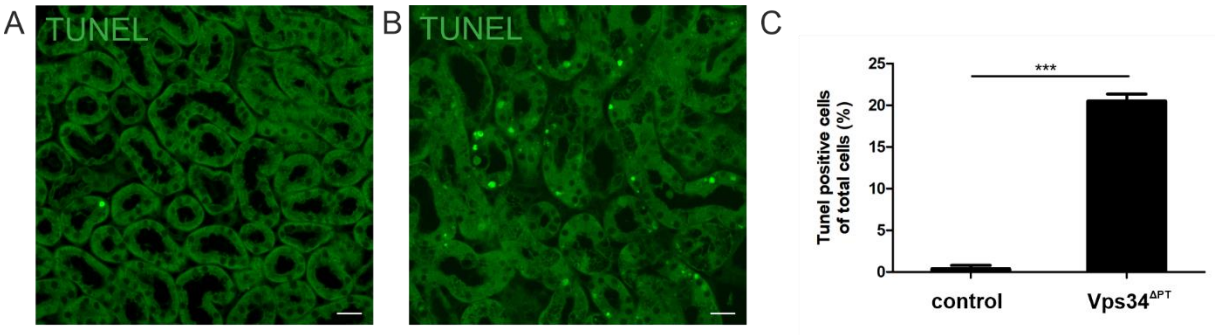

Fig. 2.12. TUNEL staining for apoptosis in Vps34 $^{\Delta PT}$ mice. *(A) Representative image of cortex of wild-type mouse kidney shows no TUNEL-positive apoptotic cells (green). (B) Representative image of cortex of Vps34 deficient mice showing many proximal tubule with TUNEL-positive cells (green). Scale bar: 25 µm. C) TUNEL-positive cells were expressed as percentage of total number of cells. The percentage of TUNEL-positive cells were shown as mean ± SD (n=3). *** p < 0,001 compared to control group; Mann-Whitney test.*

2.3.7 Vps34 deficiency protects against SARS-CoV-2 infection

The endocytic pathway represents for many viruses a way of entering the cell. It has been previously shown in respiratory cells that internalization through receptor-ligand complex is used by SARS-CoV-2 virus for invasion and replication. In this contex is still not clear which role play the Vps34 inhibition in a SARS-CoV-2 infection of the kidney. ACE2 and its co-factor TMPRSS2 are two receptors expressed in the apical side of proximal tubule cells in the kidney. Analysis of protein expression of ACE2 and TMPRSS2 in cortex of kidney of control and Vps34 deficient mice were done by immunofluorescence and Western blot. Figure 2.13; A and B

shows expression of ACE2 and TMPRSS2 respectively in the apical side of proximal tubule cells. In wild-type cells, a strong expression of ACE2 and TMPRSS2 can be observed at the apical side of the proximal tubule cells. In Vps34 deficient cells, there is a strong reduction of the expression of ACE2 and TMPRSS2 receptors at the apical side. ACE2 protein expression was also analyzed by western blotting confirming a significant reduction of ACE2 in Vps34 $^{\Delta PT}$ mice compared to control mice (Figure 2.13; C).

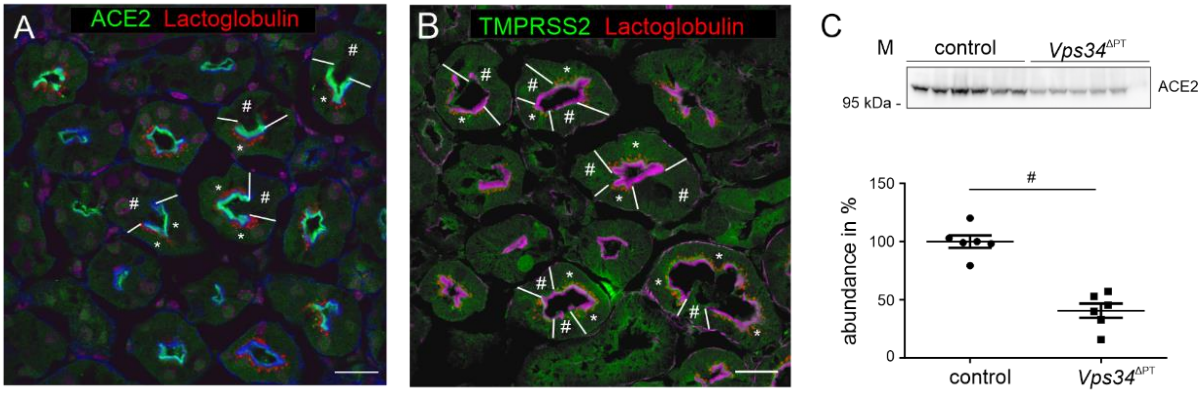

Fig. 2.13. Down-regulation of SARS-CoV2 receptors ACE2 and TMPRSS2 in proximal tubules of Vps34 $^{\Delta PT}$. *(A) ACE2 receptor in proximal tubule cells of Vps34 $^{\Delta PT}$ mice (green). Alexa Fluor®555-lactoglobulin (red) and Alexa Fluor®647-Phalloidin (blue) as marker of brush border membrane for indentification of proximal tubules. (B) TMPRSS2 receptor in proximal tubule cells of Vps34 $^{\Delta PT}$ mice (green). Alexa Fluor®555-lactoglobulin (red) and Alexa Fluor®647-Phalloidin (magenta) as marker of brush border membrane for indentification of proximal tubules. Mosaicism is indicated by two white lines. Vps34 wild-type proximal tubule cells are indicated by an asterisk and by the presence of Alexa Fluor®555-lactoglobulin (red). Vps34 $^{\Delta PT}$ cells are indicated by a hash. Scale bar: 20 µm. (C) Effect of Vps34 deletion on ACE2 protein and corresponding analysis of protein abundance in Vps34 $^{\Delta PT}$ mice normalized to control mice (p < 0,05 vs. control, n=6). Mann-Whitney test.*

2.3.8 Vps34 inhibition reduce SARS-CoV-2 infection in proximal tubule cells *in vitro*

In cooperation with Dr. Markus M. Rinschen from the Department of Medicine, University Medical Center Hamburg-Eppendorf, the effect of Vps34 inhibition after a SARS-CoV-2 infection was analyzed *in vitro*. For that purporse, control OK cells were infected with the Wuhan-like early european SARS-CoV-2 B.1 lineage (FR-4286). OK cells were pretreated with the VPS34 inhibitor SAR405 (1 µM) for one hour and subsequently infected with SARS-CoV-2. 48 hours post infection, the presence of SARS-CoV-2 spike was analyzed in the two groups and could be demonstrated that Vps34 inhibition led to a diminished viral reproduction (Figure 2.14; AG Theilig).

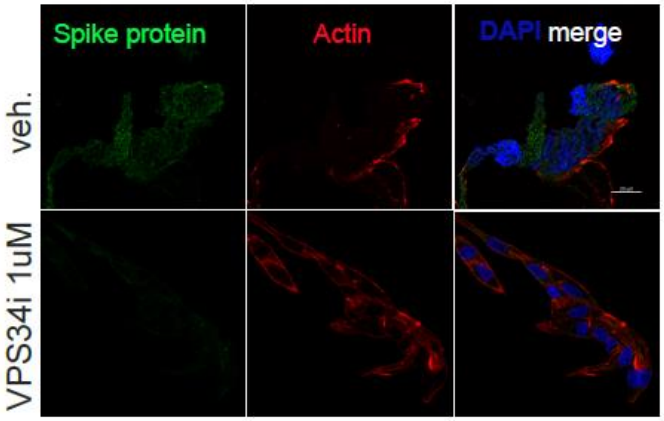

Fig. 2.14. SARS-CoV-2 infection of OK cells. *Representative confocal images of OK cells pretreated for 1h with VPS34 inhibitor SAR405 (1 µM) and infected with SARS-CoV-2. SARS-Cov-2 spike protein (green); Actin (red); DAPI (blue). Scale bar: 50 µm (AG-Theilig).*

2.3.9 VPS34 inhibition reduces albumin uptake in opossum kidney cells

The mechanisms of SARS-CoV-2 entry into the host cell and binding of the spike protein to its receptor ACE2 has been focus of attention in the last years because of the impact of the SAR-CoV-2 infection on the world population. Recent studies have reported two different pathways of SARS-CoV-2 entry into the cell. When the target cell does not express sufficient TMPRSS2 (serine 2 transmembrane protease), the SARS-CoV-2-ACE2 complex enters the cell via clathrin mediated endocytosis. In presence of membrane TMPRSS2, viral RNA is released into the cell after fusion of the virus with the membrane. [100]. In order to show that VPS34 inhibition disrupts the endocytic machinery, endocytosis assay of alexa-555-coupled albumin in Opossum kidney cells were performed. Therefore cells were set to starvation and subsequently were treated either with 4 mM glutamine, 0,5 mM glutamine, 1 µM of VPS34 inhibitor SAR405 or the appropiate vehicle control. Cells were incubated for 15 minutes at 37°C after addition of 1mg/ml alexa-555-coupled albumin and analyzed by confocal microscopy after fixation and antibody staining with Alexa-647 phalloidin and DAPI nuclear stain. Figure 3.12 evidences that after 2 hours of incubation with VPS34 inhibitor SAR405 (1 µm), the internalized amount of labelled albumin was significantly inferior in cells treated with the VPS34 inhibitor SAR405 (1 µm) than in cells treated with 0,5 or 4 mM Glutamine or in the control cells (Figure 2.15; A and B).

A

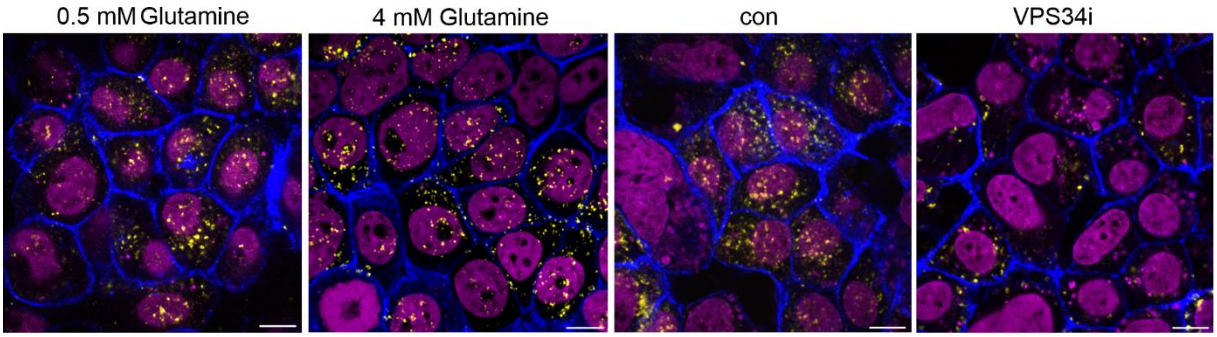

B

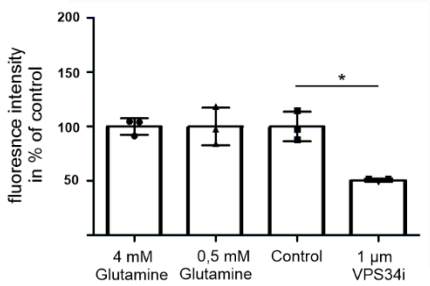

Fig. 2.15. Endocytosis assay of Alexa555-coupled albumin on OK cells after 2h treatment with 0,5 Mm, 4 mM glutamine or 1 µM VPS34 inhibitor SAR405*. A) Representative confocal images of endocytosis assay using Alexa555-coupled albumin on opossum kidney cells treated for 2 hours with 0.5 mM and 4 mM glutamine or VPS34 inhibitor SAR405 at 1 µM concentration. Representative images are shown with endocytosed albumin in yellow, nuclei in magenta and actin filaments at the cells border in blue. Scale bar = 10 µm. B) Quantitative analysis of endocytosis assay of Alexa555-coupled albumin on OK cells after 2h treatment with 0,5 Mm, 4 mM glutamine or 1 µM VPS34 inhibitor SAR405. Data represent means ± SD; *p < 0,05 vs. control, n=3). T-test with Welch´s correction.*

After no significant changes in the internalization of alexa-555 coupled albumin were observed, Opossum kidney cells were treated either with 4 mM glutamine, 0,5 mM glutamine for 24 hours. Cells were incubated for 15 minutes at 37°C after addition of 1 mg/ml alexa-555-coupled albumin and analyzed by confocal microscopy after fixation and antibody staining with Alexa-647 phalloidin and DAPI nuclear stain. Treatment of cells with 0,5 mM for 24 led to a significant reduction in the amount of internalized albumin compared to control (4 mM glutamine) (Figure 2.16; A and B).

A

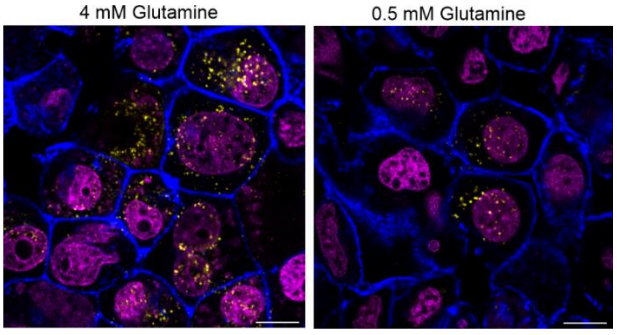

B

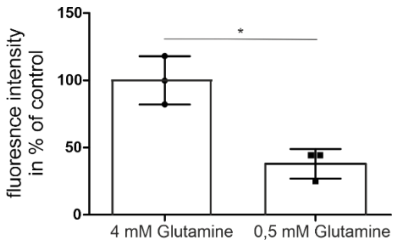

Fig. 2.16. Endocytosis assay of Alexa555-coupled albumin on OK cells after 24h treatment with 0,5 mM or 4 mM glutamine. *A) Representative confocal images of endocytosis assay using Alexa555-*

*coupled albumin on opossum kidney cells treated for 24 hours with 0.5 mM and 4 mM. Representative images are shown with endocytosed albumin in yellow, nuclei in magenta and actin filaments at the cells border in blue. Scale bar = 10 µm. B) Quantitative analysis of endocytosis assay of Alexa555-coupled albumin on OK cells after 24h treatment with 0,5 Mm, 4 mM glutamine. Data represent means ± SD; *p < 0,05 vs. control, n=3). T-test with Welch´s correction.*

2.4 Discussion

VPS34 has been studied for nearly three decades since it was discovered in budding yeast as part of a mechanism regulating the traffic to the vacuoles. The yeast orthologue of hVPS34 was originally discovered in screenings for genes involved in vacuolar protein localization and processing. Studies in both yeast and mammalian cells, have indicated that endosomal trafficking and protein sorting requires derivatives of phosphatidylinositol, in particular phosphatidylinositol-3-phosphate (PI3P). PI3P acts as a second messenger molecule, recruiting proteins that contain either a FYVE zinc finger domain or a PX domain, including phosphatase, kinases and adaptor proteins and is implicated in membrane receptor sorting, intralumenal vesicle formation and autophagy. PI3P is generated by two complexes containing the lipid kinase VPS34: complex I (VPS34/VPS15/Beclin-1/Atg14L) localized at the phagophore promoting autophagosome formation and complex II (VPS34/VPS15/Beclin-1/UVRAG) found at the endosomes and involved in endocytic sorting [50].

VPS34 role as a scaffold protein beyond its lipid kinase activity suggest that is involved in a broader range of cellular functions. This doctoral thesis presents a new molecular landscape of VPS34 regulation in the kidney proximal tubule describing its impact on vesicular trafficking and sorting, cell growth as well as new insights in its metabolic and lipidomic activity. Studies of the activation of VPS34 complex I and II in the last decade have brought new information about regulatory mechanisms that control the class III PI3K kinase activity in cell-cycle progression, stress response, nutrient signaling and human diseases such as cancer and neurodegenerative diseases. The implications of the discovery of new VPS34 functions in other signaling pathways represent a new horizon for the development of specific catalytic VPS34 inhibitors for therapeutical purposes.

2.4.1 Characterization of a VPS34 deficient mouse model

The scope of this study was to test the role of VPS34 in kidney proximal tubule cells by conditional deletion of Vps34 in the proximal tubule. For this purpose, a novel Vps34 deficient adult mouse model was generated with a doxycycline inducible Pax8 promotor driven tubular deletion of Vps34 (Vps34fl/fl*Pax8rtTA*TetOCre) formally termed as Vps34 $^{\Delta PT}$. The

mosaicism that was observed in proximal tubule cells upon Pax8-Cre driven recombination was due to differential Cre activity in the tubular cells. A remnant mosaic pattern in the kidney has been previously observed in inducible mouse lines targeting the proximal tubule [99]. Mosaicism was also evident in a study of Vps34 KO mice with conditional target excision of Vps34 exon 21 (Pax8-Vps34 $^{\Delta/\Delta}$) in the proximal tubules [52]. In our mouse model, the conditional knockout of Vps34 was confirmed through analysis of protein expression of VPS34 in the proximal tubule cells by confocal immunofluorescence. Examination of the expression of VPS34 in proximal tubule cells, revealed that VPS34 was localized at the apical membrane of few proximal tubule cells, considered wild type cells because Vps34 was not depleted. On the contrary, Vps34 depleted cells, showed no expression of VPS34 at the apical membrane. The knockout efficiency was also calculated and resulted in approximately 85% ± 15 % deletion of VPS34 in Vps34 $^{\Delta PT}$ mice (data not shown).

2.4.2 Micropinocytosis is impaired in Vps34 $^{\Delta PT}$ mice

Receptor-mediated endocytosis (micropinocytosis) in proximal tubule cells, is a highly specialized process for uptake of filtered proteins and small bioactive molecules from the glomerular ultrafiltrate to maintain a protein-free urine. To study the effects of Vps34 deletion on proximal tubule cell function, micropinocytosis was analyzed in Vps34 $^{\Delta PT}$ mice and control mice. Red labeled lactoglobulin had been injected 5 minutes prior perfusion-fixation of Vps34 $^{\Delta PT}$ mice and control mice. Results of visualization of fluorescent labeled lactoglobulin by immunofluorescence microscopy, showed inhibition of lactoglobulin uptake in Vps34 deficient cells compared to wild-type cells. This result is consistent with impairment of receptor-mediated endocytosis reported in mice with conditional deletion of Vps34 in kidney proximal tubule cells [51] and in podocytes [102]. Impairment of endocytic uptake of filtered ligands in proximal tubule cells has been associated with low molecular weight proteinuria in numerous genetic, acute and chronic diseases such as Type 2 diabetes mellitus, Dent disease and Fanconi syndrome.

2.4.3 Defective clathrin mediated endocytosis in Vps34 $^{\Delta PT}$ mice

The uptake of molecules from the ultrafiltrate and the regulation of the plasma membrane turnover relies on endocytosis and functional endocytic pathways. In kidney proximal tubule cells, the clathrin-dependent endocytic pathway is uniquely specialized to respond the the high capacity needs for reabsorption. The development of the clathrin-coated pits and the

formation of clathrin-coated vesicles in these cells is acutely regulated as well as the recognition of cargo via specific receptors [103].

In Vps34 $^{\Delta PT}$ cells, immunofluorescence showed a strong decreased expression of clathrin and clathrin-coated vesicles at the apical membrane of the proximal tubule cells compared to wild-type cells. The function of clathrin in the endocytic process has been studied in many cellular organisms through genetic disruption of the clathrin heavy chain gene. In single-cell organisms, such as yeast and *Dictiostelium discoideum*, clathrin inactivation led to a slow growth and reduced endocytosis [104]. Repression of clathrin in mammalian cell culture experiments revealed concrete reduced endocytosis of transferrin, epidermal growth factor and LDL receptor. The reduction of clathrin in Vps34 $^{\Delta PT}$ cells and clathrin associated proteins such as adaptor protein-2 suggest that the coordination between the surface delivery of molecules and the endocytosis/recyling pathways is altered upon the absence of VPS34, resulting in reduced endocytosis and loss of many membrane proteins.

2.4.4 Defective apical endocytic recycling in Vps34 $^{\Delta PT}$ mice

The multiligand receptors megalin and cubilin coordinate the internalization of the majority of the filtered proteins and other small molecules from the glomerular ultrafiltrate. Proximal tubule cells are characterized by high levels of expression of the endocytic receptors megalin and cubillin and by a fast recycling of the megalin receptor to the plasma membrane after cargo internalization. The abundance of megalin expression in the proximal tubule shows its relevance as a multiligand scavenger receptor for ligans such as albumin, hemoglobin, insulin, retinol-binding protein (RBP) and vitamin D-binding protein (DBP). The absence of megalin in mice is associated with increased proteinuria, increased urinary levels of albumin, α1 microglobulin and DBP [105]. An additional megalin knockout mouse model study has highlighted the importance of megalin receptor endocytosis for the lysosomal biogenesis. In this model, decreased megalin-mediated reuptake of acid hydrolases for example Cathepsin B, was shown to alter the efficient biogenesis of the lysosome [106].

I found that another effect of VPS34 depletion in the proximal tubule was the mislocalization of the megalin receptor towards the basolateral membrane. One of the reasons for the displacement of the megalin receptor from the apical subcompartments of the cell is probably the observed reduction in the expression of the small GPTase Rab11. Rab11 is mainly localized in perinuclear recycling endosomes and regulates the slow recycling from sorting endosomes to the plasma membrane [107, 108]. Immunofluorescence of Vps34 $^{\Delta PT}$ cells showed

mislocalization of recycling apical membrane receptor megalin and reduction of the cubilin receptor compared to wild-type cells.

Perturbations of the endosomal system have been observed in a wide range of cancers and neurodegenerative diseases such as Alzheimer´s disease and Parkinson´s disease. Defective trafficking of growth factor receptors, impaired recycling or reduced degradation of proteins are common characteristics of tumor development. Investigations carried out in the field of neurodegeneration revealed that defects in endosomal function, that cause protein mislocalizations or aberrant secretion of proteins are involved in the nascent of these disorders.

2.4.5 Functional impairment of late endosomes/lysosomes in Vps34 $^{\Delta PT}$ mice

Lysosomes are cellular compartments for degradation of macromolecules and are regulated by acid hydrolases and lysosomal membrane proteins. In eurkaryotic cells, lysosomes maintain cellular self-renewal capacity and energy supply. Besides being a mechanism of waste disposal, lysosomes act as an active signaling hub involved in multiple signaling pathways such as mammalian target of rapamycin complex 1 (mTORC1) and adenosine 5´monophosphate-activated protein kinase (AMPK). The structural function and integrity of the lysosomes is essential for the cell function and viability. Abnormalities in the lysosomal function have been observed in lysosomal storage disorders, neurodegenerative diseases, cancer and cardiovascular and metabolic diseases. For example, disruption of lysosomal biogenesis leading to impairment of autophagy activation and cell toxicity has been observed in experimental models of diabetic nephropathy and Parkinson´s disease [109, 110].

Comparison of proteomes from urine and cortical kidney tissue from Vps34 $^{\Delta PT}$ mice, revealed that several lysosomal related proteins such as NPC2, NEU1, CTSZ and MAN2b were reduced in kidney cortices and increased in urine as a consequence of Vps34 depletion. This result indicates depletion of lysosomal components in Vps34 $^{\Delta PT}$ mediated by loss into the urine.

The result of LAMP-2 labelling to visualize late endosomes/lysosomes in kidneys of Vps34 $^{\Delta PT}$ mice, showed that the number of LAMP-2 positive lysosomes increased significantly in proximal tubule cells as a result of VPS34 depletion compared to wild-type cells. Late endosomes are trafficked toward the perinuclear space in wild-type cells where the lysosomes are localized. In VPS34 deficient cells, LAMP-2 structures are more abundant and extend to the basal cytoplasm impairing its interaction with other cytoplasmatic organelles.

Nutrient signaling, extracellular pH changes and cellular stress have been reported to influence lysosome positioning and movement [111]. Although these mechanisms are not completely ellucidated, it seems that lysosomal distribution appears to modulate the intensity of mTORC1 signaling in response to nutrients and the signaling events to regulate autophagy [112]. Lysosome positioning is therefore a highly regulated process and impairment of lysosome dynamics, is an important determinant of lysosomal disfunction.

These observations are consistent with previous *in vitro* evidence of accumulation of enlarged late endosomes/lysosomes and reduced amount of late endosomes/lysosomes markers [113]. VPS34 inhibition with SAR405 in RKO colorectal cancer cells for 16h also showed formation of large LAMP-1 organelle vacuoles and impairment of maturation of the lysosomal enzyme cathepsin D [94].

2.4.6 Disregulation of amino acid and sugar transporters in Vps34 $^{\Delta PT}$ mice

Amino acid transporters are membran-bound proteins that are localized in the plasma membrane and facilitate the uptake, exit or exchange of amino acids across the membrane. Specific amino acids are involved in processes such as energie production, nitrogen balance and regulation of metabolism. Amino acid transporters play an important role in amino acid-dependent mTOR signaling and cell growth by increasing the cellular uptake of amino acids [114]. In addition to the vesicular trafficking defects observed in VPS34 deficient mice, I found a significant decreased expression of amino acid transporters such as B^0AT1, 4F2hc, γ^+LAT1 and γ^+LAT2 and the sodium transporters NBC1 and SGLT2 on a protein level in Vps34 $^{\Delta PT}$ mice. Phosphoproteomic analysis of control and Vps34 $^{\Delta PT}$ kidney homogenates revealed that these amino acid and sodium transporters had a reduced phosphorylation in their respective serin sites (data not shown).

These results are consistent with previous published data of RAPTOR deficient mice which showed reduced expression of the amino acid transporters SLC6A19 (B^0AT1), SLC7A7 (γ^+LAT1) and SLC3A2 (4F2*hc*) as a principal cause for the observed aminoaciduria [99]. Considering that specific amino acids serve as oxidative fuel for ATP generation, the potential loss of amino acids caused by depletion of Vps34 may alter the energy balance of the cell. Recent sudies have shown that methionine and leucin restriction alters lipid metabolism, including the lipid synthesis and the lipolysis pathway [115].

Interestingly, our data revealed also a compensatory reaction of the proximal tubule cell to conserve its cell function consisting in maintaining free fatty acid transporters (FAPTs, SLC27,

SLC27A), increased glutamin metabolism (L-Gln is transported into renal proximal tubule cells via the basolateral transporter SLC38A3) and increasing beta oxidation enzymes for augmented reabsorption of free fatty acids and keton bodies.

2.4.7 Reduced retromer complex activity in Vps34 $^{\Delta PT}$ mice

The endocytic machinery serves as a major instrument for sorting proteins in vesicles where they are directed to degradative pathways, recycled back to the plasma membrane or retrieved to the TGN through a retrograde pathway. Five proteins encoded by vacuolar protein sorting genes (Vps35p, Vps29p, Vps26p, Vps17p and Vps5p) form in yeast the retromer complex [116]. The retromer complex ist highly conserved in eukaryotes and comprises a cargo-selective trimer of VPS35, VPS29 and VPS26 that operates with a sorting nexin dimer (containing SNX-BAR proteins) of SNX1 or SNX2 paired with either SNX5 or SNX6 to regulate the retrieval of several proteins from endosomes to the Golgi such as lysosomal hydrolase receptors. Its function has been linked to the endosomal maturation pathway and to the rescue of cargo proteins from being degraded in lysosomes [117].

The disruption of the retromer complex leads to a number of cellular phenotypes including defective recycling of receptors and perturbation of cellular degradation pathways such as autophagy and mitophagy. The importance of the retromer complex in the regulation of the homeostasis of different transmembrane proteins at the plasma membrane and within the endosomal system has been established in several pathologies such as Parkinson´s disease or Alzheimer´s disease [118, 119]. I studied the retromer complex in proximal tubule cells of VPS34 depleted mice by analyzing one of the components of the sub-complex VPS35. Analysis of immunofluorescence of VPS35 revealed an ubiquitous localization of VPS35 in wild-type proximal tubule cells with a strong signal in subapical compartments. In Vps34 $^{\Delta PT}$ cells, VPS35 localization is not concentrated at subapical compartments of the cell where the endocytic vesicles are located but unequally redistributed throughout the cytoplasma. Westen Blot analysis confirmed a reduction in the protein expression of VPS35 in Vps34 $^{\Delta PT}$ cells compared to wild-type cells. Proteomic data revealed a reduction of proteins of the retromer complex and its interacting proteins (sorting nexins). Another finding linked to the function of the retromex complex was the unsual increased phosphorylation of SNX3 and SNX12 at sites essential for retromer assembly and membran docking. The reduction of the retromer complex formation and its activity is likely linked to the loss of VPS34 in the proximal tubule cell and may affect the regulation of endosomal pathways due to the absence of specific lipids and protein modifications.

2.4.8 Defective apical sorting of membrane proteins

Although a large number of reports confirm impairments in endocytic process by inhibition or depletion of VPS34, little is known about the interaction of this lipid kinase with secretory pathways. Galectins are mainly known for regulation of cell-cell and cell-matrix interactions as well as participation in vital processes such as growth, proliferation and differentiation. GAL-3 is predominantly located in the cytoplasm, but it has also been detected in the cell surface, the extracellular environment and also in the nucleus, what confirms the multifunctional role of this molecule. In our study, Galectin-3 (GAL-3) and galectin-9 (GAL-9) were both strongly increased in proteomic data of Vps34 $^{\Delta PT}$ mice. High-resolution microscopy of wild-type proximal tubule cells, showed apical and basolateral localization of GAL-3 outside the plasma membrane indicating secretion processes. In Vps34 $^{\Delta PT}$ mice, strong accumulation of GAL-3 was observed in the cytosol of proximal tubule cells, reflecting mistrafficking of these protein.

In kidney tubules, GAL-9 binds to syalilated glycoproteins facilitating apical targeting and sorting of these proteins [120] and GAL-3 binds to carbohydrates on cargo proteins enabling polarized transport for delivery of vesicles to the plasma apical membrane followed by secretion [121]. Special mention deserve the novel role of GAL-3 in recognising damaged lysosomes. GAL-3 in cooperation with TRIM16 orchestrates autophagic responses to remove and extrude damaged lysosomes to maintain intracellular homeostasis [122]. Altogether, these observations suggest that the VPS34 depletion-mediated mislocalization of galectins in addition to abnormal expression in cytosol interferes with the regulation of the proximal tubule cell physiology, development and homeostasis.

2.4.9 Vps34 inhibition and low glutamine reduce SARS-CoV-2 infection in PTC

The severe acute respiratory syndrome coronavirus 2 (SARS-CoV-2), a virus that belongs to the coronavirus family was responsible for the Coronavirus Disease (Covid-19) characterized by fever, severe respiratory illness, pneumonia and lung failure and caused millions of human casualties worldwide. Several studies have highlighted the mechanisms of entry of SARS-CoV-2 into human host cells. SARS-CoV-2 enters the host cell by attaching its spike protein to the ACE2 receptor localized at the plasma membrane. This attachment activates several host cell proteases leading to cleavage of the spike protein which in turn facilitates its entry into the cell [123]. TMPRSS2 is one of the proteases involved in the cleavage and activation of the spike protein of SARS-CoV-2 to facilitate the viral entry into the host cell [95]. Many DNA viruses including adenovirus, human papilloma virus, Epstein-Barr virus as well as multiple RNA

viruses such as hepatitis C virus and influenza A, manipulate the host cell metabolic network to support the production of high amounts of viral progeny [124]. The concentration and metabolic processing of sugars and amino acids such as glucose, mannose, glutamine and glutamat play a key role in cellular homeostasis and are therefore targeted by viruses for their replication. The abrogation of Vps34 in proximal tubule cells of Vps34 $^{\Delta PT}$ mice, led to an unexpected upregulation of proteins involved in the antiviral defense. Among the most upregulated proteins found in the proteomic analysis of Vps34 $^{\Delta PT}$ mice, could be listed IFN-induced protein with tetratricopeptide repeats (IFIT) which are known to contribute to defense against certain viruses by different mechanisms of action. One of them is through binding to components of the eukaryotic initiation factor 3 translation initiation complex and impeding protein translation [125]. Furthermore, proteomic analysis revelead a reduced expression of ACE2 and TMPRSS2 in Vps34 $^{\Delta PT}$ mice. Western blot analysis confirmed a significant reduction of ACE2 in Vps34 $^{\Delta PT}$ mice compared to control mice. Immunhistochemistry analysis of ACE2 and TMPRSS2 revealed a significant reduction in ACE2 and TMPRSS2 in the brush border membrane of Vps34 $^{\Delta PT}$ cells compared to wild-type cells.

To confirm this hypothesis, SARS-CoV-2 infection of OK cells was analyzed after VPS34 inhibition with SAR405, a specific VPS34 kinase inhibitor [126]. SAR405 prevention of SARS-CoV-2 activity in OK cells was confirmed by measuring SARS-CoV-2 mRNA 24h after inhibition of the OK cells with SAR405 at a concentration of one micromolar. The anti-viral response observed in the cell culture experiment was also dependent on glutamin levels. OK cells infected with SARS-CoV-2 and incubated with low glutamine revealed similar results as OK cells treated with SAR405 inhibitor. In addition, analysis of amino acids in OK cells that were treated with SAR405, revealed an increase in the supernatant glutamate concentration but not in the cell concentration. Performance of isotope tracing of 13-labeled glutamine in OK cells in the presence and absence of SAR405, showed increased glutamine metabolism via TCA cycling in OK cells treated with SAR405 compared to untreated cells. Additionally, the rewiring of glutamine metabolism in proximal tubule cells during VPS34 inhibition indicates that VPS34 plays a role in the promotion of SARS-CoV-2 replication. These data support the idea that inhibition of VPS34 kinase activity could be used as a potential therapeutic target after SARS-CoV-2 infection.

2.4.10 Potential implications of VPS34 inhibition

VPS34 is required for a functional membrane trafficking route and machinery and is involved in the regulation of the secretory membrane and protein trafficking processes essential for

the proximal tubule cell homeostasis. The critical role of VPS34 in cellular and organismic functions has been manifested in phenotypes of Vps34 deletion in yeast and invertebrate organisms. *Saccharomyces cerevisiae* strains deleted for Vps34 or carrying point mutations without PI3-kinase activity, exhibited mis-sorting of vacuolar hydrolases and osmoregulation defects [127]. In *Caenorhabditis elegans* und in *Drosophila melanogaster*, deletion of Vps34 causes arrested development and larval lethality respectively [128, 129]. The importance of VPS34 for the embryogenesis in mammals, has been examined in Vps34 homozygous mice. Vps34 gene knockout embryos died 7-8 days after birth failing to form mesoderm, showing that VPS34 is essential for embryogenesis and organ function in mammals [130, 131]. Our data provided evidence of increased apoptosis in proximal tubule cells of mice with conditional depletion of Vps34 compared to control mice. I found a significant increase in TUNEL-positive cells in Vps34 $^{\Delta PT}$ mice, indicactive of an active apoptotic process.

In order to get a detailed view of the cell functions of VPS34, investigations have been centred in the formation of a VPS34 molecule without active kinase activity while keeping the VPS34 protein expression. The goal of this strategy is to mimic the impact of a systemically administered small molecule ATP-competitive kinase inhibitor. A recent discovery in heterozygous Vps34$^{D761A/+}$ mice, suggested that partial Vps34 deletion enhances insulin sensitivity and glucose tolerance, indicating that VPS34 might be a new drug target for the treatment of insulin resistance in type-2 diabetes [51]. VPS34 is also known as a core component regulating autophagy and dysregulation of autophagy has been described in many cancers and infectious diseases. Promising results in tumor growth inhibition via pharmacological inactivation of VPS34 kinase activity, has turned disruption of autophagy into a new approach for cancer treatment.

Disruption of Vps34 activity in neurons *in vivo* and *in vitro*, has also revealed an impairment of autophagy, lysosomal degradation and endolysosomal membrane damage [132, 133]. The defects in vesicular trafficking and autophagy observed in mice with conditional depletion of Vps34 in this thesis match with neuronal defects reported upon VPS34 inactivation in early stages of neurodegenerative disorders such as Alzheimer´s disease [134]. Altogether, these findings demonstrate that VPS34 is a master switch adjusting endocytosis, nutrient transport, autophagy and antiviral response. Nonetheless, according to these and previously published results, VPS34 inhibition should be reconsidered as a possible therapeutic target.

3. Chapter 2: Targeted deletion of von-Hippel-Lindau in the proximal tubule conditions the kidney against early diabetic kidney disease

3.1 Abstract

The proximal tubule has to deal in diabetes mellitus with high amounts of solutes and albumin as a consequence of diabetes-associated glomerular hyperfiltration with a resulting augmentation of tubular transport, growth and hypoxia. Hypoxia has been suggested to be a potent driver of the progression to diabetic kidney disease .

To study the role of hypoxia in the proximal tubule, a conditional PT-von Hippel-Lindau (*Vhl*-deleted mouse model, specific for S1/S2 segments, in combination with streptozotocin-induced type 1 diabetes mellitus was analyzed. Decreased NOS1 expression in the macula densa as well as a reduction of sodium and glucose transporters are involved in the prevention of the glomerular hyperfiltration observed in PT-*Vhl*-deleted streptozotocin-induced type 1 DM mice compared to diabetic control mice. PT-*Vhl*-deletion and DKD share common alterations in gene expression profiles, glomerular morphology, tubular transport and metabolism. STRING network analysis of the Gene ontology term

Alignment of *Vhl*-deletion related genes of diabetic mice in heat maps revealed that HIF-1α stabilization preconditioned the animals against diabetic kidney disease as a result of histone modification and chromatin remodelling of the genes altered in DKD. Hypoxia also controls the expression of L-wnk1. As L-wnk1 is known to modulate angiogenesis, proliferation and autophagy, this evidence underlines the participation of a dysregulated WNK1 signalling in the pathophysiology of diabetic kidney disease.

Our data demonstrate that hypoxia is a hallmark of early DKD and that targeting hypoxia in the proximal tubule prior to the onset of diabetes mellitus type 1 normalizes renal cell homeostasis and prevents the development and progression of DKD.

3.2 Introduction

3.2.1 Diabetic kidney disease

Diabetic kidney disease (DKD) is a common complication that develope 20% to 40% of the individuals with either type 1 or type 2 diabetes and is considered the major cause of chronic and end-stage renal disease (ESRD). The prevalence of diabetes worldwide has been estimated in more than 350 million people, reaching the rate of 550 million people by the end of the next decade [135]. Initially considered as a microvascular disorder, DKD is the result of

hyperglycemia, uncontrolled hemodynamics, inflammatory processes and hypoxia [136]. Complex alterations in metabolic milieu have been hypothesized to contribute to the initiation of DKD including hyperglycemia, changes in fatty acid metabolism, oxidative stress and mitochondrial dysfunction.

A prolonged hyperglycemia is one of the factors that contribute to the initiation of DKD. High glucose concentrations are known to induce specific cellular changes within the kidney affecting endothelial cells, mesangial cells, podocytes and tubular cells. Hyperglycemia enhances glucose reabsorption in the proximal tubule and the amount of glucose reabsorbed depends on the expression of sodium-glucose transporters. There is evidence for upregulation of SGLT1 and SGLT2 mRNA and increased protein expression of SGLT1 in the cortex of STZ-diabetic rats [137, 138]. The enhanced expression of tubular sodium-glucose transporters has been attributed to the growth of proximal tubular epithelia observed in the cortex of diabetic kidneys [139]. The increased electrolyte reabsorption in the proximal tubule implies that reduced amounts of sodium, chloride and potassium are delivered to the macula densa, increasing the glomerular filtration rate through suppression of the tubuloglomerular feedback mechanism [140].

3.2.2 Effects of hyperglycemia on the proximal tubule

3.2.2.1 Glomerular hyperfiltration

Hyperglycemia is one of the main factors leading to glomerular hyperfiltration in diabetes mellitus resulting in inhibition of the tubuloglomerular feedback [141]. Initially was considered that abnormalities in renal haemodinamic function were determinants of glomerular hyperfiltration. But a new tubular hypothesis considers glomerular hyperfiltration as a consequence of interactions between the glomerulus and the proximal tubule.

The tubular theory proposes that enhanced sodium and glucose reabsorption in the proximal tubule through upregulation of sodium-glucose cotransporter 2 and sodium-hydrogen exchanger NHE3 leads to a reduced sodium-chloride delivery to the macula densa. These effects lead to an inhibition of the tubuloglomerular feedback signal and consequently to an increase in intraglomerular hydraulic pressure and glomerular filtration rate [142].

One of the best interventions to reduce glomerular hyperfiltration has been achieved with the use of SGLT2 inhibitors. Clinical trials in T2DM patients have demonstrated SGLT2 inhibitors reduce glucose reabsorption from the renal filtrate and ameliorate glomerular hyperfiltration through reduction of the intraglomerular pressure [143].

3.2.2.2 Advanced glycation end products

One of the results of the prolonged exposure to hyperglycemia is the formation of advanced glycation end products (AGEs). AGEs are heterogeneous substances that are produced through a non-enzymatic reaction, known as glycation [144] between the aldehyde groups of reducing sugars such as glucose, fructose and ribose and free amino groups of protein, lipids or nucleic acids. The pathological effects of AGEs are mainly related to the promotion of oxidative stress and inflammation as a consequence of the formation of cross-links between key molecules in the basement membrane of the extracellular matrix (ECM) and through interaction of AGEs with their cellular receptors RAGE activating a series of intracellular signaling pathways. The formation of AGEs, impairs the assembly of basement membrane proteins with severe implications for its structure and function [145]. In the glomerular basement membrane, for example, the accumulation of AGEs disrupts the balance between synthesis and degradation of components of the ECM, especially collagen causing membrane thickening and impaired filtration [146]. In DKD, circulating AGEs also induce renal inflammation and fibrosis. The activation of RAGEs by AGEs in endothelial cells, leads to activation and translocation of NF-κB resulting in transcription of endothelin-1, vascular cell adhesion molecule-1 (VCAM-1), intercellular adhesion molecule-1, vascular endothelial growth factor (VEGF) and some inflammatory cytokines such as IL-1α, IL-6 and TNF-α [147]. The upregulation of TGF-β after RAGE stimulation increases the production of collagen IV, laminin and fibronectin contributing to membrane thickening in tubular and mesangial cells [148]. Early studies have suggested that AGEs can trigger ROS production [149]. One of the mechanisms might be the stimulation of membrane bound NAD(P)H oxidase via RAGE receptors [150]. There is also evidence that glycation of antioxidative enzymes such as SOD, may enhance ROS production and cellular oxidative damage [151].

3.2.2.3 Hypoxia

Intrarenal hypoxia is present in kidneys from diabetic patients and constitutes a mechanism for DKD [152]. Kidney hypoxia is the result of an imbalance between oxygen delivery and oxygen demand [153]. In diabetes, the oxygen balance is compromised through several mechanisms causing an increase in ATP demand and

therefore in oxygen demand with a subsequent decrease in ATP generation. The ATP demand is affected by increased renal sodium transport as a result of tubular growth and sodium-glucose transporter upregulation [154]. In addition, a decrease in ATP generation is due to a metabolic shift from glucose oxidation to free fatty acid oxidation and inhibition of adenosine monophosphate-activated protein kinase (AMPK) [155, 156]. Various studies have provided information about the extent of hypoxia during the development of DKD [157]. One of the most important components of the response to correct hypoxia correspond to hypoxia-inducible factors [158].

3.2.2.4 Hypoxia-inducible factor

Hypoxia-inducible factor (HIF), the transcription factor that regulates the transcriptional response to hypoxia is composed of an inducible alpha subunit (HIF-α) and a constitutively expressed β subunit (HIF-β)[159]. Under conditions of normoxia, HIF-α polypeptides are hydroxylated in two prolin residues by prolyl hydroxylases promoting the binding of HIF-α subunits to the von Hippel-Lindau tumor suppressor pVHL, the recognition component of a E3 ubiquitin-ligase complex [160]. After association with pVHL, the HIF-α subunits are degraded via the ubiquitin proteasome mechanism [161]. In hypoxia, HIF-1α is stabilized against degradation and can translocate to the nucleus where it forms a dimer with the HIF-1β subunit on the HRE of target genes and up-regulates a series of genes that enable the cell to overcome the reduced oxygen availability. The HIF-1 complex activates the expression of target genes involved in processes such as angiogenesis, oxygen transport, glycolysis, growth factor signaling, cell survival and cell proliferation [162]. Increased HIF-1α levels have been shown to upregulate genes involved in angiogenesis, such as VEGF, matrix metalloproteinase 2 (MMP2) and cathepsin D [163]. HIF activation under hypoxia also increased the expression of GLUT1 and GLUT3 transporter and enzymes of the glycolytic process in order to generate more energy [164]. Furthermore, increased expression of TGF-α and IGF-2 under hypoxic conditions, may indicate that processes such as cell proliferation and cell survival are promoted through transcriptional activation of HIF-1 [165].Data from gene expression studies revealed that VHL deficiency can cause different effects in fully hydroxylated HIFs. Overexpression of HIF-1α by deletion of renal VHL can cause adverse renal outcomes [166]. However, the

increase of HIF-1α with cobalt chloride has been shown to improve renal outcomes in diabetes models [167]. Positive effects of HIF stabilization have been reported in several kidney diseases as for example in acute kidney injury or chronic kidney disease. HIF induction has been shown to exert a protective effect in a rat glomerulonephritis model [168]. In a chronic kidney disease animal model, cobalt treatment for HIF induction resulted in improvement of the tubulointerstitial injury and preservation of the peritubular capillary network [169].

3.2.3 WNK1 regulation in ion homeostasis and human diseases

WNKs (With No lysine [K]) are a family of kinases known to have roles in the regulation of salt homeostasis in response to osmotic stress. The WNK kinases comprise four serine-threonine kinases (WNK1 to WNK4) that lack the catalytic lysine residue in the kinase subdomain II responsible for docking ATP and phosphoryl transfer and are highly sensitive to intracellular chloride [170, 171]. WNKs have been shown to regulate the activity of several sodium, potassium and chloride transporters, among them, the sodium-potassium-chloride cotransporter 2 (NKCC2) which is expressed in the ascending limb of the loop of Henle. The WNK1 gene is ubiquitously expressed but, in the kidney, WNK1 has a specific expression pattern comprising two distinct isoforms, one with its intact catalytic activity (L-WNK1) and a truncated form lacking most of the kinase domain and expressed only in the distal nephron (KS-WNK1) [172]. Although the WNK pathway is best known by its regulation of ion transport, implications of the WNK signaling pathway in the pathologies of several human diseases is drawing more attention in the scientific community. In humans, increased expression of WNK1 due to deletions in the intron between exons 1 and 2, led to a rare form of hypertension [173]. The WNK phosphorylation cascade has been associated with pathological conditions such as salt-sensitive hypertension, which has been reported in patients with metabolic syndrome, diabetes mellitus and chronic kidney disease (CKD) [174]. Several mouse models and *in vitro* assays have studied the *WNK1* gene in relation to blood vessel architecture. Although a complete understanding of the relationship between WNK1 and endothelial migration and angiogenesis is missing, reduced expression of WNK1 caused decreased expression of factors related to angiogenesis such as Slug, VEGF-A or matrix metalloproteinases [175]. *WNK1* has also been implicated in the regulation of autophagy as depletion of *WNK1* leads to increase in the number of autophagosomes [176]. Autophagy is a degradation process to maintain cellular physiology. Alterations in different forms of autophagy processes are involved mainly in neurological diseases but have also been reported

in diabetes [177]. The molecular signature of the proximal tubular changes in hypoxia and DKD is complex and still there is no evidence for the involvement of the WNK kinases in the formation of the diabetic state.

3.2.4 Aim of the study

The incidence of diabetes mellitus and its complications is increasing worldwide. The high incidence of kidney disfunction in diabetes patients has turn diabetic kidney disease in the leading cause of end-stage renal disease. The identification of the early factors that lead to diabetic kidney disease is critical for the development of new therapeutic strategies against the progression of DKD.

The diabetic renal proximal tubule is exposed to high amounts of solutes and albumin due to diabetes-associated hyperfiltration. The proximal tubule is the most metabolically active region of the kidney and dotted with a membrane surface for transepithelial transport and high amounts of mitochondria, reabsorbs nutrients, small proteins, electrolytes and trace elements. The early diabetic kidney is characterized by glomerular hyperfiltration and albuminuria subjecting the proximal tubule with growth, hypoxia and higher nutrient overload.

Inhibition of sodium-glucose uptake by gliflozins has revolutionized the treatment of DKD by preventing the decline in the kidney function and the progression to end-stage renal disease. Renal hypoxia is frequently observed in DKD. The aim of this study is to explain the role of proximal tubule hypoxia and determine the effects of hypoxia in the development and progression of DKD using a genetic approach targeting the proximal tubule-specific deletion of *Vhl* in diabetic and non-diabetic mice.

3.3 Results

3.3.1 *Vhl*-knockout in proximal tubules

To study the effect of hypoxia, characterized by HIF-stabilization under conditions of type 1 diabetes mellitus, mice with deletion of the *Vhl* gene in the early segments of the proximal tubule were generated by cross-breeding VHL^{flox} mice with $Sglt2^{cre}$ mice. Mice with *Vhl* deletion were termed $VHL^{\Delta PT}$. The induction of diabetes mellitus in 3-months-old mice with and without deletion of *Vhl*, was done by administration of STZ. 10 weeks after diabetes was induced, tissue was collected for correspondent analysis.

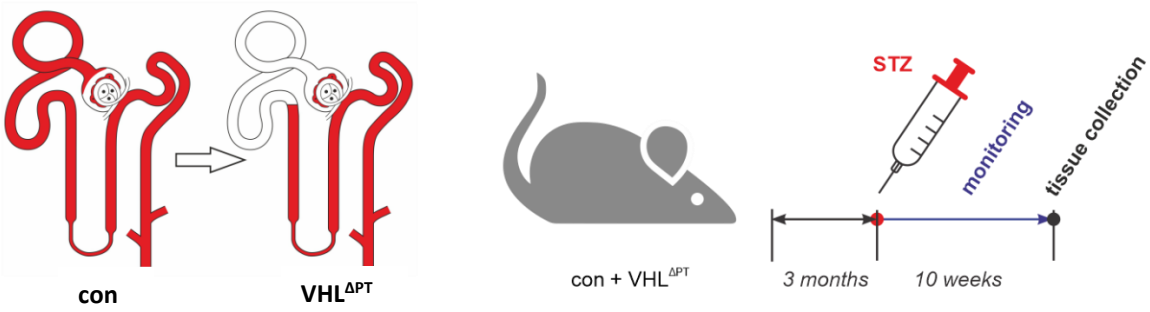

A Generation of $VHL^{\Delta PT}$ mice through knockout of *Vhl* in PT

B Generation of mice con/STZ and $VHL^{\Delta PT}$/STZ by treatment with streptozotocin

Fig. 3.1. Graphic representation of generation of the mouse models con, $VHL^{\Delta PT}$, con/STZ and $VHL^{\Delta PT}$/STZ. *The Vhl knockout in S1 and S2 segments of the proximal tubule was generated using Sglt2 specific promotor by breeding VHL ^{flox} mice, with Sglt2 ^{cre} mice (left). Diabetic mice were generated with two injections of streptozotocin (STZ) in 24 h and all animals were monitored for a 10 weeks period before perfusion/fixation and tissue collection (AG Theilig).*

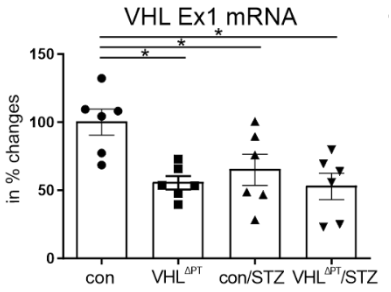

Fig. 3.2. Determination of the degree of *Vhl* knockout in $VHL^{\Delta PT}$ vs control mice. *For the determination of the degree of Vhl knockout in $VHL^{\Delta PT}$ mice, the mRNA expression of Vhl-Exon 1 was quantified in SGLT2- positive proximal tubule cells. The results revealed a 44,5 ± 5,2% deletion of Vhl in S1-S2 segments in $VHL^{\Delta PT}$ mice, n= 6 per group; *P < 0,05, Kruskal-Wallis/Dunn´s test (AG Theilig).*

3.3.2 Increase of HIF-1α in *Vhl* knockout mice

The expression of HIF-1α is increased in many pathological conditions such as human malignancies and diabetes. To confirm that *Vhl* depleted mice and mice with streptozotocin-induced diabetes presented an increase in HIF-1α expression, immunoblotting was performed from soluble nuclear fractions of kidneys from control (con), Vhl $^{\Delta PT}$, con/STZ and Vhl $^{\Delta PT}$/STZ mice. As showed in figure 3.3 the Vhl $^{\Delta PT}$ group showed a significant increase in HIF-1α expression compared to the control group. Also in the con/STZ group, HIF-1α was significantly augmented. The Vhl $^{\Delta PT}$/STZ group though, showed no significant changes compared to the control group.

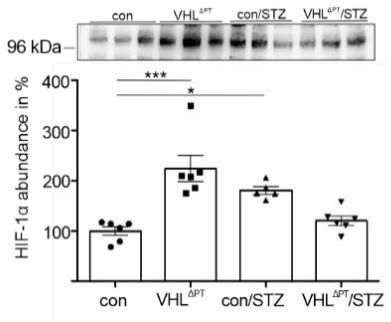

Fig. 3.3. Representative Western blot of HIF-1α. *Western Blot analysis of soluble nuclear fractions and quantification of HIF-1α protein expression in control group (con), Vhl $^{\Delta PT}$, con/STZ and Vhl $^{\Delta PT}$/STZ. Values are means ± SEM, n= 5-7 per group. *P < 0,05 ***P < 0,001, Mann-Whitney test.*

3.3.3 Deletion of *Vhl* in the proximal tubule prevents diabetic glomerular hyperfiltration and proteinuria after induction of diabetes

Plasma analysis of mice 10 weeks after induction of diabetes revealed significantly higher blood glucose levels in con/STZ group and in Vhl $^{\Delta PT}$/STZ group compared to the control group and *Vhl* knockout group both presenting normoglycemia. In order to evaluate the renal function, the GFR was measured in conscious mice through the exogenous GFR tracer, fluorescein-isothiocyanate conjugated sinistrin, an inulin analog. As shown in figure 3.4; B, animals of the con/STZ group revealed a significantly augmented GFR compared to control littermates. Surprisingly, animals from the Vhl $^{\Delta PT}$/STZ group did not showed glomerular hyperfiltration which is an early clinical hallmark in diabetes mellitus. Proteinuria is a marker of kidney damage and a risk factor for progression of chronic kidney disease. Analysis of samples from 24-hour urine collections of mice 10 weeks after STZ treatment revealed significantly higher protein excretion in con/STZ compared to control mice. No changes were observed in the Vhl $^{\Delta PT}$/STZ group compared to control mice. Additional measure of urine volume, revealed greater urinary flow rate in con/STZ and in Vhl $^{\Delta PT}$/STZ compared to control and Vhl $^{\Delta PT}$ groups. The amount of sodium, glucose and phosphate in con/STZ were also

significantly higher in the urine of con/STZ and in Vhl $^{\Delta PT}$/STZ compared to control and Vhl $^{\Delta PT}$ groups.

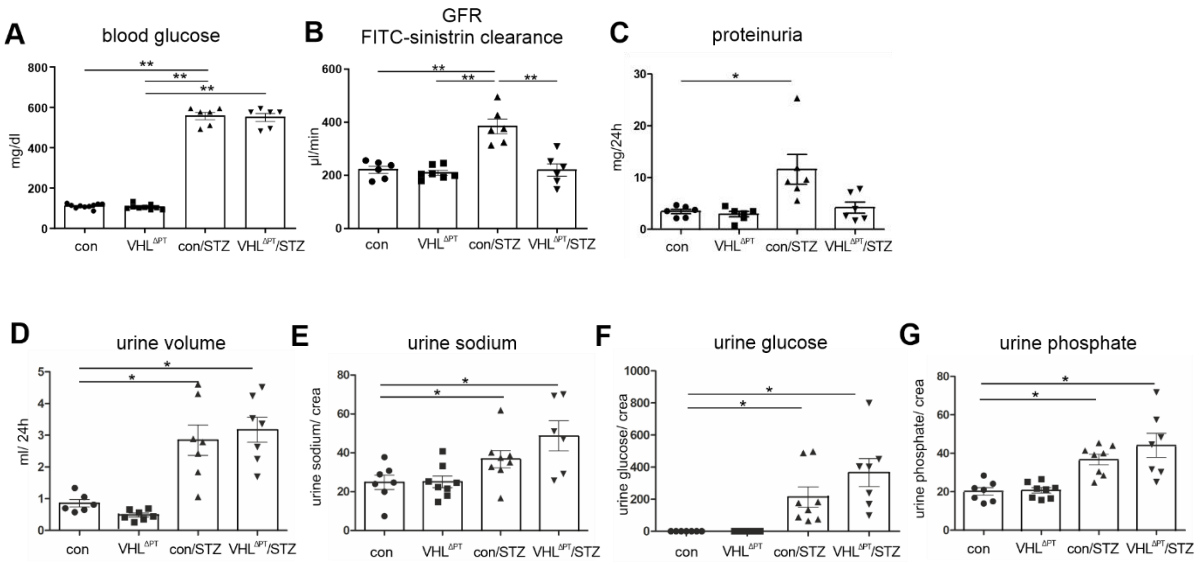

Fig. 3.4. Renal functionsparameter and glomerular filtrationsrate after induction of diabetes with streptozotocin. *Renal functionsparameter of blood glucose (A), Glomerular filtrationsrate (B) and proteinuria (C) as well as urine volume (D), urine sodium (E), urin glucose (F) and urine phosphate (G) of control group (con), VHL$^{\Delta PT}$, con/STZ and VHL$^{\Delta PT}$/STZ. The GFR was determined by kinetic measure of FITC-sinistrin in plasma of control group (con), Vhl $^{\Delta PT}$, con/STZ and Vhl $^{\Delta PT}$/STZ. Mean value ± SEM; n = 6-7 per group; *P < 0,05 **P < 0,01, Kruskal-Wallis/Dunn´s test (AG Theilig).*

3.3.4 Altered expression of tubular sodium and glucose transporters and NOS1 upon genetic PT deletion of *Vhl* after STZ-induced type 1 DM

After evaluation of renal function data, proteins involved in glomerular hyperfiltration and urinary solute excretion in the proximal tubule and thick ascending limb such as SGLT2, GLUT1, NKCC2 and NOS1 were analyzed by immunohistochemistry and Western blot analyses. Filtered glucose is almost entirely reabsorbed across the luminal membrane via sodium-glucose co-transporter 2 (SGLT2) in the proximal convoluted tubule. SGLT2 expression was analyzed by immunhistochemistry in the S1 and S2 segments of the proximal tubule of con, VHL$^{\Delta PT}$, con/STZ and VHL$^{\Delta PT}$/STZ mice. The protein expression of SGLT2 showed no significant differences in the VHL$^{\Delta PT}$, con/STZ and VHL$^{\Delta PT}$/STZ groups compared to the control group (Figure 3.5; A). However, the glucose transporter 1 (GLUT1) expressed most prominently in the basolateral membrane of the distal tubules, the connecting tubules and the collecting ducts, revealed a significant increased protein expression in the animal groups VHL$^{\Delta PT}$, con/STZ and VHL$^{\Delta PT}$/STZ with the strongest difference found in the con/STZ group (Figure 3.5; B).

The sodium hydrogen exchanger-3 (NHE3) has been postulated to have a role in NaCl homeostasis and in the regulation of blood pressure. NHE3 is localized apically in the proximal tubule and in thick ascending limb. The NHE3 expression in the VHL$^{\Delta PT}$ group was slightly higher compared to controls and significantly increased in both diabetic groups with the highest expression levels in con/STZ (Figure 3.5; C). The NKCC2 transporter showed very similar results in the immunohistochemistry analysis as the NHE3 transporter. The protein levels of NKCC2 in TAL were higher in VHL$^{\Delta PT}$ and significantly increased in both diabetic groups with highest expression levels in con/STZ (Figure 3.5; D).

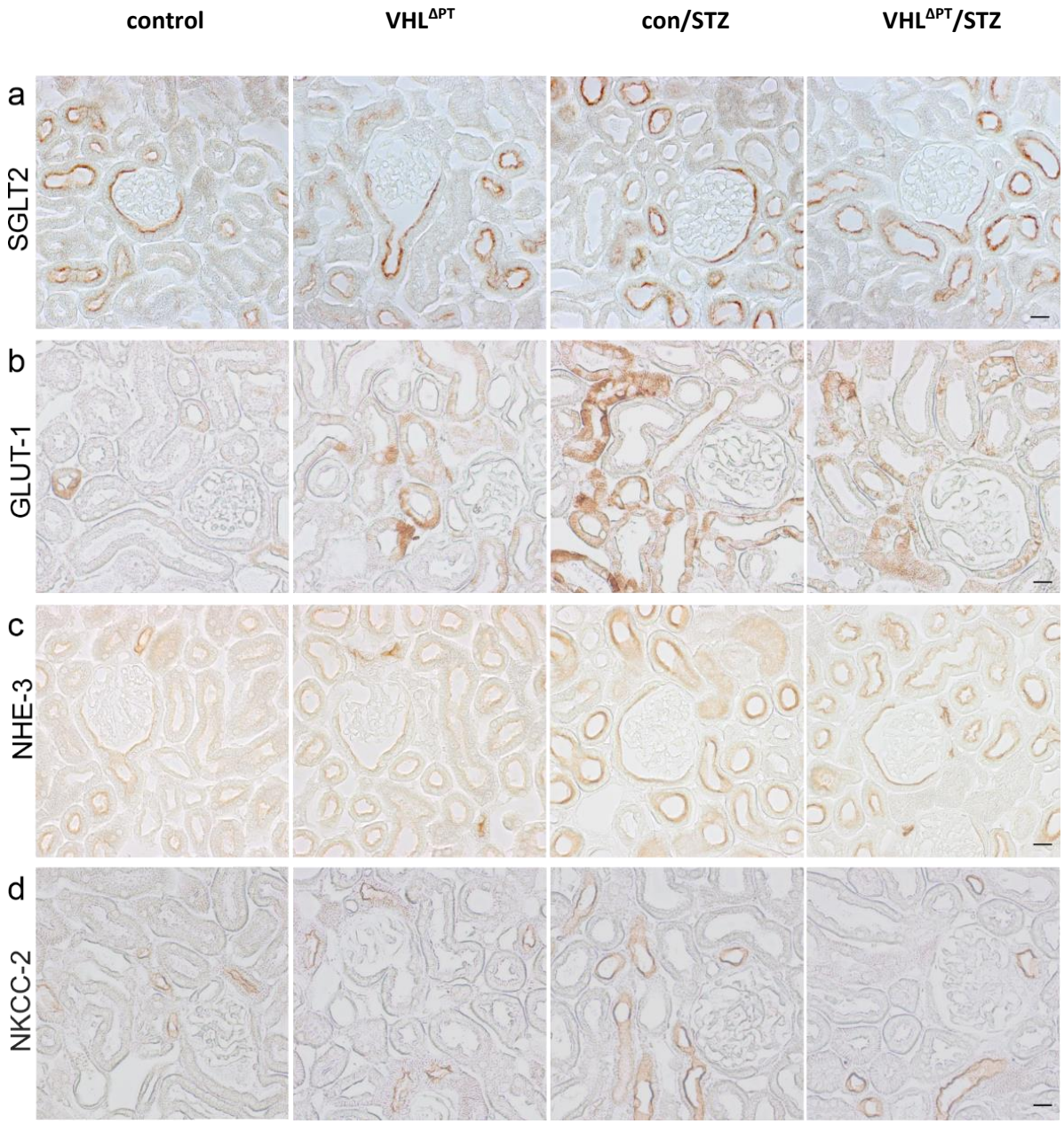

Fig. 3.5. Expression of sodium and glucose transporters in proximal tubules and distal tubules of Vhl $^{\Delta PT}$, con/STZ and Vhl $^{\Delta PT}$/STZ mice. *Immunhistochemistry analyses of SLGT2 (a), GLUT1 (b), NHE3*

(c) and NKCC2 (d) in proximal tubules and distal tubules of control group (con), VHL$^{\Delta PT}$, con/STZ and VHL$^{\Delta PT}$/STZ (AG Theilig). Scale bar: 20 µm.

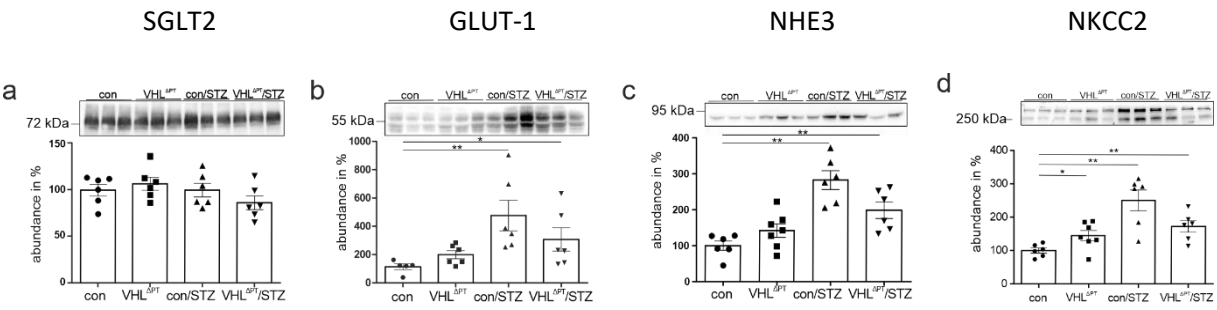

Fig. 3.6 Representative Western blots of SLGT2, GLUT-1, NHE3 and NKCC2. *Western Blot analysis and quantification of SGLT2 (a), GLUT-1 (b), NHE3 (c) and NKCC2 (d) in control group (con), Vhl $^{\Delta PT}$, con/STZ and Vhl $^{\Delta PT}$/STZ. Values are means ± SEM, n= 5-7 per group. *P < 0,05 **P < 0,01. Kruskal-Wallis-test.*

NO has been suggested to be involved in the pathogenesis of diabetic nephropathy due to its role in the control of renal and glomerular hemodynamics. Because the tubular hypothesis proposes that TGF is the main controller of the GFR in early diabetes and elevated glucose exposure modifies NOS activity and NO release, the expression of NOS1 in the macula densa was analyzed in the four experimental groups. NOS1 expressed in the macula densa was significantly increased only in the con/STZ group compared to the control group. Interestlingly, animals from the Vhl $^{\Delta PT}$/STZ group showed a significantly decreased expression of NOS1 compared to animals from the con/STZ group (Figure 3.7).

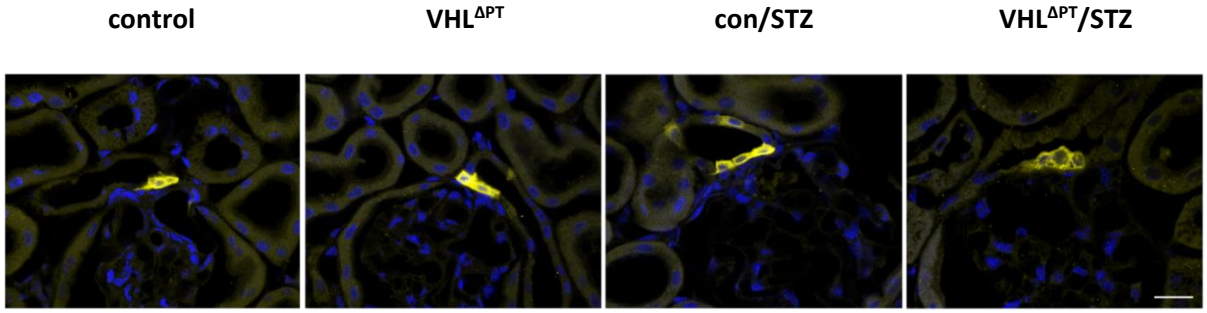

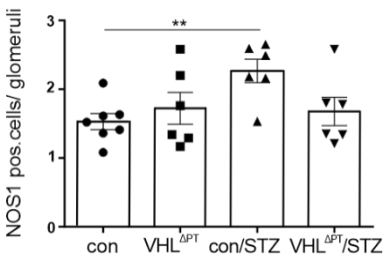

Fig. 3.7. Expression of NOS1 in Macula densa of con, Vhl $^{\Delta PT}$, con/STZ and Vhl $^{\Delta PT}$/STZ mice. *Immunofluorescence analysis of NOS1 in cells of the macula densa in control group (con), VHL$^{\Delta PT}$, con/STZ and VHL$^{\Delta PT}$/STZ and evaluation of NOS1 positive cells per glomeruli.* Values are means ± SEM, n= 5-7 per group. *P < 0,05 **P < 0,01. Mann Whitney´s test. *Scale bar: 20 µm. (AG Theilig).*

3.3.5 Deletion of *Vhl* induces gene alterations similar as in STZ-induced diabetes

RNA sequencing of kidney samples from all experimental groups was performed. To see the impact of *Vhl* deletion and subsequent HIF-1α stabilization on the development of DKD, we analyzed the gene expression profiles of commonly regulated genes of *Vh*l $^{\Delta PT}$, con/STZ and *Vhl* $^{\Delta PT}$/STZ mice compared to control group. We found that PT-Vhl-deletion and DKD share common alterations in gene expression profiles, glomerular and tubular morphology, tubular transport and metabolism. Among the altered genes between both diabetic groups we identified *Zbtb16*, Klotho, Glucocorticoid receptor, NKCC2 and WNK1.

3.3.5.1 Gene set enrichment of upregulated pathways is related to glomerular and tubular morphology and function

Figure 3.8 shows a heatmap of genes significantly upregulated in the VHL$^{\Delta PT}$ and the con/STZ group compared to the control group. The rectangles are scaled with a range of colors that are proportional to the gene expression values. In the rows of the table are represented the genes object of analysis and in the columns are represented the samples of each group. Genes that are changed are represented by red and blue tone red color means increased gene expression and blue color means reduced gene expression. Figure 3.8; A shows the results of the RNA Seq analysis representing genes affecting the glomerular morphology and function in five categories: podocyte function, glomerular basement membrane thickening, mesangial protein expression, angiogenesis and vasculogenesis and endocytosis. Higher *Tjp1* (ZO-1) levels were found in Vhl $^{\Delta PT}$ and in con/STZ, as well as higher levels of roundabout homologue 2 (*Robo2*) associated with disruption of the glomerular filter barrier. Vhl $^{\Delta PT}$ and in con/STZ showed higher expression of Nid2, Lamc1, Col4a3 and Col4a5, which is consistent with thickening of the GBM. Vhl $^{\Delta PT}$ and in con/STZ also demonstrated to have higher levels of *ltgb8* and *Vcl*, consistent with proliferation of mesangial cells and higher *Ptprb* and *Ogt*, associated with increased angiogenesis. Interestingly, Vhl $^{\Delta PT}$ and in con/STZ showed decreased levels of Cathepsin S, a biomarker associated with GFR decline. Figure 2.8; B) shows the results of the RNA sequencing obtained by grouping genes for epithelial function in five categories including cell polarity, stress, celullar transport, metabolism and endocytosis. Higher mRNA levels for *Notch1*, *Btbd7* and *Fryl* were observed in the Vhl $^{\Delta PT}$ and in the con/STZ group compared to the control group. These genes are known to play a critical role in early stages of nephrogenesis. In Vhl $^{\Delta PT}$ and in con/STZ, were found also higher mRNA levels for *Hif1α*, a known gene induced by hypoxia and for *Nox4* and *Rictor*, genes that are induced by cellular stress. Increased levels of genes that regulate epithelial transport such as *Slc12a1*

(NKCC2), *Slc9a3* (NHE3), *Slc4a4* (NBC1) and *Slc2a2* (GLUT2) were also observed in In Vhl $^{\Delta PT}$ and in con/STZ as well as higher levels of genes that play a critical role in endocytosis such as *Cltc* (Clathrin), the major component of coated vesicles and coated pits and *Eea1* and *Rab38* in early/Recycling endosomes.

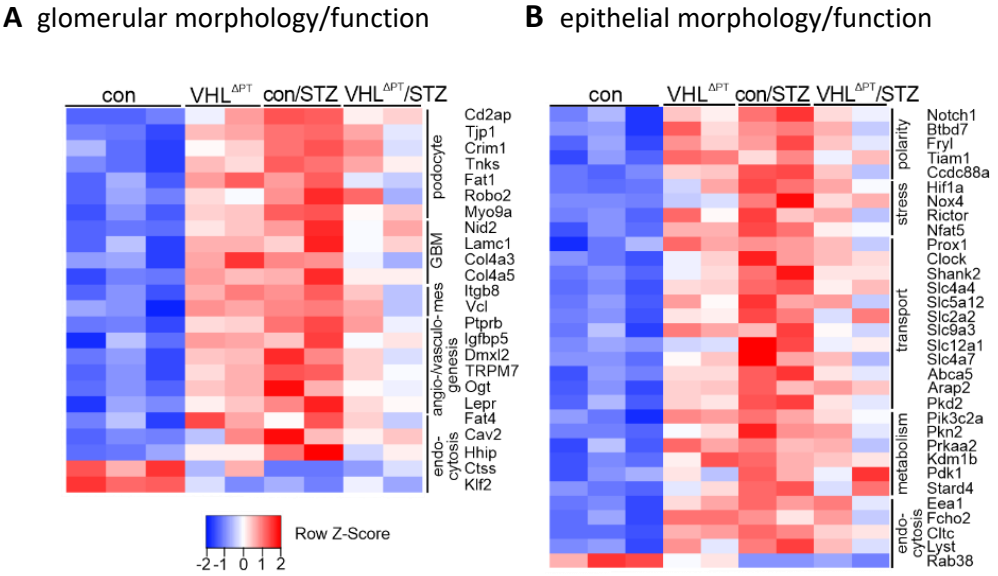

Fig. 3.8. Altered gene expression between control, Vhl $^{\Delta PT}$, con/STZ and Vhl $^{\Delta PT}$/STZ mice. *Heatmap representation of significantly changed genes between control and VHL$^{\Delta PT}$mice, based on filtering criteria DESeq P-Values ≤ 0,05, x-fold change ≥ 1,5. (F.Theilig, AG Theilig).*

3.3.5.2 Altered WNK1 gene expression under hypoxia and DKD

Among the significantly altered genes between the diabetic groups con/STZ and Vhl $^{\Delta PT}$/STZ in the category tubular transport, we indentified alterations in the *Slc12a1* gene coding for the NKCC2 transporter, that regulates sodium transport in the thick ascending limb of the loop of Henle. The WNK-SPAK-NCC/NKCC2 signalling network is one of the fundamental regulatory pathways involved in ion homeostasis. We therefore tested the expression of the *WNK1* gene and *WNK1*-related genes in our experimental animal groups to identify if these genes could be related to the pathology of DKD. Alterations in the gene expression of *WNK1* were identified in RNA-seq analysis from kidneys of the experimental mouse groups con, Vhl $^{\Delta PT}$, con/STZ and Vhl $^{\Delta PT}$/STZ. RNA-seq dataset revealed higher mRNA levels for *WNK1* in Vhl $^{\Delta PT}$ mice and specially in con/STZ and Vhl $^{\Delta PT}$/STZ mice as well as higher mRNA levels for several genes related to ionic transport regulation like *kcnj1* (ROMK), *slc12a3* (NCC), *slc12a2* (NKCC2), *scnn1a* (α-ENaC) and *WNK4* (Figure 3.9).

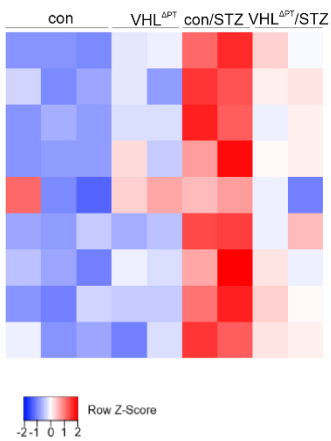

gene	protein	function
WNK1	WNK1	regulation of electrolyte homeostasis, cell proliferation
WNK4	WNK4	positive regulation of NCC
Slc12a1	NKCC2	reabsorption of sodium, potassium and chloride ions
Slc12a3	NCC	reabsorption of sodium and chloride ions
Nedd4-2	NEDD4-2	negative regulation of NCC, ENaC and WNK1
Kcnj1	ROMK	regulation of potassium secretion and blood pressure
Klhl3	KLHL3	ubiquitination of WNK1 and WNK4
Trpv5	TRPV5	regulation of calcium homeostasis
Scnn1	ENaC	mediation of sodium reabsorption and fluid balance

Figure 3.9. Altered WNK1 expression between con, Vhl $^{\Delta PT}$, con/STZ and Vhl $^{\Delta PT}$/STZ. *Heaptmap significant altered gene expression between con, Vhl $^{\Delta PT}$, con/STZ and Vhl $^{\Delta PT}$/STZ groups, based on filtering criteria DESeq P-Values ≤ 0,05, x-fold change ≥ 1,5. Genes were selected after its functionality in proximal tubule in the categories regulation of electrolyte homeostasis, cell proliferation and regulation of sodium, potassium and chloride ions (AG Theilig).*

3.3.6 Analysis of WNK1 transcriptional regulation

3.3.6.1 Verification of WNK1 antibody

The WNK1 antibody used in the experiments that correspond to this section of the thesis was verified using CRIPSR/Cas technik in the cell line HEK293T. Blots reveal a band at ~250 kDa corresponding to the molecular weight of L-WNK1 and a lower band likely for the KS-WNK1.

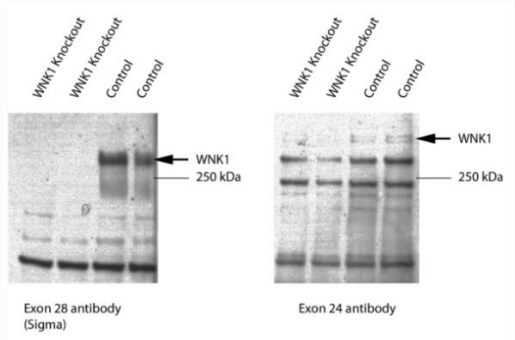

Fig. 3.10. Validation of WNK1 antibody. *Immunoblots showing total amount of WNK1 in HEK293T control cells and in WNK1 knockout cells. Validation of Pan-WNK1 antibody (Sigma) against exon 28 and WNK1 antibody against exon 24 using CRISPR/Cas in HEK293T cells. (AG Theilig).*

3.3.6.2 WNK1 localization in the adult murine kidney

WNK1 is encoded by a gene located on chromosome 12, extends over more than 150 kb, contains 28 exons and generates two transcripts termed L-wnk1 and Kidney-Specific wnk1 (Ks-wnk1). The BaseScope method was used to determine the distribution of mRNA transcripts of *L-wnk1* in cortex and medulla of the kidney of adult mice. WNK1 protein localization was

determined by immunohistochemical analysis. For the establishment of the localization of *L-wnk1* transcripts in the glomeruli, podocin, integrin-α-8 and renin were used for cell-type identification. Podocin was used as marker of podocytes and is exclusively localized to the slit diaphragm, integrin-α-8 was used as marker for mesangial cells and renin as marker for juxtaglomerular cells. *L-wnk1* mRNA puncta (red) could be detected in podocytes, confirmed by staining slices with podocin (Figure 3.11; A). Also mesangial cells were positive for *L-wnk1* mRNA puncta confirmed by staining with integrin-α-8 (Figure 3.11; B). Juxtaglomerular cells, confirmed by staining with renin, presented also evidence of *L-wnk1* mRNA puncta (Figure 3.11; C. Results of WNK1 staining in mouse glomeruli using confocal microscopy, showed that WNK1 (green) is expressed in the cytoplasma of glomerular podocytes. Synaptopodin was used as a marker for podocytes (Figure 3.11; D). A strong WNK1 expression was observed in the cytoplasma of mesangial cells. Integrin-α-8, was used as a marker for mensangial cells. Also in juxtaglomerular cells, WNK1 expression could be detected in the cytoplasma (figure 3.11; E). Renin, which is expressed in vesicles in juxtaglomerular cells (red) was used as a marker for this type of cell (Figure 3.11; F).

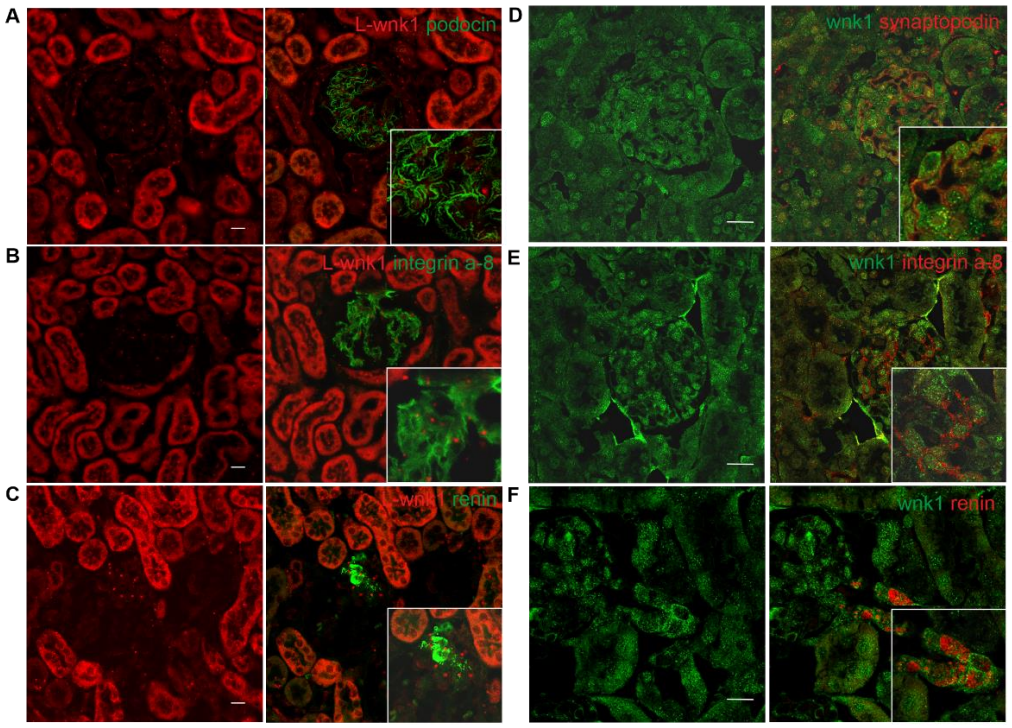

Fig. 3.11. WNK1 localization in the adult murine kidney. *A-C) Representative confocal images of cortex of paraffin kidney sections of adult WT mice, labeled using BaseScope for L-wnk1 targeting exon 2. L-wnk1 mRNA expresssion colocalized in podocytes (A), mesangial cells (B) and in renin cells (C). D-F) Representative confocal images of cortex of paraffin kidney sections of adult ks-wnk1 knockout mice, labeled using anti-WNK1 antibody (green) against amino acid range 1611-1630 of the rat WNK1*

protein. Localization of WNK1 protein in podocytes (D), mesangial cells (E) and in renin cells (F). Scale bar 20 µm.

L-wnk1 mRNA puncta could also be detected in S1 and S2 segments of the mouse proximal tubule, with megalin (green) used as a marker for proximal tubule cells (Figure 3.12; A). BaseScope analysis of *L-wnk1* mRNA in thick ascending limb of Henle´s loop, revealed a strong *L-wnk1* mRNA expression in TAL. The bumetanide-sensitive Na-K-2Cl cotransporter (NKCC2) was used as marker for cells of thick ascending limb of Henle´s loop (Figure 3.12; B). *L-wnk1* mRNA puncta (red) could also be detected in distal tubule cells. As a marker for distal tubule cells was used sodium-chloride cotransporter (NCC) (Figure 3.12; C). Expression of *L-wnk1* mRNA trancripts was also found in collecting duct cells with AQP2 as marker for collecting duct cells (Figure 3.12; D).

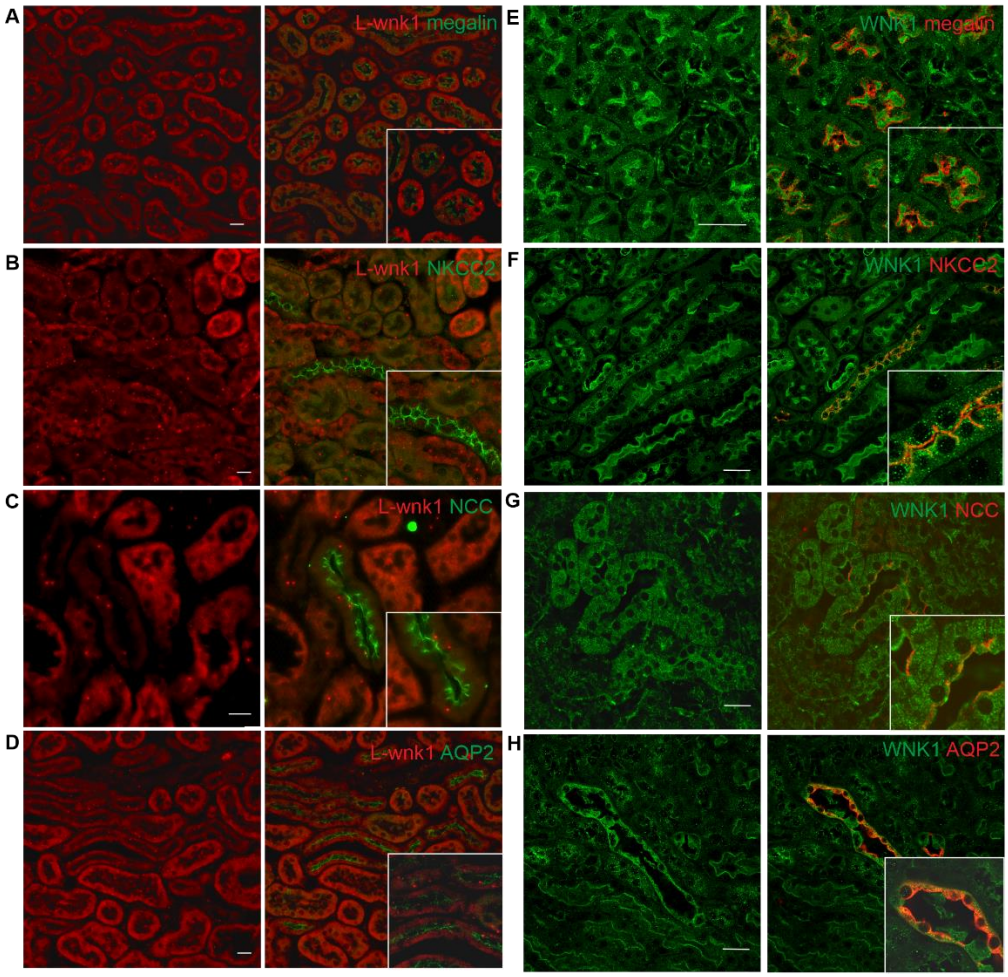

Fig. 3.12. WNK1 localization in the adult murine kidney. *A-D) Representative confocal images of cortex and medulla of kidney sections of adult WT mice, labeled using BaseScope for L-wnk1 targeting Exon 2. A) L-wnk1 mRNA expresssion colocalized on proximal tubule cells (megalin in green). B) L-wnk1 mRNA expression colocalized on thick ascending limb of Henle´s loop (NKCC2 in green). C) L-wnk1 mRNA expression colocalized on distal tubule cells (NCC in green). D) L-wnk1 mRNA expression in collecting duct cells (AQP2 in green). E-H) Representative confocal images of cortex and medulla of kidney*

sections of adult ks-wnk1 K.O mice, using anti-WNK1 antibody (green) against amino acid range 1611-1630 of the rat WNK1 protein. E) Localization of WNK1 (green) in the S1 segment of proximal tubules with megalin as proximal cell tubule marker (red). F) Localization of WNK1 (green) in thick ascending *limb of Henle´s loop with NKCC2 as marker for TAL cells (red). G) Localization of WNK1 (green) in distal tubule with NCC as marker for distal tubule cells (red). H) Localization of WNK1 (green) in collecting duct cells with AQP2, a marker for principal cells (red). Scale bar 20 µm.*

WNK1 protein expression was also found in proximal tubules stained with WNK1 (green) and megalin (red) (Figure 3.12; E). Immunofluorescence labeling for WNK1 (green) and the Na-K-2Cl cotransporter (red) in thick ascending limb of Henle´s loop, revealed a strong expression of WNK1 in cytoplasma and nuclei of cells that belong to the thick ascending limb of Henle´s loop (Figure 3.12; F). Staining of WNK1 (green) and NCC (red) in mouse distal tubule cells, revealed also a strong expression of WNK1 in cytoplasma of distal tubule cells (Figure 3.12; G). Collecting duct cells, stained with AQP2 (red), which localizes to the apical side of principal cells of collecting duct, showed abundant cytosolic expression of WNK1 (Figure 3.12; H).

3.3.6.3 Increased expression of L-wnk1 in the PT of Vhl $^{\Delta PT}$ and Vhl $^{\Delta PT}$/STZ mice

Examination of the results of the BaseScope analysis of L-wnk1 in cortex of control mice and Vhl $^{\Delta PT}$, con/STZ and Vhl $^{\Delta PT}$/STZ mice, showed that there is an increase in *L-wnk1* mRNA puncta in proximal tubule cells of Vhl $^{\Delta PT}$ mice compared to control mice (Figure 3.13). In contrast to the increase seen in the Vhl $^{\Delta PT}$ group, no increase was observed in the STZ group. However, proximal tubule cells from Vhl $^{\Delta PT}$/STZ mice showed also an increase in *L-wnk1* mRNA puncta compared to control mice.

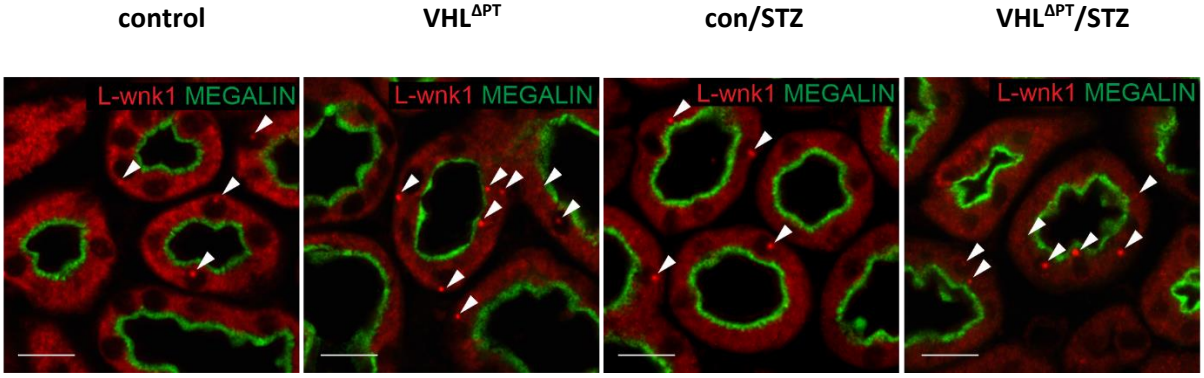

Fig. 3.13. Expression of L-wnk1 in cortex of control, Vhl $^{\Delta PT}$, con/STZ and Vhl $^{\Delta PT}$/STZ mice. *A) Representative Confocal images of L-wnk1 (red) and megalin (green) as a marker of proximal tubule cells, from paraffin sections from control group (con), Vhl $^{\Delta PT}$, con/STZ and Vhl $^{\Delta PT}$/STZ mice. Scale bar: 20 µm.*

3.3.6.4 Increased expression of ks-wnk1 mRNA in TAL and distal tubules of con/STZ and Vhl $^{\Delta PT}$/STZ mice

The analysis of the BaseScope results of ks-wnk1 in cortex of control mice and Vhl $^{\Delta PT}$, con/STZ and Vhl $^{\Delta PT}$/STZ mice, revealed in the first place no increase in the Ks-wnk1 mRNA puncta in cells of TAL of Vhl $^{\Delta PT}$ mice compared to control mice. However, a strong increase was observed in ks-wnk1 mRNA puncta in the STZ group and in the Vhl $^{\Delta PT}$/STZ group compared to control group. Examination of Ks-wnk1 mRNA puncta in distal tubule cells of control mice and Vhl $^{\Delta PT}$, con/STZ and Vhl $^{\Delta PT}$/STZ mice revealed similar results as seen in TAL. No increase was observed in the Vhl $^{\Delta PT}$ group compared to control group, but a strong increase was observed in Ks-wnk1 mRNA puncta in the STZ group and in the Vhl $^{\Delta PT}$/STZ group compared to control group (Figure 3.14).

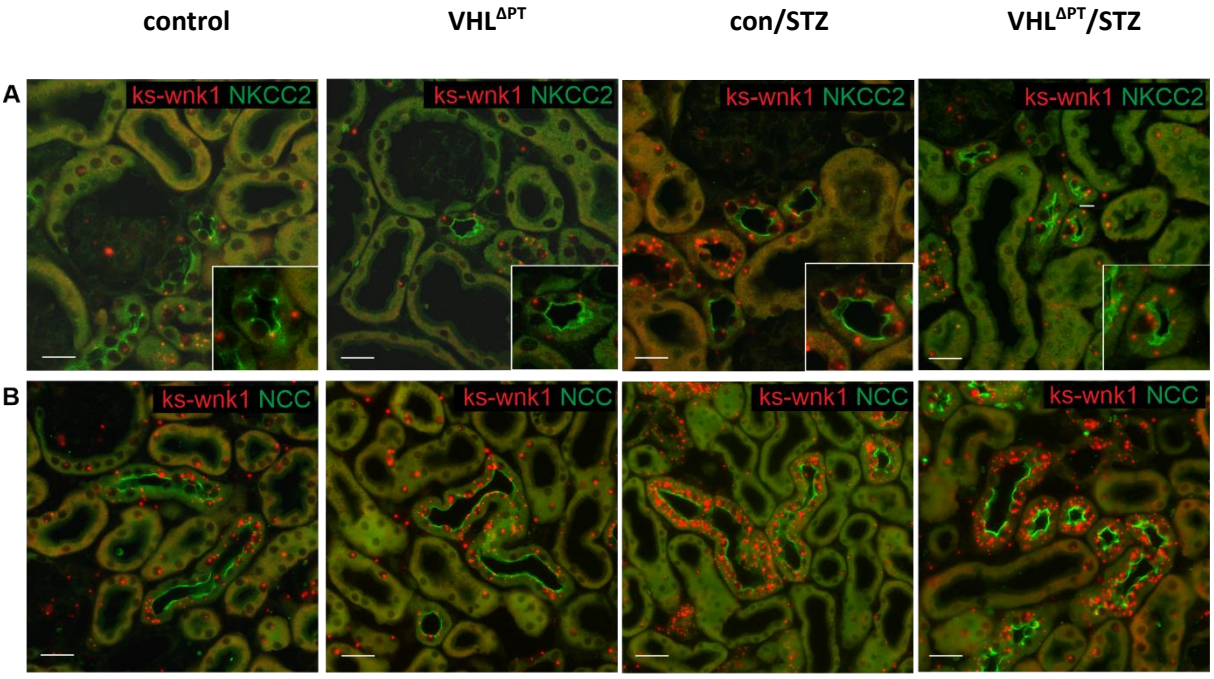

Fig. 3.14. Expression of ks-wnk1 in cortex of control, Vhl $^{\Delta PT}$, con/STZ and Vhl $^{\Delta PT}$/STZ mice. *A) Representative confocal images of ks-wnk1 (red) and NKCC2 (green) as a marker of thick ascending limb of Henle´s loop, from paraffin sections from control group (con), Vhl $^{\Delta PT}$, con/STZ and Vhl $^{\Delta PT}$/STZ mice. B) Confocal images of ks-wnk1 (red) and NCC (green) as a marker of distal tubule cells, from paraffin sections from control group (con), Vhl $^{\Delta PT}$, con/STZ and Vhl $^{\Delta PT}$/STZ mice. Scale bar: 20 µm.*

3.3.6.5 Increased mRNA expression of wnk1 (L-wnk1 and Ks-wnk1) in diabetic mice

mRNA was isolated from kidneys from con, Vhl $^{\Delta PT}$, con/STZ and Vhl $^{\Delta PT}$/STZ mice and the expression of wnk1 was assesed by real time RT-PCR (TaqMan). As shown in figure 3.15 the expression of wnk1 was significantly higher in the diabetic groups compared to control group.

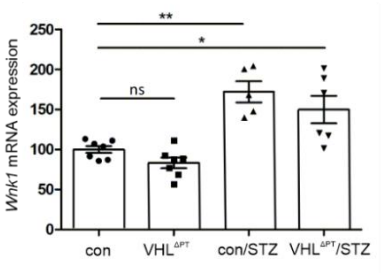

Fig. 3.15. Wnk1 (L-wnk1 and Ks-wnk1) mRNA expression by real-time RT-PCR (TaqMan). *Wnk1 mRNA expression in con, Vhl $^{\Delta PT}$, con/STZ and Vhl $^{\Delta PT}$/STZ mice, n= 6-7, *P < 0,05 **P < 0,01. Mann-Whitney test.*

3.3.6.6 Increased expression of WNK1 in proximal tubules of Vhl $^{\Delta PT}$ mice and in distal tubules of con/STZ and Vhl $^{\Delta PT}$/STZ mice

After establishing a differential WNK1 expression pattern at transcriptional level performed by BaseScope and real-time RT-PCR analysis, WNK1 regulation was next analyzed at protein level in con, Vhl $^{\Delta PT}$, con/STZ and Vhl $^{\Delta PT}$/STZ mice by IHC using a WNK1 antibody recognizing aminoacids 1611-1630 of the rat WNK1 sequence. As depicted in figure 2.16; A), the expression of WNK1 in proximal tubules was increased in Vhl $^{\Delta PT}$ group compared to control group. WNK1 expression showed no difference between control group and con/STZ and Vhl $^{\Delta PT}$/STZ groups. In distal tubules, the WNK1 protein expression did not differ in the Vhl $^{\Delta PT}$ group compared to the control group. However, the WNK1 expression was notably higher in the con/STZ and Vhl $^{\Delta PT}$/STZ groups compared to the control group (Figure 3.16; B).

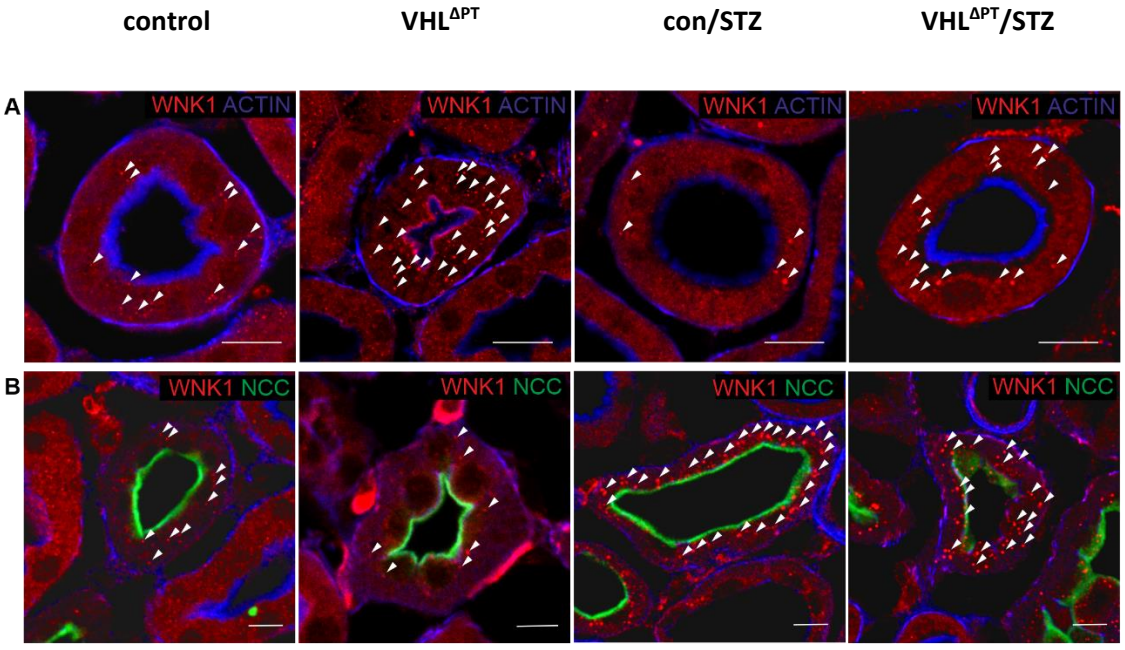

Fig. 3.16. Expression of WNK1 in cortex of control, Vhl $^{\Delta PT}$, con/STZ and Vhl $^{\Delta PT}$/STZ mice. *A) Representative confocal images of WNK1 in proximal tubules of cryo sections of mice from control,*

Vhl $^{\Delta PT}$, con/STZ and Vhl $^{\Delta PT}$/STZ groups. WNK1 (red), Alexa Fluor®647-Phalloidin (blue) as marker for proximal tubules. Scale bar: 10 µm. B) Representative confocal images of WNK1 in distal tubules of cryo sections of mice from control, Vhl $^{\Delta PT}$, con/STZ and Vhl $^{\Delta PT}$/STZ groups. WNK1 (red), NCC (green) as marker for distal tubules. Scale bar: 10 µm.

To confirm the results of the immunohistochemistry analysis of WNK1, Western blotting of WNK1 protein was performed from kidney samples of control, Vhl $^{\Delta PT}$, con/STZ and Vhl $^{\Delta PT}$/STZ mice. Figure 3.17; A) shows a significant increase in protein levels of L-WNK1 in Vhl $^{\Delta PT}$ and con/STZ group compared to the control group. Thus, the highest significant increase of KS-WNK1 protein levels can be observed only in the con/STZ group. Interestingly, the Vhl $^{\Delta PT}$/STZ group undergoes a reduction in L-WNK1 and KS-WNK1 protein levels compared to con/STZ group.

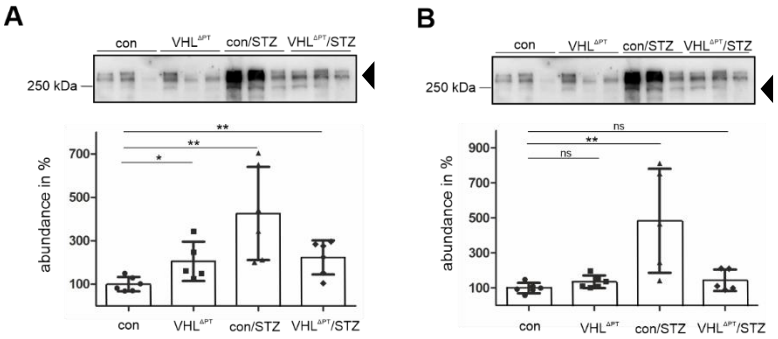

Fig. 3.17. Representative Western blot analysis of L-WNK1 and KS-WNK1. *Western Blot analysis of membrane fractions and quantification of L-WNK1 (A) and KS-WNK1 (B) in control group (con), Vhl $^{\Delta PT}$, con/STZ and Vhl $^{\Delta PT}$/STZ. Values are means ± SD, n= 5-7 per group. *P < 0,05 **P < 0,01. Mann-Whitney test.*

3.3.6.7 Discovery of transcription factor binding sites for L-wnk1 and Ks-wnk1

In order to determine which transcription factors might play a role in the regulation of L-wnk1 and Ks-wnk1 transcription activity, a comparative analysis of putative binding sites of transcription factors was done upon the promoter region of human L-wnk1 (accession no. NG 007984) in the region 4308 to 5507 upstream from the first ATG in exon 1 and human Ks-wnk1 in der region 98952 to 100056 upstream from Exon 4a (accession no. AY319934) using the software tool MatInspector Version 8.0 from Genomatix (Germany). We obtained more than 450 sequences for transcription factor binding sites in the promoter of L-wnk1 and Ks-wnk1. The results of the analysis of the L-wnk1 promoter revealed putative transcription factor binding sites for the transcription factors AP-1, KLF-15, HIF-1, CTCT, YY1, EGR1, PLZF and MAFB. Among some of the transcription factors obtained by the search under the Ks-wnk1 promoter are KLF2, NFAT5, STAT5, GATA-3, Glucocorticoid receptor and p53. A list containing

20 transcription factors that matched the promoter sequence of L-wnk1 and Ks-wnk1 and their consensus binding sites is set as supplemental table and figure 1 and 2 in appendix.

3.3.6.8 L-wnk1 and Ks-wnk1 promoter analysis with Dual-Luciferase Reporter Assay

The dual-luciferase reporter assay allows to determine rapidly and accurately the activity of a given promoter. To avoid variations in gene expression, a commercial *Renilla* luciferase reporter vector, the herpes simplex virus TK promoter pRL-TK (Promega) was chosen for normalization to reach more accurate luminescence values. The luciferase plasmids containing fragments of human L-wnk1 (accession no. NG 007984), ks-wnk1 promoter (accession no. AY319934) and the control vector pGL3-Basic (Promega, Madison, USA) were transfected into OK, medullary TAL and mpkCCD (c14) cells to analyse first the promoter activity of L-wnk1 and Ks-wnk1 at baseline level and under influence of regulatory transcription factors. The OK cell line overexpressing the transcription factor ZBTB16 (PLZF) was done with lentiviral supernatant produced by Dr. Emmanuel Di Valentin (University of Liège, GIGA-Viral Vectors Platform) using ViraSafe™ Lentiviral Packaging System, Pantropic (VPK-206) with TET-On 3G system. OK, mpkCCD (c14) and medullary TAL cells were cultured in growth medium as described in section 1.1.3 of this thesis. To analyse the effect of GATA-3 on L-wnk1 and ks-wnk1 promoter activity, L-wnk1 or Ks-wnk1 were cotransfected in mpkCCD (c14) cells with a plasmid expressing the full-length human GATA-3 (addgene plasmid pcDNA-GATA3 #1332). To assert the effect of human MAFB on L-wnk1 in OK cells, L-wnk1 was cotransfected with a plasmid expressing human MAFB (accession NM_005461). MAFB pcDNA 3.1 was kindly provided by Dr. Celio Pouponnot (Institute Curie centre de recherche, Orsay, France).

3.3.6.9 Base-Line promoter activity of L-wnk1 and Ks-wnk1

The promoter activity of the 1200-bp human L-wnk and the 1191-bp human Ks-wnk1 was detected in opposum kidney epithelial cells and in murine principal kidney cortical collecting duct cells mpkCCD (c14). Figure 3.18; A, showed promoter activity of human L-wnk1 in opposum kidney cells but almost no baseline activity of Ks-wnk1. Detection of L-wnk1 and Ks-wnk1 promoter activity in TAL cells, showed promoter activity of L-wnk1 and Ks-wnk1 promoter but in comparison we observed a reduced promoter activity of Ks-wnk1 (Figure 3.18; B). The detection of L-wnk1 and Ks-wnk1 promoter activity In mpkCCD (c14) cells, showed promoter activity of L-wnk1 and Ks-wnk1 promoter and also reduced promoter activity of Ks-wnk1 compared to L-wnk1 (Figure 3.18; C).

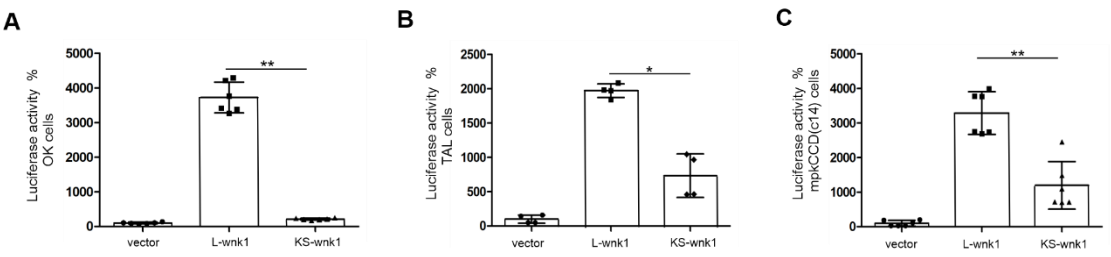

Fig. 3.18. Baseline activity of L-wnk1 and Ks-wnk1 promoters in cultured cells. *Normalized luciferase activity for constructs containing L-wnk1 and Ks-wnk1 promoter regions upstream from the luciferase gene in OK cells, TAL cells and mpkCCD(c14) cells. The relative luciferase activity of vector (pGL3-Basic) was considered 100. The pRL-TK promoter served as a positive control. Data are means ± SD, n= 4-6 per group. *P < 0,05 **P < 0,01. Mann-Whitney test.*

3.3.6.10 Effect of high glucose in L-wnk1 promoter activity in opossum kidney cells

For the luciferase assay experiments, 5 mM D-Glucose was chosen to keep the cells under normal conditions whereas 25 mM D-glucose was chosen as the optimal concentration of D-glucose to meet the metabolic requirements of the diabetes research. To examine the effect of glucose and hypoxia on L-wnk1 promoter activity, L-wnk1 transfected opossum kidney cells were estimulated with 25 mM glucose for 24 h and incubated 24h at 3% O_2 (hypoxia) and at 5% CO_2 (normoxia). Figure 3.19; A shows L-wnk1 luciferase activity in opossum kidney cells after 25 mM glucose estimulation under normoxic and hypoxic conditions. On normoxic conditions, the promoter activity of L-wnk1 was significantly reduced when cells where incubated with 25 mM glucose. On the contrary, L-wnk1 promoter activity was significantly increased when cells were incubated at hypoxic conditions (figure 3.19; A).

3.3.6.11 Effect of ZBTB16 on L-wnk1 promoter activity

The transcription factor ZBTB16 also known as PLZF (promyelocytic leukemia zinc finger) is another transcription factor that is object of investigation in this chapter. Protein expression of ZBTB16 was significantly increased in the Vhl $^{\Delta PT}$ group compared to the control group and also was significantly increased in the group con/STZ compared to the control group. In order to analyze the effect of ZBTB16 on L-wnk1 gene expression, a stable opossum kidney cell line was used that constitutively express ZBTB16 after addition of doxycycline (5 µg/ml) . As a control was used the opposum kidney cell line transfected with GPF as a reporter gene with and without addition of doxycycline. Doxycycline (5 µg/ml) was added to the cells after reaching 90% confluency. Cell medium was changed after 24h and new doxycycline was given to the cells to secure the effectivity of the induction of ZBTB16. Figure 3.19; B shows the result of ZBTB16 expression on L-wnk1 promoter activity. L-wnk1 activity showed no significant

changes in cells transfected with the GFP construct after doxycicline estimulation. Surprisingly, cells expressing ZBTB16 after induction with doxycicline showed a significant increase in the L-wnk1 luciferase activity.

3.3.6.12 Effects of GATA-3 on L-wnk1 promoter activity

GATA-3 is a member of the zink-finger transcription factors involved primarily in cell development and differentiation. In figure 3.19;C, analysis of the L-wnk1 promoter activity in mpkCCD (c14) cells showed a significant reduction in L-wnk1 luciferase activity when cells were co-transfected with GATA-3.

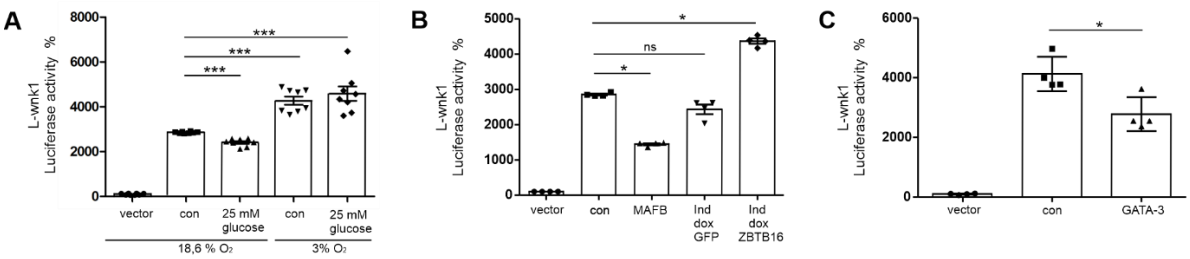

Fig. 3.19. L-wnk1 promoter activity in OK, OK LV and mpkCCD (c14) cells. *A) Normalized luciferase activity in OK cells transfected with L-wnk1 promoter construct after estimulation with 25 mM glucose for 24 h at normoxic conditions (18.6% O2 and 5% CO2) and at hypoxic conditions (3% O2 and 5% CO2). B) Normalized luciferase activity in OK cells transfected with L-wnk1 promoter construct and a control vector or plasmid expressing human MAFB and in OK LV cells after doxycycline-dependent induction of GFP or ZBTB16. C) Normalized luciferase activity in mpkCCD (c14) cells transfected with L-wnk1 promoter construct and a control vector or plasmid expressing human GATA-3.The relative luciferase activity of vector (pGL3-Basic) was considered 100. The pRL-TK promoter served as a positive control. Data are means ± SD, n= 4-8 per group. *P < 0,05 ***P < 0,001. Mann Whitney test.*

3.3.6.13 Effect of high glucose and hypoxia on Ks-wnk1 promoter activity

To examine the effect of glucose and hypoxia on Ks-wnk1 promoter activity, Ks-wnk1 transfected mpkCCD (c14) cells were incubated 24h at 3% O_2 and 5% CO_2 after stimulation with 5 mM o 25 mM D-glucose. Figure 3.20; A shows the Ks-wnk1 luciferase activity in mpkCCD (c14) cells after 25 mM glucose estimulation under hypoxic conditions. The promoter activity of Ks-wnk1 was significantly increased when cells where incubated with 25 mM glucose under hypoxic conditions. In addition, Ks-wnk1 promoter activity was significantly increased when cells were incubated at 3% O_2 and 5% CO_2 (hypoxic conditions) compared to cells incubated at 18.6% O_2 and 5% CO_2 (normoxic conditions).

These results indicate that glucose and hypoxia may induce upregulation of ks-wnk1 in distal and cortical collecting duct cells. To analyze the function of the transcription factor GATA-3 on

Ks-wnk1 promoter activity, Ks-wnk1 plasmid was contransfected with a plasmid expressing the full-length human GATA-3 (addgene plasmid pcDNA-GATA3 #1332) in mpkCCD(c14) cells. Figure 2.20; B) shows the result of GATA-3 expression on Ks-wnk1 promoter activity. Ks-wnk1 activity showed a significant reduction when mpkCCD (c14) cells were co-transfected with GATA-3. These results are indicative that the transcription factor GATA-3 may have a negative regulatory effect on Ks-wnk1 at transcriptional level.

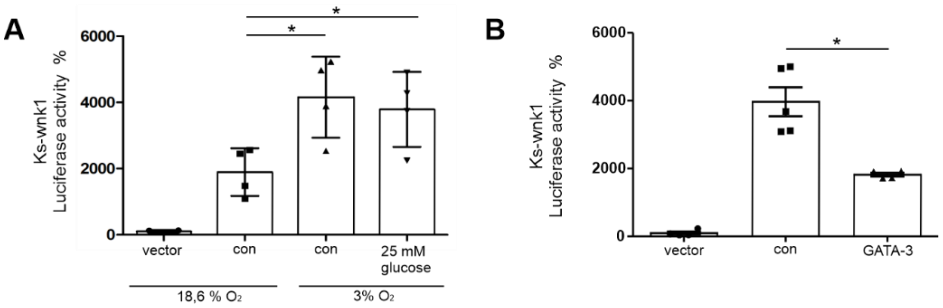

Fig. 3.20. Ks-wnk1 promoter activity in mpkCCD(c14) cells. *A) Normalized luciferase activitiy in mpkCCD (c14) cells transfected with Ks-wnk1 promoter construct after estimulation with 25 mM glucose for 24 h at normoxic conditions (18.6% O2 and 5% CO2) and at hypoxic conditions (3% O2 and 5% CO2). B) Normalized luciferase activity in mpkCCD (c14) cells transfected with Ks-wnk1 promoter construct and a control vector or plasmid expressing human GATA-3. The relative luciferase activity of vector (pGL3-Basic) is considered 100. The pRL-TK promoter served as a positive control. Data are means ± SD, n= 4-8 per group. *P < 0,05 ***P < 0,001. Mann Whitney test.*

3.3.7 *Vhl*-deletion modifies the expression of genes known to ameliorate DKD

The results of the RNA sequencing between the con/STZ group and the $VHL^{\Delta PT}$/STZ group showed that the gene expression profile in con/STZ was notably altered compared to the control group. The impact of Vhl deletion on con/STZ had as a consequence that the gene expression profile of $VHL^{\Delta PT}$/STZ analyzed by RNA sequencing, does not differ considerably from the control group. Therefore, genes were sought in the $VHL^{\Delta PT}$/STZ group, that could play a role in the improvement seen in this experimental group compared to the con/STZ group. Among the strongest candidates for further analysis were selected the genes *Nr3c1*, *Klotho* and *Zbtb16.* Figure 3.21 shows a heatmap of genes significantly upregulated in the $VHL^{\Delta PT}$ group compared to the control group. The majority of the genes listed in figure 3.21 are strongly upregulated in the $VHL^{\Delta PT}$ group compared to the control group.

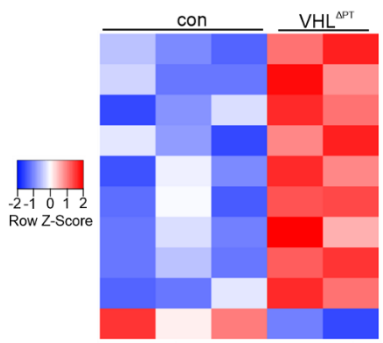

gene	protein	function
Skil	Ski-Related Oncogene	suppresses diabetic nephropathy
Cxcl14	C-X-C Motif Chemokine Ligand 14	inhibits proinflammatory cytokines
Prox1	Prospero Homeobox 1	differentiation of mTAL, lymphangiogenesis
Irs2	Insulin receptor substrate 2	improves hemodynamic and TGF, glycogen degradation
Nr3c1	Glucocorticoid receptor	antifibrotic in diabetes
Kl	Klotho	ameliorates diabetic nephropathy
Zbtb20	Zinc finger and BTB domain containing protein 20	repressing gluconeogenesis
Tfpi2	Tissue factor pathway inhibitor 2	suppressing proliferation and migration
Pfkp	Phosphofructokinase, platelet	rate-determining enzyme of glycolysis
Bmp4	Bone morphogenic protein 4	ROS production, inflammation, endothelial dysfunction

Fig. 3.21. Altered gene expression between con and Vhl $^{\Delta PT}$. *Heatmap representation of significantly changed genes between control and VHL$^{\Delta PT}$ mice, based on filtering criteria DESeq P-Values ≤ 0,05, x-fold change ≥ 1,5. (AG Theilig).*

Based on the RNA sequencing results, the protein expression of the glucocorticoid receptor and klotho was next analyzed by immunofluorescence and Western blot analyses. The protein expression of glucorcoticoid receptor resulted to be higher in the nuclei of the proximal tubules and in the distal tubule of VHL$^{\Delta PT}$ compared to control mice (Figure 3.22; A). However the expression of the glucocorticoid receptor was reduced in the con/STZ and VHL$^{\Delta PT}$/STZ groups compared to the control mice. Klotho was found to be significantly higher in distal tubules and connecting tubules of VHL$^{\Delta PT}$, con/STZ and VHL$^{\Delta PT}$/STZ groups compared to control mice (Figure 3.22; B). The protein expression of the glucocorticoid receptor, klotho and ZBTB16 in con, VHL$^{\Delta PT}$, con/STZ and VHL$^{\Delta PT}$/STZ groups was also analyzed by western blotting. The results of the western blot analysis show a significant reduction of glucocorticoid receptor protein expression in the con/STZ and VHL$^{\Delta PT}$/STZ groups compared to control mice (Figure 3.23; A). Klotho was significantly increased in the VHL$^{\Delta PT}$ and con/STZ and VHL$^{\Delta PT}$/STZ groups compared to the control group (Figure 3.23; B). Analysis of ZBTB16 protein expression showed a significant increase in the VHL$^{\Delta PT}$ and con/STZ groups compared to the control group. Interestingly, the *Vhl* knockout in the STZ-induced diabetic group revealed a significant reduction in the nuclear expression of the transcription factor ZBTB16 (Figure 3.23; C).

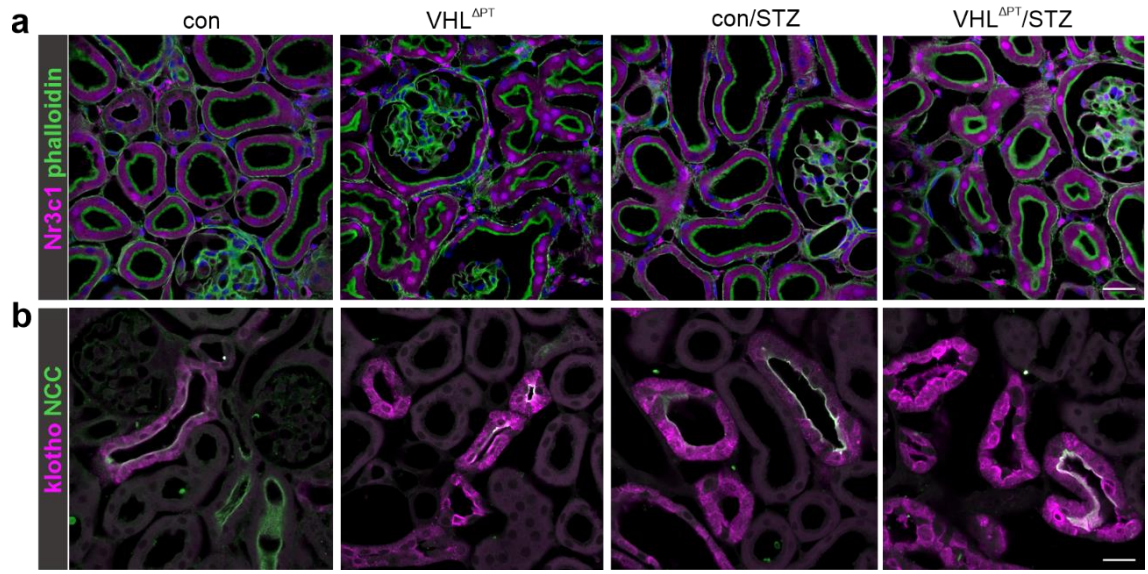

Fig. 3.22. Expression of glucorticoid receptor and Klotho in proximal and distal tubules of control, Vhl $^{\Delta PT}$, con/STZ and Vhl $^{\Delta PT}$/STZ mice. *(a) Representative confocal images of immunhistochemical fluorescence stainings of Nr3c1 (magenta) and actin (green) as marker from proximal tubule and DAPI (blue) as marker for nuclei, from 5 µm cryo sections from control group (con), Vhl $^{\Delta PT}$, con/STZ and Vhl $^{\Delta PT}$/STZ mice. (b) Representative confocal images of immunhistochemical fluorescence stainings of klotho (magenta) and NCC (green) as marker for distal tubules, from 5 µm cryo sections from control group (con), Vhl $^{\Delta PT}$, con/STZ and Vhl $^{\Delta PT}$/STZ mice. Scale bar: 20 µm.*

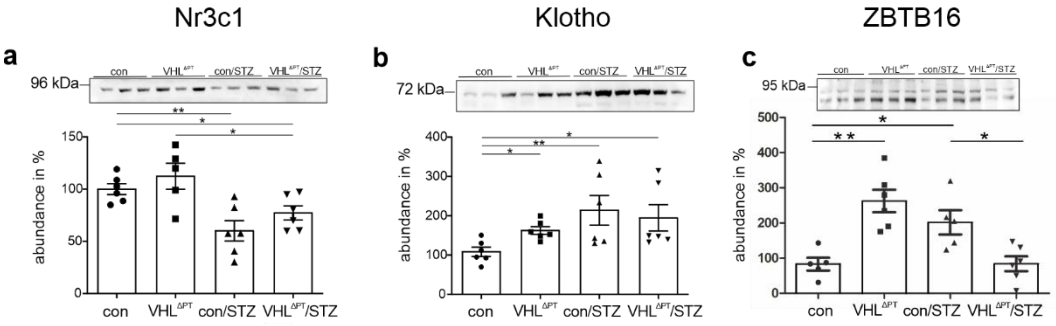

Fig. 3.23. Representative Western blots of Glucocorticoid receptor, Klotho and ZBTB16. *Western Blot analysis of nuclear fractions and quantification of Glucocorticoid receptor, (a) Klotho (b), ZBTB16 (c) in control group (con), Vhl $^{\Delta PT}$, con/STZ and Vhl $^{\Delta PT}$/STZ. Values are means ± SEM, n= 5-7 per group. *P < 0,05 **P < 0,01.Kruskal-Wallis/Dunn´s Test.*

3.4 Discussion

DKD is a multifactorial disease with a complex genetic background. A better understanding of epigenetics and transcriptional control is necessary to develop new strategies to slow the progression or to prevent the onset of diabetic kidney disease and renal failure in diabetic patients. The pathophysiology of the early diabetic kidney involves glomerular hyperfiltration and albuminuria, exposing the proximal tubule to an elevated workflow, growth and promoting cellular stress, inflammation and hypoxia.

3.4.1 Pathophysiology of the diabetic kidney disease

DKD is characterized by a serie of major structural changes in the glomerulus, including glomerular basement membrane thickening, mesangial expansion and reduced glomerular filtration surface density [178]. The thickening of the glomerular basal membrane is one of the most characterized changes in DKD. Several lines of evidence have supported the idea that increased synthesis of basement membrane components such as Type IV collagen might contribute to the thickening of the GBM [179]. Another important pathological change of DKD is mesangial expansion. The stimulation of certain growth factors and cytokines as a consequence of hyperglycemia, AGEs and oxidative stress as well as increased matrix secretion and cell enlargement are considered factors driving mesangial expansion. Numerous studies have shown that increased renal expression of TGF-β is associated with mesangial expansion and glomerulosclerosis [180]. One interesting debate topic in diabetes was centred in which cell type is more susceptible to injury due to high glucose levels. It has been suggested that the expression of glucose transporters is determinant for the toxic effects of glucose from the extracellular compartment specially in proximal tubular cells [181]. A metabolic switch from fatty acid oxidation and gluconeogenesis toward glycolysis is one of the specific cellular effects induced by high-glucose concentrations observed in acute and chronic kidney injury [182]. In an experimental STZ-induced diabetes model, the finding of proximal tubular cell defects without previous or concomitant glomerular lesions, suggest that proximal tubule injury may be a primary event in DKD.

A substantial reduction in proximal tubular uptake of albumin was also observed in streptozotocin-diabetic rats [183] indicating that altered tubular albumin reuptake is an important factor for albuminuria in early stages of DKD. In that context, urinary proteins such as albumin, transferrin and immunoglobulin G can stimulate proximal tubule cells to synthetize pro-inflammatory molecules and chemokines. For instance, albumin has been

shown to induce interleukin-8 [184] and two other NF-κB-dependent proinflammatory genes such as, RANTES and monocyte chemotactic protein 1 (MCP-1) [185, 186].

The increase in the GFR observed in the early pathogenesis of DKD, has been considered an important factor for kidney damage due to a rise in intraglomerular pressure and renal blood flow [187]. There is growing evidence that the proximal tubule can be involved in early stages of DKD. Thus, the tubular theory proposes that changes in the tubule system inhibit tubuloglomerular feedback due to increased glucose reabsorption rates, which also leads to enhanced reabsorption of sodium, chloride and fluid, reducing this way the amount of sodium and chloride that in normal conditions is delivered to the macula densa. Under normal conditions, the amount of glucose reaching the macula densa is insignificant after 99% of the filtered glucose is reabsorbed in the S1-S3 segments of the proximal tubule [188]. When the glucose concentration at the macula densa rises as a consequence of hyperglycemia, the SGLT1 in the cells of the macula densa, senses glucose to regulate the production of nitric oxide (NO) by NO synthase 1 (NOS1). The increase in the amounts of glucose stimulate the production of NO inhibiting TGF responsiveness and promotes the increase in the GFR [189, 190]. In our STZ-induced DKD mice model, we could show that increased NHE3 and NKCC2 expression led to a reduced sodium delivery to the macula densa which contributed to enhance the GFR. Furthermore, an increase in NOS1 expression was indicative of saturation of glucose transport and further increased the GFR. An increase in the abundance of NKCC2 had also been observed in previous studies in rats with STZ-induced type 1 diabetes mellitus via NAPDH oxidase and PKC [191, 192]. *Vhl*-deletion in the proximal tubule of mice before induction of diabetes, resulted in lower proximal and distal expression of tubular transporters and decreased NOS1 levels in the $VHL^{\Delta PT}$/STZ group compared to the con/STZ group. The increased urinary excretion of sodium and glucose observed in these animals is in agreement with several other studies that related the excretion of this solutes into the urine to a tubular disability [193, 194].

3.4.2 Cellular HIF stabilization

In normoxia, pVHL is a master regulator of HIF-1α proteolytic degradation. The VHL-HIF-1α interaction is highly conserved between species and the absence of pVHL results in HIF-α stabilization, metabolic reprogramming through upregulation of glycolytic metabolism and upregulation of HIF target genes [195, 196]. In this work it could be demonstrated that *Vhl*-deletion in the proximal tubule of the mouse results in HIF stabilization. The results of the RNA sequencing and protein analysis of the kidneys of *Vhl*-knockout mice showed increased

expression levels of mRNA as well as increased nuclear HIF1a expression in the treated groups $VHL^{\Delta PT}$, con/STZ and $VHL^{\Delta PT}$/STZ. This data is consistent with previous reports of augmented renal HIF as a result of adaptation to hypoxia in diabetic rats [197]. There is enough evidence to support a protective role of HIF in renal diseases (including DKD). An interesting observation of the correlation of HIF-1α stabilization and cell damage comes from a study in experimental acute renal failure where the induction of HIF in tubular and endothelial cells inversely correlates with tissue damage [198]. Although tubulointerstitial fibrosis is present at end stages of many forms of kidney diseases, including diabetic nephropathy, the accumulation of fibrotic material is one of the determinants to the progression of kidney disease [199]. Accumulated evidence has shown that HIF-1α activation is a strong regulator of fibrosis under various pathological conditions. Several *Vhl*-conditional knockout mouse models have demonstrated that HIF accumulation in collecting ducts and distal tubules promotes the development of interstitial fibrosis [166, 200]. Also in early diabetic retinopathy animal models, positive expression of HIF-1α in the retinal ganglion cell layer and concomitantly increased VEGF expression, correlated with disease progression [201].

3.4.3 Tubuloglomerular crosstalk

Glomerular hyperfiltration has been considered one of the primary events in the course of DKD but events such as tubular growth, hyperreabsorption and tubuloglomerular communication indicates a primary role of the proximal tubule in the pathogenesis of the diabetic kidney disease. As a result of functional changes in the proximal tubule cells, accompanied by morphological and ultrastructural events, it is essential that variations in the gene expression patterns within these tubular cells are understood in the onset of DKD. In our experimental animal model, we have observed through RNA sequencing of kidney samples that the deletion of *Vhl* in the proximal tubule induces alterations in certain glomerular and tubular expressed genes known to be altered in previous studies. Changes in the integrity of the glomerular basement membrane (GBM) contribute to alterations in the glomerulus and its permeability to macromolecules [202]. Among the genes upregulated in *Vhl*-deleted PT and STZ-induced type 1 diabetes we found Nid2, Lamc1, Col4a3 and Col4a5. Alterations in the synthesis and structure of the extracellular matrix as well as increased collagen IV levels associated with hyperglycemia and insulin resistance have been previously reported in diabetes mellitus [203]. Interestingly, upregulation of basement membrane proteins (COL4A1, COL4A2, LAMC1, NID1, NID2 and HSPG2) has been observed on the artery proteome in patients type 2 diabetes mellitus [204]. Angiogenesis and vasculogenesis is a hallmark of DKD.

We found significant upregulation of Ptprb and Ogt mRNA levels and downregulation of Ctss levels in Vhl-deleted PT and STZ-induced type 1 diabetes. These genes are known to be involved in vascular changes during diabetes mellitus. Ptprb is expressed in the renal endothelium and Ptprb transcript and protein levels are strongly upregulated in the microvasculature of diabetic kidney models [205]. *Ogt* is a gene coding for the O-linked β-N-acetylglucosamine transferase (OGT), an enzyme that adds the GlcNAc moiety to acceptor proteins [206]. Emerging findings have strongly suggested a role of protein O-GlcNAcylation in the pathogenesis and progression of T2DM [207]. In this context, protein O-GlcNAcylation was demonstrated to alter the function in vascular smooth muscle and endothelial cells contributing to vascular remodelling in patients with T2DM [208]. The reduced Ctss mRNA levels found in the experimental groups $VHL^{\Delta PT}$ and con/STZ is in line with lower cathepsin S expression observed in renal biopsies from patients with diabetes. However diabetes and cardiovascular diseases are associated with increased plasma levels of the cysteine protease cathepsin S. Increased cathepsin S levels have been identified with vascular diseases and overall mortality in population-based cohort studies [209]. Furthermore, increased amounts of cathepsin S in endothelial cells and macrophages have been linked to microvascular complications in diabetes [210]. We also identified genes that regulate epithelial morphology and function, including genes for cell polarity, stress, transport, metabolism and endocytosis. Genes that regulate cell polarity and are involved in renal development such as Notch1, Btdb7 and Fryl were found upregulated in the $VHL^{\Delta PT}$, con/STZ and $VHL^{\Delta PT}$/STZ group. The NOTCH pathway is a decisive pathway for developmental angiogenesis and NOTCH1 has been proposed to maintain vascular homeostasis [211]. Aberrations in NOTCH1 signaling have been found in STZ-mouse models of type 1 diabetes mellitus [212] as well as in *db/db* type 2 diabetic mice [213] indicating that Notch plays an important functional role in the development of DKD. Further studies have suggested that persistent NOTCH1 pathway activation leads to podocyte damage and kidney failure [214]. In this context, inhibition of the Notch pathway by gamma secretase inhibitors, has been shown to ameliorate fibrosis and prevent proteinuria and basement membrane thickening in different rodent models [215, 216]. Genes shown to be involved in hypoxic, oxidative or osmotic stress such as *Hif1a*, *Nox4*, *Rictor* and *Nfat5* were also found altered in the experimental groups compared to the control group. Consistent with this result, Nox4 protein expression was shown to be increased in diabetic kidney cortex compared with non-diabetic controls and mediated hypertrophy and fibronectin expression in a rat model of T1DM induced by STZ [217]. Increased evidence has suggested that Nox1 and Nox4 upregulation is required for the microvascular complications in diabetes [218]. *Nfat5* is

a known regulator of the adaptive response to oxidative stress and inflammation and has a protective role under normal conditions. Upregulation of *Nfat5* has been observed during complications of diabetes such as DKD and diabetic retinopathy [219, 220]. Furthermore, we identified an increase in mRNA levels of an important set of genes involved in epithelial transport including Slc9a3 (coding for NHE3) and Slc12a1 (coding for NKCC2). As discussed above, DKD is associated with sodium retention and expanded extracellular fluid volume. An increase of NHE3 in diabetes has been reported in human studies of type 1 and hypertensive patients with type 2 diabetes, where a 20% increase in proximal tubular reabsorption of sodium was observed as well as in vivo rodent models of diabetes mellitus using STZ.

3.4.4 Differentially altered gene expression of WNK1 upon genetic proximal tubular *Vhl*-deletion and after STZ-induced type 1 diabetes

The results of the RNA sequencing of kidney samples from all experimental groups revealed slightly elevated levels of Slc12a1 mRNA (coding for NKCC2) in *Vhl*-depleted mice and a higher expression level in the con/STZ group compared to the control group. Moreover, NKCC2 levels expressed apically in TAL were significantly higher in $VHL^{\Delta PT}$ and significantly increased in both diabetic groups. Alterations in fluid and electrolyte balance have been frequently observed in patients with diabetes mellitus. The higher expression of sodium transporters observed in con/STZ mice compared to $VHL^{\Delta PT}$/STZ mice, supports the theory that the tubuloglomerular feedback mechanism (TGF) is dysregulated in DKD and leads to glomerular hyperfiltration. Numerous studies have provided strong evidence that increased sodium reabsorption through sodium-chloride cotransporter (NCC) in the distal convoluted tubule (DCT) and sodium-potassium-chloride cotransporter (NKCC2) in the thick ascending limb of Henle´s loop is regulated by WNK1 and WNK4 kinases [221, 222]. We therefore decide to analyze the gene expression of WNK1 and WNK1-related genes in our hypoxia and diabetes animal models. Interestingly, $VHL^{\Delta PT}$ mice demonstrated higher levels of WNK1 and WNK4 kinases whereas con/STZ mice showed the strongest differences in the WNK kinases compared to control mice. A similar result was observed in genes mediating sodium reabsorption. Thoroughly, higher levels of *Slc12a1* (coding for NKCC2), *Slc12a3* (coding for NCC) and *Scnn1* (coding for ENaC) were observed in $VHL^{\Delta PT}$ mice and strong differences in con/STZ mice compared to control mice. These results are consistent with increased NKCC2 mRNA expression and increased mRNA and protein expression of NCC observed in mice with a diet-induced obesity [223, 224]. Increased ENaC mRNA expression has also been reported in studies with human and animals suggesting an association of diabetes and DKD with increased ENaC activity and protein

expression [225, 226]. In the last twenty years, the majority of the studies on WNK1 have been centered in their role in hypertension and kidney function. There are two main WNK1 transcripts in the kidney, a long transcript (L-WNK1) and a shorter transcript without kinase activity (KS-WNK1) exclusively expressed in the distal nephron under the control of a different promoter [227]. The different expression pattern of the KS-WNK1 isoform in the kidney and the absence of a kinase domain suggest that L-WNK1 and KS-WNK1 might be regulated by different mechanisms. In our study, *Vhl*-depletion resulted in increased L-WNK1 transcripts in proximal tubule cells in $VHL^{\Delta PT}$ compared to control mice. In both groups with STZ-induced diabetes, higher distal expression of KS-WNK1 was observed compared to the control group. Several *in vitro* studies on L-WNK1 localization have been focused to stablish novel regulatory functions for L-WNK1. It has been discovered that L-WNK1 overlaps with some cell structures and proteins such as clathrin-coated vesicles and autophagy interacting proteins suggesting that the L-WNK1 pathway may affect important cell processes including endocytosis, growth and proliferation [228, 229].

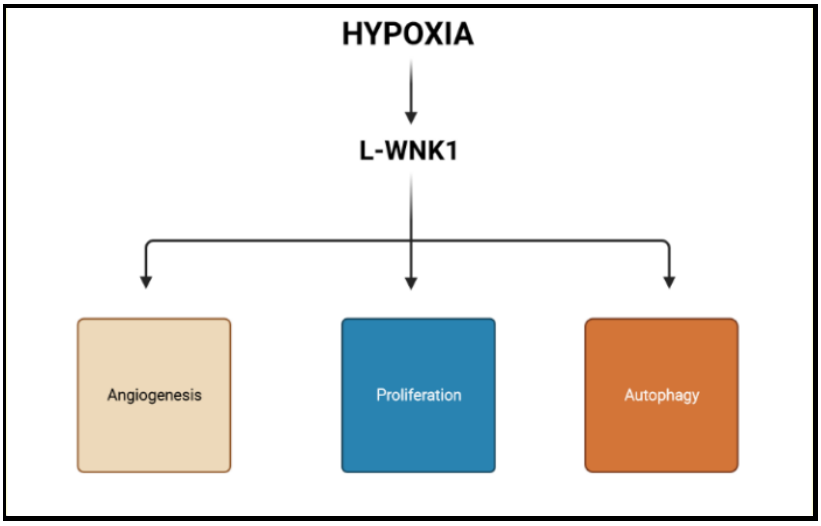

Fig 3.24. Possible pathological impacts of L-WNK1 in diabetic kidney disease*. L-WNK1 might regulate the expression of various signaling pathways involved in different aspects of controlling cell processes to hypoxic stress in DKD.*

Hypoxia is an important regulator of VEGF gene expression, which is essential for endothelial cell differentiation and development of new capillaries from pre-existing vessels [230]. There is also strong evidence that WNK1 is required for regulation of angiogenesis and vascular remodeling. WNK1 homozygous knockout mice presented endothelial defects and died during embryonic development due to impaired angiogenesis [231]. It has also been proposed that WNK1 might induce angiogenesis through regulation of factors that promote angiogenesis such as Slug, VEGF and matrix metallo-proteinases. Besides the induction of angiogenesis in

proximal tubule cells, L-WNK1 might play an important role in the regulation of cell proliferation and autophagy in diabetes. A key feature in patients with diabetes is kidney hypertrophy. Cellular proliferation and hypertrophy of proximal tubular epithelial cells has been previously reported in diabetes and mostly attributed to hyperglycemia-induced oxidative stress and elevated growth factors [189, 232]. Although many mechanisms are involved in this process, a detailed understanding of this particular phenotype is still lacking. The WNK1 axis has been shown to support tumor malignancy through regulation of cell proliferation in cancer cells [233]. Furthermore, effects of WNK1 in cell proliferation have been reported in in vitro experiments with vascular smooth muscle cells where overexpression of WNK1 led to accelerated cell cycle transition form G_1 to S phase [234]. The process of autophagy has been shown to be highly induced in type 1 diabetes mellitus. We have demonstrated that ZBTB16 acts as a negative regulator of autophagy. Several studies have suggested that WNK1 participates in the regulation of autophagy [228]. L-WNK1 increase in proximal tubule cells in $VHL^{\Delta PT}$ mice, might be a manifestation of the response to hypoxia to counteract the mechanism of autophagy initiation. The increase of KS-WNK1 in TAL and DT of con/STZ and $VHL^{\Delta PT}$/STZ mice may result from differential transcriptional regulation of Ks-wnk1 in these cells independently of the hypoxia effect. It is possible that the pathological role of KS-WNK1 in TAL und DT cells render the pleiotropic roles of L-WNK1 in these cells.

3.4.5 L-WNK1 and KS-WNK1 promoter analysis

Gene transcriptional regulation is controlled by a different set of regulatory factors. Gene expression patterns are mainly regulated by upstream and/or downstream elements that serve as a binding site for multiple transcription factors. The results of the analysis of a promoter fragment of 1200 bp, upstream from the first ATG in exon 1 of the WNK1 gene, specific for the full-length transcript of L-WNK1 revealed numerous consensus transcription factor binding sites including AP-1, HIF-1, CTCT, YY1, EGR1, ZBTB17 and MAFB which are associated with kidney diseases. Among the transcription factor binding sites found in the analysis of a promoter fragment present in intron 4 and specific for the kidney specific defective isoform (KS-WNK1) were found KLF2, NFAT5, STAT5, GATA-3 and p53. We tested the human transcription factors ZBTB16, MAFB and GATA-3 on the promoter activity of L-WNK1 and KS-WNK1 and found that ZBTB16 enhanced the transcription of L-WNK1 while MAFB and GATA-3 both showed downregulation of the transcription of L-WNK1 and KS-WNK1 in the luciferase assays. The role of MAFB in kidney disease is not well characterized but its activity could be related to increased oxidative stress. Indication of a protective role of MAFB in

diabetic nephropathy has been suggested in a study of STZ-induced diabetic mice overexpressing MAFB in podocytes [235]. This effect was observed through increased transcriptional regulation of gluthatione peroxidase 3 and Nephrin. Despite its role in the development of the kidney [236], little is known about the role of GATA-3 in the adult kidney. A recent study reported GATA-3 is increased by hyperglycemia and mediates tissue inflammation [237]. However the downregulation of L-WNK1 and KS-WNK1 by GATA-3 might have beneficial effects in the DKD. Although there is no clear evidence that L-WNK1 and KS-WNK1 have different functional roles, one of the explanations of the observed increased expression of L-WNK1 in the proximal tubule in hypoxia and increased expression of KS-WNK1 in TAL in diabetes, might be the existence of two proximal promoters with distinct transcription binding sites. CpG methylation at promoter regions is another factor that might contribute to epigenetic modification affecting the recruitment of transcription factors. These epigenetic mechanisms might be the cause of changes in gene expression and phenotype in diabetes. There is evidence of aberrant DNA methylation of genes regulated in the proximal tubule of *db/db* mice [238].

3.4.6 *Vhl*-deletion modifies the expression of genes known to ameliorate DKD

The analysis of genes differentially expressed in the experimental group with proximal tubule *Vhl* deletion, revealed a group of genes upregulated in $VHL^{\Delta PT}$ compared to control mice whose related proteins might result protective against DKD. The glucocorticoid receptor is a nuclear hormone receptor that is expressed in most cell types and has a critical role in many disease states. Thus, the roles of glucocorticoids and GR signaling in kidney diseases is very intricate. We observed increased mRNA levels of *Nr3c1* in mice with *Vhl* deletion compared to control mice. Analysis of protein expression of the GR indicated increased expression of GR in the nuclei of proximal tubule cells and to a lesser extent in distal tubule cells of animals with Vhl-deletion compared to control littermates and reduced expression level in the con/STZ and $VHL^{\Delta PT}$/STZ groups. A positive role for the GR was reported in a mouse model with podocyte-specific deletion of the glucocorticoid receptor. Control mice showed decreased proteinuria compared to GR knockout mice after glomerular injury [239]. Besides its role as negative regulator of vascular inflammation, endothelial GR performs anti-fibrotic effects by targeting the Wnt signalling pathway [240]. A functional enhancement of glucocorticoid signalling in hypoxic conditions might be possible due to its association with inflammatory processes [241]. Hypoxia might be able to produce an effect on GR mRNA and protein levels either through nuclear translocation of the GR or by binding of HIF1 to HREs in the Nr3c1 promotor [242].

Our results are in line with the hypothesis that enhanced glucocorticoid activity in hypoxia is mediated through an increase in the GR expression. Klotho is a multifunctional protein involved in processes such as cell senescence, antioxidant response and renal fibrosis, thus the mechanism underlying the function and signalling pathways of klotho are controversial. Klotho is predominantly expressed in renal tubules, parathyroid glands and choroid plexus of the brain and may function as a paracrine or endocrine hormone [243]. The klotho gene was described to have anti-aging properties. In this context, Klotho deficiency in mice resulted in premature aging, arteriosclerosis and skin atrophy [244]. Decreased serum and urine Klotho levels are associated with vascular aging and endothelial dysfunction, two hallmarks of cardio-renal complications in diabetes. Furthermore, a renoprotective activity has also been reported in various rodent models of acute kidney injury and chronic kidney disease [245]. The upregulation of Klotho in our *Vhl*-depleted mice compared to control mice, suggests that hypoxia might ameliorate DKD by upregulating Klotho in epithelial tubular cells.

3.4.7 HIF-stabilization preconditions the kidney against diabetes-induced changes

Alterations of renal metabolism have been observed under situations of systemic metabolic disorders for example in hyperglycaemic and lipidemic conditions. Hyperglycaemia may induce cellular hypoxia, a key event in the pathogenesis of diabetic kidney disease. As a consequence of tissue hypoxia, HIF induces the expression of various genes related to energy metabolism but how these metabolic alterations affect the progression of DKD is still unknown. Studies have suggested that alterations in energy metabolism caused by increased energy metabolic flux and accumulation of glucose metabolites in diabetic kidneys are probably linked to mitochondrial disfunction [246]. In a STZ-induced diabetes mellitus rat model, HIF stabilization led to downregulation of fatty-acid and amino-acid metabolism and to upregulation of glycolysis which are considered beneficial effects to reverse the metabolic alterations observed in the diabetic renal tissue [247].

In our experimental model, we have demonstrated that *Vhl*-deletion before induction of diabetes prevents the changes in gene expression observed in STZ-induced diabetes mellitus that are responsible for the pathophysiology of the DKD. We analysed the gene expression profile in the four experimental groups through gene ontology enrichment analysis and found that in the $VHL^{\Delta PT}$/STZ group histone lysine modification, peptidyl-lysine methylation and histone modification were terms strongly altered in this group compared to the control group (AG Theilig, data not shown). By comparing the genes significantly altered in the $VHL^{\Delta PT}$/STZ group with respect to the con/STZ group in our RNA Seq data, we obtained lower expression

of Slc12a1, Abca13 and Zbtb16. The promyelocytic leukemia zinc finger (PLZF), also known as ZBTB16 (Zinc finger and BTB domain containing 16) is a transcriptional regulator with effects on growth, self-renewal and differentiation [248].

PLZF has been involved in the pathogenesis of metabolic diseases. The importance of PLZF in adipogenesis was confirmed by a study showing that increased expression of ZBTB16 in brown adipocytes, led to induction of genes involved in fatty acid oxidation, glycolysis and mitochondrial function [249]. There are also multiple lines of evidence that indicates that PLZF has a critical role in the pathogenesis of hypertension, cardiac hypertrophy and fibrosis [250]. According to data from a spontaneously hypertensive rat experimental model, mutations in the *Plzf* gene are associated with gene alterations that can affect intracellular pathways important for the regulation of the cell energetic status [251]. Analysis of the involvement of PLZF in energy metabolism has also been carried out in *db/db* mice and cultured liver cells, where the effect of downregulation of PLZF was beneficial for the metabolic disease. In these experiments was demonstrated that PLZF has the ability to promote gluconeogenic gene expression increasing glucose output and leading to hyperglycemia, whereas knockdown of ZBTB16 improved glucose homeostasis in the db*/db* mice [252]. Another study in *db/db* mice, showed an association between the downregulation of ZBTB16 and upregulation of autophagy [253]. The dysregulation of the autophagy process might contribute to the progression of DKD. Enhanced ZBTB16 activity has been implicated in negative regulation of autophagy through ubiquitination and degradation of Atg14L, a key factor in the autophagy process [254]. The negative regulation of autophagy by ZBTB16 has also been demonstrated in an OK/LV cell cultured model, where the induction of ZBTB16 led to downregulation of LC3II, another key element necessary to trigger cell autophagy (AG Theilig unpublished data). In this context, the physiologic induction of autophagy through downregulation of the *Plzf* gene may be effective to reduce the progression of DKD. As mentioned before in this chapter, multiple pathophysiological processes are involved in the progression of DKD, but the mechanisms leading to the pathogenesis of diabetic complications and the interaction between them still remain poorly understood. A large number of pharmacological studies have been conducted to obtain an effective treatment against the incidence of DKD and its associated cardiovascular risks. The Renin-angiotensin-aldosterone system (RAAS) blockade using angiotensin-converting-enzyme (ACE) inhibitors and angiotensin-receptor blockers is one of the fundamental therapies of DKD and has shown positive effects in type 1 and 2 diabetes mellitus patients. Angiotensin-receptor blockers have shown to have antialbuminuric effects und have demonstrated clinical efficiency in type 2 diabetes patients [255].

In addition to therapies based on classical mechanisms, two novel antihyperglycemic drugs, sodium-glucose cotransporter 2 inhibitors and glucagon-like peptide-1 receptor agonists (GLP-1RA) have emerged as renoprotective agents in DKD. The effects of SGLT2 inhibitors are caused by blocking the reabsorption of filtered glucose in the proximal tubule with the consequence of decreased glycated haemoglobin (HbA1c) and increased urinary glucose excretion. SGLT2 inhibitors and GLP-1RA have been suggested to modulate renal hemodynamics, reduce inflammation and preserve the renal function by attenuating hyperfiltration and reducing proteinuria [256, 257]. However, the genetic and pathologic heterogeneity of patients with diabetes mellitus may be the reason why monotherapies with insulin, metformin or dapaglifozin has not been able to reduce the progression of DKD in many cases. In the onset of type 1 diabetes mellitus, combined therapeutical targeting of immune and β-cell axis with SGLT2 inhibitors might be of great benefit for the pathological consequences of this diabetic state [258]. A combined therapy might delay the progression to DKD in type 2 diabetes mellitus patients based on two aspects. On one hand, based on the different action sites of SGLT2 inhibitors and RAAS inhibitors and second, through the potential synergistic effects of the combined intervention. Because reduction of AGEs has been a powerful measure to ameliorate the complications of diabetes via effects on ROS formation, new strategies have emerged such as treatment with cross-link breakers of the advanced glycation end products. In experimental models of diabetic complications, the direct targeting of AGEs has led to reduce UAE, blood pressure and attenuated glomerulosclerosis and proteinuria [259]. Alagebrium (ALT-711) represents one example of a direct AGE inhibitor whose administration in *db/db* mice has resulted in improvement of large-vessel elasticity, decrease in peripheral resistance and attenuation of renal fibrosis [260]. In our study of genetic PT *Vhl* deletion in STZ-induced type 1 diabetic mice, we could find an association between HIF-1 stabilization and preservation of renal function and prevention of the morphological pattern of glomerular and tubular lesions. Our observations are in consonance with recent studies using HIF stabilizers which have been shown to normalize GFR in STZ-treated rats [167] and reduce albuminuria and to ameliorate glomerular and endothelial damage in obese type 2 diabetic mice [261]

Most importantly, we could demonstrate that PT *Vhl*-deletion prior to induction of diabetes, normalized the metabolism and ameliorated the abnormal expression of genes observed in diabetic mice by histone modification and chromatin remodeling suggesting that HIF-1α stabilization preconditions the kidney against DKD. This nephroprotective effect of HIF-1 stabilizers could have implications in the pharmacological management of type 1 diabetes.

4. Conclusion

Numerous diseases are associated with protein kinases as they regulate many signaling pathways that trigger physiological and pathological processes. Based on extensive body of research around protein kinase structure and cellular mode of action, kinases have emerged as major drug targets in the field of disease treatment. The lipid kinase VPS34 has been implicated in cancer, neurodegenerative disorders and metabolic disease and is a key regulator of metabolism, autophagy and endocytosis. We have highlighted that the molecular landscape of the proximal tubule is controlled by the PI3-kinase VPS34. Our characterization of conditional VPS34 depleted mice revealed impaired nutrient signaling caused by transporter regulation, phosphorylation of the retromer complex and exocytotic inhibition of galectin 3 and 9 and increased abundance of beta oxidation, reduced gluconeogenesis and usage of glutamine for energy consumption. Interestingly, we also discovered a strong antiviral response through induction of antiviral proteins and reduction of the virus receptor ACE-2. The in vitro inhibition of VPS34 marked a strong reduction of SARS-CoV-2 infection based on swift rewiring of glutamine metabolism. Though the control that VPS34 exerts over the cell may be a significant factor for metabolic interventions in certain diseases, the unwilling effects of targeting VPS34 in the kidney as a drug should led repurpose the use of VPS34 inhibitors in the future.

Diabetic kidney disease is a kidney complication caused by diabetes mellitus leading to augmentation of renal tubular transport, growth and hypoxia. The identification of the early factors that lead to diabetic kidney disease is critical to develop new therapeutic strategies against the onset of DKD and the progression to chronic kidney disease and renal failure. The proximal tubule is emerging as a central player in the early events of diabetic kidney. Our results confirmed that glomerular hyperfiltration is related to tubular hyperreabsorption, abnormal growth of the proximal tubule and tubuloglomerular communication. Based on the results of our diabetic PT-Vhl-deficient mouse model, we demonstrated that in diabetic mice, renal function, morphology and metabolism is preserved upon HIF-1α stabilization as a result of genetic reprogramming. For a better understanding of the contribution of hypoxia to the diabetic kidney disease environment, we analyzed the molecular signature of proximal tubule cells and the genetic profile of the diabetic kidney under HIF-1α stabilization. We found that PT Vhl-deletion, ameliorated glomerular and endothelial damage by inducing alterations in genes related to glomerular and tubular morphology and function. Our study found genes

showing differential histone modification and chromatin remodeling leading to a precondition of the kidney against the development of DKD.

We also found alterations in the WNK1 gene. These results suggest that the WNK1 might have, beyond the regulation of electrolyte and fluid homeostasis, related actions in angiogenesis, autophagy and proliferation. These new findings could make the WNK1 kinase and HIF-1 stabilizers an additional therapeutical option to prevent DKD.

References

1. Grahammer, F., et al., *mTOR Regulates Endocytosis and Nutrient Transport in Proximal Tubular Cells.* J Am Soc Nephrol, 2017. **28**(1): p. 230-241.

2. Haase, V.H., et al., *Vascular tumors in livers with targeted inactivation of the von Hippel-Lindau tumor suppressor.* Proc Natl Acad Sci U S A, 2001. **98**(4): p. 1583-8.

3. Wang, T., et al., *Role of NHE isoforms in mediating bicarbonate reabsorption along the nephron.* Am J Physiol Renal Physiol, 2001. **281**(6): p. F1117-22.

4. Gluck, S.L., et al., *Physiology and biochemistry of the kidney vacuolar H+-ATPase.* Annu Rev Physiol, 1996. **58**: p. 427-45.

5. Weiner, I.D. and J.W. Verlander, *Role of NH3 and NH4+ transporters in renal acid-base transport.* Am J Physiol Renal Physiol, 2011. **300**(1): p. F11-23.

6. Goltzman, D., *Physiology of Parathyroid Hormone.* Endocrinol Metab Clin North Am, 2018. **47**(4): p. 743-758.

7. Traebert, M., et al., *Luminal and contraluminal action of 1-34 and 3-34 PTH peptides on renal type IIa Na-P(i) cotransporter.* Am J Physiol Renal Physiol, 2000. **278**(5): p. F792-8.

8. Bacic, D., et al., *The renal Na+/phosphate cotransporter NaPi-IIa is internalized via the receptor-mediated endocytic route in response to parathyroid hormone.* Kidney International, 2006. **69**(3): p. 495-503.

9. Ekberg, K., et al., *Contributions by kidney and liver to glucose production in the postabsorptive state and after 60 h of fasting.* Diabetes, 1999. **48**(2): p. 292-8.

10. Meyer, C., et al., *Renal substrate exchange and gluconeogenesis in normal postabsorptive humans.* Am J Physiol Endocrinol Metab, 2002. **282**(2): p. E428-34.

11. Meyer, C., et al., *Relative importance of liver, kidney, and substrates in epinephrine-induced increased gluconeogenesis in humans.* American Journal of Physiology-Endocrinology and Metabolism, 2003. **285**(4): p. E819-E826.

12. McGuinness, O.P., et al., *Impact of chronic stress hormone infusion on hepatic carbohydrate metabolism in the conscious dog.* Am J Physiol, 1993. **265**(2 Pt 1): p. E314-22.

13. Tiwari, S., et al., *Deletion of the insulin receptor in the proximal tubule promotes hyperglycemia.* J Am Soc Nephrol, 2013. **24**(8): p. 1209-14.

14. Sasaki, M., et al., *Dual Regulation of Gluconeogenesis by Insulin and Glucose in the Proximal Tubules of the Kidney.* Diabetes, 2017. **66**(9): p. 2339-2350.

15. Legouis, D., et al., *Renal gluconeogenesis: an underestimated role of the kidney in systemic glucose metabolism.* Nephrol Dial Transplant, 2022. **37**(8): p. 1417-1425.

16. Mettlen, M., et al., *Regulation of Clathrin-Mediated Endocytosis.* Annu Rev Biochem, 2018. **87**: p. 871-896.

17. Ferguson, S.M., et al., *Coordinated Actions of Actin and BAR Proteins Upstream of Dynamin at Endocytic Clathrin-Coated Pits (vol 17, pg 811, 2009).* Developmental Cell, 2010. **18**(2): p. 332-332.

18. O'Sullivan, M.J. and A.J. Lindsay, *The Endosomal Recycling Pathway-At the Crossroads of the Cell.* Int J Mol Sci, 2020. **21**(17).

19. Grant, B.D. and J.G. Donaldson, *Pathways and mechanisms of endocytic recycling.* Nat Rev Mol Cell Biol, 2009. **10**(9): p. 597-608.

20. Swanson, J.A., *Shaping cups into phagosomes and macropinosomes.* Nature Reviews Molecular Cell Biology, 2008. **9**(8): p. 639-649.

21. Junemann, A., et al., *A Diaphanous-related formin links Ras signaling directly to actin assembly in macropinocytosis and phagocytosis.* Proc Natl Acad Sci U S A, 2016. **113**(47): p. E7464-E7473.

22. Swanson, J.A. and S. Yoshida, *Macropinosomes as units of signal transduction.* Philosophical Transactions of the Royal Society B-Biological Sciences, 2019. **374**(1765).

23. Birn, H. and E.I. Christensen, *Renal albumin absorption in physiology and pathology.* Kidney Int, 2006. **69**(3): p. 440-9.

24. Kerjaschki, D. and M.G. Farquhar, *The Pathogenic Antigen of Heymann Nephritis Is a Membrane Glycoprotein of the Renal Proximal Tubule Brush-Border.* Proceedings of the National Academy of Sciences of the United States of America-Biological Sciences, 1982. **79**(18): p. 5557-5561.

25. Zou, Z., et al., *Linking receptor-mediated endocytosis and cell signaling: evidence for regulated intramembrane proteolysis of megalin in proximal tubule.* J Biol Chem, 2004. **279**(33): p. 34302-10.

26. Nagai, M., et al., *The adaptor protein ARH escorts megalin to and through endosomes.* Molecular Biology of the Cell, 2003. **14**(12): p. 4984-4996.

27. Gallagher, H., et al., *The adaptor disabled-2 binds to the third psi xNPxY sequence on the cytoplasmic tail of megalin.* Biochimie, 2004. **86**(3): p. 179-82.

28. Morris, S.M., et al., *Myosin VI binds to and localises with Dab2, potentially linking receptor-mediated endocytosis and the actin cytoskeleton.* Traffic, 2002. **3**(5): p. 331-41.

29. Morris, S.M., et al., *Dual roles for the Dab2 adaptor protein in embryonic development and kidney transport.* EMBO J, 2002. **21**(7): p. 1555-64.

30. Perez Bay, A.E., et al., *The fast-recycling receptor Megalin defines the apical recycling pathway of epithelial cells.* Nat Commun, 2016. **7**: p. 11550.

31. Limbutara, K., C.L. Chou, and M.A. Knepper, *Quantitative Proteomics of All 14 Renal Tubule Segments in Rat.* Journal of the American Society of Nephrology, 2020. **31**(6): p. 1255-1266.

32. Christensen, E.I., et al., *Endocytic receptors in the renal proximal tubule.* Physiology (Bethesda), 2012. **27**(4): p. 223-36.

33. Storm, T., et al., *Detailed investigations of proximal tubular function in Imerslund-Grasbeck syndrome.* Bmc Medical Genetics, 2013. **14**.

34. He, Q.C., et al., *Amnionless function is required for cubilin brush-border expression and intrinsic factor-cobalamin (vitamin B-12) absorption in vivo.* Blood, 2005. **106**(4): p. 1447-1453.

35. Haraldsson, B., *Tubular Reabsorption of Albumin: It's All About Cubilin.* Journal of the American Society of Nephrology, 2010. **21**(11): p. 1810-1812.

36. Hughes, R.C., *Secretion of the galectin family of mammalian carbohydrate-binding proteins.* Biochim Biophys Acta, 1999. **1473**(1): p. 172-85.

37. Dumic, J., S. Dabelic, and M. Flogel, *Galectin-3: an open-ended story.* Biochim Biophys Acta, 2006. **1760**(4): p. 616-35.

38. Moar, P. and R. Tandon, *Galectin-9 as a biomarker of disease severity.* Cellular Immunology, 2021. **361**.

39. Thijssen, V.L., et al., *Galectin expression in cancer diagnosis and prognosis: A systematic review.* Biochim Biophys Acta, 2015. **1855**(2): p. 235-47.

40. Sheppard, K., et al., *Targeting PI3 kinase/AKT/mTOR signaling in cancer.* Crit Rev Oncog, 2012. **17**(1): p. 69-95.

41. Manning, B.D. and L.C. Cantley, *AKT/PKB signaling: navigating downstream.* Cell, 2007. **129**(7): p. 1261-74.

42. Falasca, M. and T. Maffucci, *Regulation and cellular functions of class II phosphoinositide 3-kinases.* Biochem J, 2012. **443**(3): p. 587-601.

43. Alliouachene, S., et al., *Inactivation of the Class II PI3K-C2beta Potentiates Insulin Signaling and Sensitivity.* Cell Rep, 2015. **13**(9): p. 1881-94.

44. Backer, J.M., *The intricate regulation and complex functions of the Class III phosphoinositide 3-kinase Vps34.* Biochem J, 2016. **473**(15): p. 2251-71.

45. Herman, P.K. and S.D. Emr, *Characterization of VPS34, a gene required for vacuolar protein sorting and vacuole segregation in Saccharomyces cerevisiae.* Mol Cell Biol, 1990. **10**(12): p. 6742-54.

46. Kihara, A., et al., *Two distinct Vps34 phosphatidylinositol 3-kinase complexes function in autophagy and carboxypeptidase Y sorting in Saccharomyces cerevisiae.* J Cell Biol, 2001. **152**(3): p. 519-30.

47. Rostislavleva, K., et al., *Structure and flexibility of the endosomal Vps34 complex reveals the basis of its function on membranes.* Science, 2015. **350**(6257): p. aac7365.

48. Reidick, C., F. Boutouja, and H.W. Platta, *The class III phosphatidylinositol 3-kinase Vps34 in Saccharomyces cerevisiae.* Biol Chem, 2017. **398**(5-6): p. 677-685.

49. Martinez, J., et al., *Molecular characterization of LC3-associated phagocytosis reveals distinct roles for Rubicon, NOX2 and autophagy proteins.* Nat Cell Biol, 2015. **17**(7): p. 893-906.

50. Funderburk, S.F., Q.J. Wang, and Z.Y. Yue, *The Beclin 1-VPS34 complex - at the crossroads of autophagy and beyond.* Trends in Cell Biology, 2010. **20**(6): p. 355-362.

51. Ohashi, Y., et al., *Membrane characteristics tune activities of endosomal and autophagic human VPS34 complexes.* Elife, 2020. **9**.

52. Nemazanyy, I., et al., *Class III PI3K regulates organismal glucose homeostasis by providing negative feedback on hepatic insulin signalling.* Nat Commun, 2015. **6**: p. 8283.

53. Bilanges, B., et al., *Vps34 PI 3-kinase inactivation enhances insulin sensitivity through reprogramming of mitochondrial metabolism.* Nat Commun, 2017. **8**(1): p. 1804.

54. Grieco, G., et al., *Vps34/PI3KC3 deletion in kidney proximal tubules impairs apical trafficking and blocks autophagic flux, causing a Fanconi-like syndrome and renal insufficiency.* Sci Rep, 2018. **8**(1): p. 14133.

55. Christoforidis, S., et al., *The Rab5 effector EEA1 is a core component of endosome docking.* Nature, 1999. **397**(6720): p. 621-625.

56. Futter, C.E., et al., *Human VPS34 is required for internal vesicle formation within multivesicular endosomes.* Journal of Cell Biology, 2001. **155**(7): p. 1251-1263.

57. Siddhanta, U., et al., *Distinct roles for the p110alpha and hVPS34 phosphatidylinositol 3'-kinases in vesicular trafficking, regulation of the actin cytoskeleton, and mitogenesis.* J Cell Biol, 1998. **143**(6): p. 1647-59.

58. Wallroth, A. and V. Haucke, *Phosphoinositide conversion in endocytosis and the endolysosomal system.* J Biol Chem, 2018. **293**(5): p. 1526-1535.

59. Henne, W.M., N.J. Buchkovich, and S.D. Emr, *The ESCRT pathway.* Dev Cell, 2011. **21**(1): p. 77-91.

60. Corvera, S., *Phosphatidylinositol 3-kinase and the control of endosome dynamics: new players defined by structural motifs.* Traffic, 2001. **2**(12): p. 859-66.

61. Itakura, E., et al., *Beclin 1 forms two distinct phosphatidylinositol 3-kinase complexes with mammalian Atg14 and UVRAG.* Mol Biol Cell, 2008. **19**(12): p. 5360-72.

62. Wandinger-Ness, A. and M. Zerial, *Rab proteins and the compartmentalization of the endosomal system.* Cold Spring Harb Perspect Biol, 2014. **6**(11): p. a022616.

63. Gillingham, A.K., et al., *Toward a comprehensive map of the effectors of rab GTPases.* Dev Cell, 2014. **31**(3): p. 358-373.

64. Murray, J.T., et al., *Role of Rab5 in the recruitment of hVps34/p150 to the early endosome.* Traffic, 2002. **3**(6): p. 416-27.

65. Tremel, S., et al., *Structural basis for VPS34 kinase activation by Rab1 and Rab5 on membranes.* Nat Commun, 2021. **12**(1): p. 1564.

66. Li, W.W., J. Li, and J.K. Bao, *Microautophagy: lesser-known self-eating.* Cell Mol Life Sci, 2012. **69**(7): p. 1125-36.

67. Kaushik, S. and A.M. Cuervo, *The coming of age of chaperone-mediated autophagy.* Nat Rev Mol Cell Biol, 2018. **19**(6): p. 365-381.

68. Ohashi, Y., S. Tremel, and R.L. Williams, *VPS34 complexes from a structural perspective.* J Lipid Res, 2019. **60**(2): p. 229-241.

69. Kihara, A., et al., *Beclin-phosphatidylinositol 3-kinase complex functions at the trans-Golgi network.* Embo Reports, 2001. **2**(4): p. 330-335.

70. Russell, R.C., et al., *ULK1 induces autophagy by phosphorylating Beclin-1 and activating VPS34 lipid kinase.* Nature Cell Biology, 2013. **15**(7): p. 741-+.

71. Pyo, K.E., et al., *ULK1 O-GlcNAcylation Is Crucial for Activating VPS34 via ATG14L during Autophagy Initiation.* Cell Reports, 2018. **25**(10): p. 2878-+.

72. Seaman, M.N.J., *The Retromer Complex: From Genesis to Revelations.* Trends Biochem Sci, 2021. **46**(7): p. 608-620.

73. Attar, N. and P.J. Cullen, *The retromer complex.* Adv Enzyme Regul, 2010. **50**(1): p. 216-36.

74. Harterink, M., et al., *A SNX3-dependent retromer pathway mediates retrograde transport of the Wnt sorting receptor Wntless and is required for Wnt secretion.* Nat Cell Biol, 2011. **13**(8): p. 914-923.

75. Raiborg, C., K.O. Schink, and H. Stenmark, *Class III phosphatidylinositol 3-kinase and its catalytic product PtdIns3P in regulation of endocytic membrane traffic.* FEBS J, 2013. **280**(12): p. 2730-42.

76. Rojas, R., et al., *Regulation of retromer recruitment to endosomes by sequential action of Rab5 and Rab7.* J Cell Biol, 2008. **183**(3): p. 513-26.

77. Verges, M., et al., *The mammalian retromer regulates transcytosis of the polymeric immunoglobulin receptor.* Nat Cell Biol, 2004. **6**(8): p. 763-9.

78. Burda, P., et al., *Retromer function in endosome-to-Golgi retrograde transport is regulated by the yeast Vps34 PtdIns 3-kinase.* Journal of Cell Science, 2002. **115**(20): p. 3889-3900.

79. Ruck, A., et al., *The Atg6/Vps30/Beclin 1 ortholog BEC-1 mediates endocytic retrograde transport in addition to autophagy in C. elegans.* Autophagy, 2011. **7**(4): p. 386-400.

80. Gallon, M. and P.J. Cullen, *Retromer and sorting nexins in endosomal sorting.* Biochem Soc Trans, 2015. **43**(1): p. 33-47.

81. Ansell-Schultz, A., et al., *Reduced retromer function results in the accumulation of amyloid-beta oligomers.* Mol Cell Neurosci, 2018. **93**: p. 18-26.

82. Schmelzle, T. and M.N. Hall, *TOR, a central controller of cell growth.* Cell, 2000. **103**(2): p. 253-62.

83. Laplante, M. and D.M. Sabatini, *mTOR signaling in growth control and disease.* Cell, 2012. **149**(2): p. 274-93.

84. Kim, D.H., et al., *MTOR interacts with Raptor to form a nutrient-sensitive complex that signals to the cell growth machinery.* Cell, 2002. **110**(2): p. 163-175.

85. Sarbassov, D.D., et al., *Rictor, a novel binding partner of mTOR, defines a rapamycin-insensitive and raptor-independent pathway that regulates the cytoskeleton.* Current Biology, 2004. **14**(14): p. 1296-1302.

86. Byfield, M.P., J.T. Murray, and J.M. Backer, *hVps34 is a nutrient-regulated lipid kinase required for activation of p70 S6 kinase.* Journal of Biological Chemistry, 2005. **280**(38): p. 33076-33082.

87. Mohan, N., et al., *VPS34 regulates TSC1/TSC2 heterodimer to mediate RheB and mTORC1/S6K1 activation and cellular transformation.* Oncotarget, 2016. **7**(32): p. 52239-52254.

88. Gulati, P., et al., *Amino acids activate mTOR complex 1 via Ca2+/CaM signaling to hVps34.* Cell Metab, 2008. **7**(5): p. 456-65.

89. Yoon, M.S., *Vps34 and PLD1 take center stage in nutrient signaling: their dual roles in regulating autophagy.* Cell Communication and Signaling, 2015. **13**.

90. Munson, M.J., et al., *mTOR activates the VPS34-UVRAG complex to regulate autolysosomal tubulation and cell survival.* EMBO J, 2015. **34**(17): p. 2272-90.

91. Hong, Z., et al., *PtdIns3P controls mTORC1 signaling through lysosomal positioning.* Journal of Cell Biology, 2017. **216**(12): p. 4217-4233.

92. Powis, G., et al., *Wortmannin, a potent and selective inhibitor of phosphatidylinositol-3-kinase.* Cancer Res, 1994. **54**(9): p. 2419-23.

93. Bago, R., et al., *Characterization of VPS34-IN1, a selective inhibitor of Vps34, reveals that the phosphatidylinositol 3-phosphate-binding SGK3 protein kinase is a downstream target of class III phosphoinositide 3-kinase.* Biochem J, 2014. **463**(3): p. 413-27.

94. Ronan, B., et al., *A highly potent and selective Vps34 inhibitor alters vesicle trafficking and autophagy.* Nat Chem Biol, 2014. **10**(12): p. 1013-9.

95. Hoffmann, M., et al., *SARS-CoV-2 Cell Entry Depends on ACE2 and TMPRSS2 and Is Blocked by a Clinically Proven Protease Inhibitor.* Cell, 2020. **181**(2): p. 271-280 e8.

96. Yao, T., et al., *Clinical characteristics of a group of deaths with COVID-19 pneumonia in Wuhan, China: a retrospective case series.* BMC Infect Dis, 2020. **20**(1): p. 695.

97. Shulla, A., et al., *A Transmembrane Serine Protease Is Linked to the Severe Acute Respiratory Syndrome Coronavirus Receptor and Activates Virus Entry.* Journal of Virology, 2011. **85**(2): p. 873-882.

98. Su, H., et al., *Renal histopathological analysis of 26 postmortem findings of patients with COVID-19 in China.* Kidney Int, 2020. **98**(1): p. 219-227.

99. Chen, Z., et al., *SARS-CoV-2 Causes Acute Kidney Injury by Directly Infecting Renal Tubules.* Front Cell Dev Biol, 2021. **9**: p. 664868.

100. Jackson, C.B., et al., *Mechanisms of SARS-CoV-2 entry into cells.* Nature Reviews Molecular Cell Biology, 2022. **23**(1): p. 3-20.

101. Shang, C., et al., *Inhibition of Autophagy Suppresses SARS-CoV-2 Replication and Ameliorates Pneumonia in hACE2 Transgenic Mice and Xenografted Human Lung Tissues.* J Virol, 2021. **95**(24): p. e0153721.

102. Bechtel, W., et al., *Vps34 deficiency reveals the importance of endocytosis for podocyte homeostasis.* J Am Soc Nephrol, 2013. **24**(5): p. 727-43.

103. Doherty, G.J. and H.T. McMahon, *Mechanisms of endocytosis.* Annu Rev Biochem, 2009. **78**: p. 857-902.

104. Royle, S.J., *The cellular functions of clathrin.* Cell Mol Life Sci, 2006. **63**(16): p. 1823-32.

105. Leheste, J.R., et al., *Megalin knockout mice as an animal model of low molecular weight proteinuria.* American Journal of Pathology, 1999. **155**(4): p. 1361-1370.

106. Nielsen, R., et al., *Endocytosis provides a major alternative pathway for lysosomal biogenesis in kidney proximal tubular cells.* Proceedings of the National Academy of Sciences of the United States of America, 2007. **104**(13): p. 5407-5412.

107. Casanova, J.E., et al., *Association of Rab25 and Rab11a with the apical recycling system of polarized Madin-Darby canine kidney cells.* Mol Biol Cell, 1999. **10**(1): p. 47-61.

108. Li, H.W., et al., *Rab4 and Rab11 coordinately regulate the recycling of angiotensin II type I receptor as demonstrated by fluorescence resonance energy transfer microscopy.* Journal of Biomedical Optics, 2008. **13**(3).

109. Yu, C.Y., et al., *Lysosome Dysfunction Enhances Oxidative Stress-Induced Apoptosis Through Ubiquitinated Protein Accumulation in Hela Cells.* Anatomical Record-Advances in Integrative Anatomy and Evolutionary Biology, 2013. **296**(1): p. 31-39.

110. Pan, T., et al., *The role of autophagy-lysosome pathway in neurodegeneration associated with Parkinson's disease.* Brain, 2008. **131**(Pt 8): p. 1969-78.

111. Pu, J., et al., *Mechanisms and functions of lysosome positioning.* J Cell Sci, 2016. **129**(23): p. 4329-4339.

112. Korolchuk, V.I., et al., *Lysosomal positioning coordinates cellular nutrient responses.* Nat Cell Biol, 2011. **13**(4): p. 453-60.

113. Bertovic, I., et al., *Vps34 derived phosphatidylinositol 3-monophosphate modulates megakaryocyte maturation and proplatelet production through late endosomes/lysosomes.* J Thromb Haemost, 2020. **18**(7): p. 1756-1772.

114. Kandasamy, P., et al., *Amino acid transporters revisited: New views in health and disease.* Trends Biochem Sci, 2018. **43**(10): p. 752-789.

115. Xiao, F. and F. Guo, *Impacts of essential amino acids on energy balance.* Mol Metab, 2022. **57**: p. 101393.

116. Seaman, M.N., J.M. McCaffery, and S.D. Emr, *A membrane coat complex essential for endosome-to-Golgi retrograde transport in yeast.* J Cell Biol, 1998. **142**(3): p. 665-81.

117. Burd, C. and P.J. Cullen, *Retromer: A Master Conductor of Endosome Sorting.* Cold Spring Harbor Perspectives in Biology, 2014. **6**(2).

118. Zimprich, A., et al., *A mutation in VPS35, encoding a subunit of the retromer complex, causes late-onset Parkinson disease.* Am J Hum Genet, 2011. **89**(1): p. 168-75.

119. Small, S.A., et al., *Model-guided microarray implicates the retromer complex in Alzheimer's disease.* Ann Neurol, 2005. **58**(6): p. 909-19.

120. Mo, D., et al., *Sialylation of N-linked glycans mediates apical delivery of endolyn in MDCK cells via a galectin-9-dependent mechanism.* Mol Biol Cell, 2012. **23**(18): p. 3636-46.

121. Shafaq-Zadah, M., E. Dransart, and L. Johannes, *Clathrin-independent endocytosis, retrograde trafficking, and cell polarity.* Curr Opin Cell Biol, 2020. **65**: p. 112-121.

122. Chauhan, S., et al., *TRIMs and Galectins Globally Cooperate and TRIM16 and Galectin-3 Co-direct Autophagy in Endomembrane Damage Homeostasis.* Dev Cell, 2016. **39**(1): p. 13-27.

123. Shang, J., et al., *Cell entry mechanisms of SARS-CoV-2.* Proc Natl Acad Sci U S A, 2020. **117**(21): p. 11727-11734.

124. Goodwin, C.M., S. Xu, and J. Munger, *Stealing the Keys to the Kitchen: Viral Manipulation of the Host Cell Metabolic Network.* Trends Microbiol, 2015. **23**(12): p. 789-798.

125. Diamond, M.S. and M. Farzan, *The broad-spectrum antiviral functions of IFIT and IFITM proteins.* Nat Rev Immunol, 2013. **13**(1): p. 46-57.

126. Pasquier, B., *SAR405, a PIK3C3/Vps34 inhibitor that prevents autophagy and synergizes with MTOR inhibition in tumor cells.* Autophagy, 2015. **11**(4): p. 725-726.

127. Schu, P.V., et al., *Phosphatidylinositol 3-kinase encoded by yeast VPS34 gene essential for protein sorting.* Science, 1993. **260**(5104): p. 88-91.

128. Roggo, L., et al., *Membrane transport in Caenorhabditis elegans: an essential role for VPS34 at the nuclear membrane.* EMBO J, 2002. **21**(7): p. 1673-83.

129. Juhasz, G., et al., *The class III PI(3)K Vps34 promotes autophagy and endocytosis but not TOR signaling in Drosophila.* J Cell Biol, 2008. **181**(4): p. 655-66.

130. Zhou, X.A., J. Takatoh, and F. Wang, *The Mammalian Class 3 PI3K (PIK3C3) Is Required for Early Embryogenesis and Cell Proliferation.* Plos One, 2011. **6**(1).

131. Jaber, N., et al., *Class III PI3K Vps34 plays an essential role in autophagy and in heart and liver function.* Proc Natl Acad Sci U S A, 2012. **109**(6): p. 2003-8.

132. Zhou, X., et al., *Deletion of PIK3C3/Vps34 in sensory neurons causes rapid neurodegeneration by disrupting the endosomal but not the autophagic pathway.* Proc Natl Acad Sci U S A, 2010. **107**(20): p. 9424-9.

133. He, F., et al., *Critical Role for Phosphatidylinositol-3 Kinase Vps34/PIK3C3 in ON-Bipolar Cells.* Invest Ophthalmol Vis Sci, 2019. **60**(8): p. 2861-2874.

134. Miranda, A.M., et al., *Neuronal lysosomal dysfunction releases exosomes harboring APP C-terminal fragments and unique lipid signatures.* Nature Communications, 2018. **9**.

135. Andersen, A.R., et al., *Diabetic Nephropathy in Type-1 (Insulin-Dependent) Diabetes - an Epidemiological-Study.* Diabetologia, 1983. **25**(6): p. 496-501.

136. Thomas, M.C., et al., *Diabetic kidney disease.* Nat Rev Dis Primers, 2015. **1**: p. 15018.

137. Vestri, S., et al., *Changes in sodium or glucose filtration rate modulate expression of glucose transporters in renal proximal tubular cells of rat.* Journal of Membrane Biology, 2001. **182**(2): p. 105-112.

138. Vidotti, D.B., et al., *Effect of long-term type 1 diabetes on renal sodium and water transporters in rats.* American Journal of Nephrology, 2008. **28**(1): p. 107-114.

139. Wolf, G. and F.N. Ziyadeh, *Molecular mechanisms of diabetic renal hypertrophy.* Kidney International, 1999. **56**(2): p. 393-405.

140. Vallon, V. and S.C. Thomson, *Renal Function in Diabetic Disease Models: The Tubular System in the Pathophysiology of the Diabetic Kidney.* Annual Review of Physiology, Vol 74, 2012. **74**: p. 351-375.

141. Cherney, D.Z., J.W. Scholey, and J.A. Miller, *Insights into the regulation of renal hemodynamic function in diabetic mellitus.* Curr Diabetes Rev, 2008. **4**(4): p. 280-90.

142. Vallon, V. and R. Komers, *Pathophysiology of the diabetic kidney.* Compr Physiol, 2011. **1**(3): p. 1175-232.

143. Bailey, C.J., C. Day, and S. Bellary, *Renal Protection with SGLT2 Inhibitors: Effects in Acute and Chronic Kidney Disease.* Curr Diab Rep, 2022. **22**(1): p. 39-52.

144. Perrone, A., et al., *Advanced Glycation End Products (AGEs): Biochemistry, Signaling, Analytical Methods, and Epigenetic Effects.* Oxidative Medicine and Cellular Longevity, 2020. **2020**.

145. Tsilibary, E.C., et al., *The Effect of Nonenzymatic Glucosylation on the Binding of the Main Noncollagenous Nc1 Domain to Type-Iv Collagen.* Journal of Biological Chemistry, 1988. **263**(9): p. 4302-4308.

146. Kumar Pasupulati, A., P.S. Chitra, and G.B. Reddy, *Advanced glycation end products mediated cellular and molecular events in the pathology of diabetic nephropathy.* Biomol Concepts, 2016. **7**(5-6): p. 293-309.

147. Rhee, S.Y. and Y.S. Kim, *The Role of Advanced Glycation End Products in Diabetic Vascular Complications.* Diabetes & Metabolism Journal, 2018. **42**(3): p. 188-195.

148. Singh, V.P., et al., *Advanced glycation end products and diabetic complications.* Korean J Physiol Pharmacol, 2014. **18**(1): p. 1-14.

149. Forbes, J.M., et al., *Role of advanced glycation end products in diabetic nephropathy.* Journal of the American Society of Nephrology, 2003. **14**: p. S254-S258.

150. Wautier, M.P., et al., *Activation of NADPH oxidase by AGE links oxidant stress to altered gene expression via RAGE.* American Journal of Physiology-Endocrinology and Metabolism, 2001. **280**(5): p. E685-E694.

151. Fujii, J., et al., *Oxidative stress caused by glycation of Cu,Zn-superoxide dismutase and its effects on intracellular components.* Nephrology Dialysis Transplantation, 1996. **11**: p. 34-40.

152. Nangaku, M., *Chronic hypoxia and tubulointerstitial injury: A final common pathway to end-stage renal failure.* Journal of the American Society of Nephrology, 2006. **17**(1): p. 17-25.

153. Hansell, P., et al., *Determinants of kidney oxygen consumption and their relationship to tissue oxygen tension in diabetes and hypertension.* Clinical and Experimental Pharmacology and Physiology, 2013. **40**(2): p. 123-137.

154. Korner, A., et al., *Increased Renal Metabolism in Diabetes Mechanism and Functional Implications.* Diabetes, 1994. **43**(5): p. 629-633.

155. Murea, M., et al., *Lipotoxicity in Diabetic Nephropathy: The Potential Role of Fatty Acid Oxidation.* Clinical Journal of the American Society of Nephrology, 2010. **5**(12): p. 2373-2379.

156. Li, H., et al., *Interactions between HIF-1 alpha and AMPK in the regulation of cellular hypoxia adaptation in chronic kidney disease.* American Journal of Physiology-Renal Physiology, 2015. **309**(5): p. F414-F428.

157. Hesp, A.C., et al., *The role of renal hypoxia in the pathogenesis of diabetic kidney disease: a promising target for newer renoprotective agents including SGLT2 inhibitors?* Kidney Int, 2020. **98**(3): p. 579-589.

158. Gunton, J.E., *Hypoxia-inducible factors and diabetes.* J Clin Invest, 2020. **130**(10): p. 5063-5073.

159. Wang, G.L. and G.L. Semenza, *General involvement of hypoxia-inducible factor 1 in transcriptional response to hypoxia.* Proc Natl Acad Sci U S A, 1993. **90**(9): p. 4304-8.

160. Hon, W.C., et al., *Structural basis for the recognition of hydroxyproline in HIF-1 alpha by pVHL.* Nature, 2002. **417**(6892): p. 975-8.

161. Lee, J.W., et al., *Hypoxia-inducible factor (HIF-1)alpha: its protein stability and biological functions.* Exp Mol Med, 2004. **36**(1): p. 1-12.

162. Semenza, G.L., *HIF-1 and mechanisms of hypoxia sensing.* Curr Opin Cell Biol, 2001. **13**(2): p. 167-71.

163. Dery, M.A., M.D. Michaud, and D.E. Richard, *Hypoxia-inducible factor 1: regulation by hypoxic and non-hypoxic activators.* Int J Biochem Cell Biol, 2005. **37**(3): p. 535-40.

164. Iyer, N.V., et al., *Cellular and developmental control of O2 homeostasis by hypoxia-inducible factor 1 alpha.* Genes Dev, 1998. **12**(2): p. 149-62.

165. Brocato, J., Y. Chervona, and M. Costa, *Molecular Responses to Hypoxia-Inducible Factor 1 alpha and Beyond.* Molecular Pharmacology, 2014. **85**(5): p. 651-657.

166. Kimura, K., et al., *Stable expression of HIF-1 alpha in tubular epithelial cells promotes interstitial fibrosis.* American Journal of Physiology-Renal Physiology, 2008. **295**(4): p. F1023-F1029.

167. Nordquist, L., et al., *Activation of Hypoxia-Inducible Factors Prevents Diabetic Nephropathy.* Journal of the American Society of Nephrology, 2015. **26**(2): p. 328-338.

168. Kudo, Y., et al., *Hypoxia-inducible factor-1 alpha is involved in the attenuation of experimentally induced rat glomerulonephritis.* Nephron Experimental Nephrology, 2005. **100**(2): p. 95-103.

169. Tanaka, T., et al., *Cobalt promotes angiogenesis via hypoxia-inducible factor and protects tubulointerstitium in the remnant kidney model.* Laboratory Investigation, 2005. **85**(10): p. 1292-1307.

170. Xu, B., et al., *WNK1, a novel mammalian serine/threonine protein kinase lacking the catalytic lysine in subdomain II.* J Biol Chem, 2000. **275**(22): p. 16795-801.

171. Piala, A.T., et al., *Chloride Sensing by WNK1 Involves Inhibition of Autophosphorylation.* Science Signaling, 2014. **7**(324).

172. O'Reilly, M., et al., *WNK1, a gene within a novel blood pressure control pathway, tissue-specifically generates radically different isoforms with and without a kinase domain.* Journal of the American Society of Nephrology, 2003. **14**(10): p. 2447-2456.

173. Wilson, F.H., et al., *Human hypertension caused by mutations in WNK kinases.* Science, 2001. **293**(5532): p. 1107-12.

174. Morris, R.C., et al., *Renal Dysfunction, Rather Than Nonrenal Vascular Dysfunction, Mediates Salt-Induced Hypertension Response.* Circulation, 2016. **133**(9): p. 907-907.

175. Dbouk, H.A., et al., *Actions of the protein kinase WNK1 on endothelial cells are differentially mediated by its substrate kinases OSR1 and SPAK.* Proc Natl Acad Sci U S A, 2014. **111**(45): p. 15999-6004.

176. Kankanamalage, S.G., et al., *WNK1 is an unexpected autophagy inhibitor.* Autophagy, 2017. **13**(5): p. 969-970.

177. Gonzalez, C.D., et al., *Autophagy Dysregulation in Diabetic Kidney Disease: From Pathophysiology to Pharmacological Interventions.* Cells, 2021. **10**(9).

178. Anil Kumar, P., et al., *Molecular and cellular events mediating glomerular podocyte dysfunction and depletion in diabetes mellitus.* Front Endocrinol (Lausanne), 2014. **5**: p. 151.

179. Suzuki, D., et al., *Renal in situ hybridization studies of extracellular matrix related molecules in type 1 diabetes mellitus.* Nephron, 2002. **92**(3): p. 564-72.

180. Isono, M., et al., *Stimulation of TGF-beta type II receptor by high glucose in mouse mesangial cells and in diabetic kidney.* Am J Physiol Renal Physiol, 2000. **278**(5): p. F830-8.

181. Morrisey, K., et al., *Renal proximal tubular cell fibronectin accumulation in response to glucose is polyol pathway dependent.* Kidney Int, 1999. **55**(6): p. 2548-72.

182. Faivre, A., et al., *Tubular Cell Glucose Metabolism Shift During Acute and Chronic Injuries.* Front Med (Lausanne), 2021. **8**: p. 742072.

183. Russo, L.M., et al., *Impaired tubular uptake explains albuminuria in early diabetic nephropathy.* J Am Soc Nephrol, 2009. **20**(3): p. 489-94.

184. Tang, S., et al., *Albumin stimulates interleukin-8 expression in proximal tubular epithelial cells in vitro and in vivo.* Journal of Clinical Investigation, 2003. **111**(4): p. 515-527.

185. Zoja, C., et al., *Protein overload stimulates RANTES production by proximal tubular cells depending on NF-kappa B activation.* Kidney Int, 1998. **53**(6): p. 1608-15.

186. Wang, Y.P., et al., *Induction of monocyte chemoattractant protein-1 by albumin is mediated by nuclear factor kappa B in proximal tubule cells.* Journal of the American Society of Nephrology, 1999. **10**(6): p. 1204-1213.

187. Tonneijck, L., et al., *Glomerular Hyperfiltration in Diabetes: Mechanisms, Clinical Significance, and Treatment.* J Am Soc Nephrol, 2017. **28**(4): p. 1023-1039.

188. Vallon, V. and S.C. Thomson, *Targeting renal glucose reabsorption to treat hyperglycaemia: the pleiotropic effects of SGLT2 inhibition.* Diabetologia, 2017. **60**(2): p. 215-225.

189. Vallon, V. and S.C. Thomson, *The tubular hypothesis of nephron filtration and diabetic kidney disease.* Nat Rev Nephrol, 2020. **16**(6): p. 317-336.

190. Zhang, J., et al., *Macula Densa SGLT1-NOS1-Tubuloglomerular Feedback Pathway, a New Mechanism for Glomerular Hyperfiltration during Hyperglycemia.* J Am Soc Nephrol, 2019. **30**(4): p. 578-593.

191. Cipriani, P., et al., *The role of nitric oxide in the dysregulation of the urine concentration mechanism in diabetes mellitus.* Front Physiol, 2012. **3**: p. 176.

192. Yang, J., J.S. Pollock, and P.K. Carmines, *NADPH oxidase and PKC contribute to increased Na transport by the thick ascending limb during type 1 diabetes.* Hypertension, 2012. **59**(2): p. 431-6.

193. Ichinose, K., E. Kawasaki, and K. Eguchi, *Recent advancement of understanding pathogenesis of type 1 diabetes and potential relevance to diabetic nephropathy.* Am J Nephrol, 2007. **27**(6): p. 554-64.

194. Dronavalli, S., I. Duka, and G.L. Bakris, *The pathogenesis of diabetic nephropathy.* Nat Clin Pract Endocrinol Metab, 2008. **4**(8): p. 444-52.

195. Maxwell, P.H., et al., *The tumour suppressor protein VHL targets hypoxia-inducible factors for oxygen-dependent proteolysis.* Nature, 1999. **399**(6733): p. 271-275.

196. Jaakkola, P., et al., *Targeting of HIF-alpha to the von Hippel-Lindau ubiquitylation complex by O-2-regulated prolyl hydroxylation.* Science, 2001. **292**(5516): p. 468-472.

197. Rosenberger, C., et al., *Adaptation to hypoxia in the diabetic rat kidney.* Kidney Int, 2008. **73**(1): p. 34-42.

198. Rosenberger, C., et al., *Up-regulation of HIF in experimental acute renal failure: evidence for a protective transcriptional response to hypoxia.* Kidney Int, 2005. **67**(2): p. 531-42.

199. Tonolo, G. and S. Cherchi, *Tubulointerstitial disease in diabetic nephropathy.* Int J Nephrol Renovasc Dis, 2014. **7**: p. 107-15.

200. Pritchett, T.L., et al., *Conditional inactivation of the mouse von Hippel-Lindau tumor suppressor gene results in wide-spread hyperplastic, inflammatory and fibrotic lesions in the kidney.* Oncogene, 2015. **34**(20): p. 2631-2639.

201. Yan, H.T. and G.F. Su, *Expression and significance of HIF-1 alpha and VEGF in rats with diabetic retinopathy.* Asian Pacific Journal of Tropical Medicine, 2014. **7**(3): p. 237-240.

202. Ponchiardi, C., M. Mauer, and B. Najafian, *Temporal profile of diabetic nephropathy pathologic changes.* Curr Diab Rep, 2013. **13**(4): p. 592-9.

203. Muona, P., et al., *Hyperglycemic glucose concentrations up-regulate the expression of type VI collagen in vitro. Relevance to alterations of peripheral nerves in diabetes mellitus.* Am J Pathol, 1993. **142**(5): p. 1586-97.

204. Steffensen, L.B., et al., *Basement membrane proteins in various arterial beds from individuals with and without type 2 diabetes mellitus: a proteome study.* Cardiovascular Diabetology, 2021. **20**(1).

205. Carota, I.A., et al., *Targeting VE-PTP phosphatase protects the kidney from diabetic injury.* J Exp Med, 2019. **216**(4): p. 936-949.

206. Yang, X. and K. Qian, *Protein O-GlcNAcylation: emerging mechanisms and functions.* Nat Rev Mol Cell Biol, 2017. **18**(7): p. 452-465.

207. Hameed, I., et al., *Type 2 diabetes mellitus: From a metabolic disorder to an inflammatory condition.* World J Diabetes, 2015. **6**(4): p. 598-612.

208. Bolanle, I.O., et al., *Revascularisation of type 2 diabetics with coronary artery disease: Insights and therapeutic targeting of O-GlcNAcylation.* Nutr Metab Cardiovasc Dis, 2021. **31**(5): p. 1349-1356.

209. Lutgens, S.P., et al., *Cathepsin cysteine proteases in cardiovascular disease.* FASEB J, 2007. **21**(12): p. 3029-41.

210. Kumar Vr, S., et al., *Cathepsin S Cleavage of Protease-Activated Receptor-2 on Endothelial Cells Promotes Microvascular Diabetes Complications.* J Am Soc Nephrol, 2016. **27**(6): p. 1635-49.

211. Gridley, T., *Notch signaling in the vasculature.* Curr Top Dev Biol, 2010. **92**: p. 277-309.

212. Miloudi, K., et al., *NOTCH1 signaling induces pathological vascular permeability in diabetic retinopathy.* Proceedings of the National Academy of Sciences, 2019. **116**(10): p. 4538-4547.

213. Feng, X., et al., *PPAR-alpha Agonist Fenofibrate Prevented Diabetic Nephropathy by Inhibiting M1 Macrophages via Improving Endothelial Cell Function in db/db Mice.* Front Med (Lausanne), 2021. **8**: p. 652558.

214. Niranjan, T., et al., *The Notch pathway in podocytes plays a role in the development of glomerular disease.* Nat Med, 2008. **14**(3): p. 290-8.

215. Bielesz, B., et al., *Epithelial Notch signaling regulates interstitial fibrosis development in the kidneys of mice and humans.* J Clin Invest, 2010. **120**(11): p. 4040-54.

216. Nishad, R., et al., *Growth hormone induces Notch1 signaling in podocytes and contributes to proteinuria in diabetic nephropathy.* Journal of Biological Chemistry, 2019. **294**(44): p. 16109-16122.

217. Gorin, Y., et al., *Nox4 NAD(P)H oxidase mediates hypertrophy and fibronectin expression in the diabetic kidney.* J Biol Chem, 2005. **280**(47): p. 39616-26.

218. Etoh, T., et al., *Increased expression of NAD(P)H oxidase subunits, NOX4 and p22phox, in the kidney of streptozotocin-induced diabetic rats and its reversibity by interventive insulin treatment.* Diabetologia, 2003. **46**(10): p. 1428-37.

219. Choi, S.Y., W. Lee-Kwon, and H.M. Kwon, *The evolving role of TonEBP as an immunometabolic stress protein.* Nature Reviews Nephrology, 2020. **16**(6): p. 352-364.

220. Park, J., et al., *Tonicity-responsive enhancer binding protein regulates the expression of aldose reductase and protein kinase C delta in a mouse model of diabetic retinopathy.* Experimental Eye Research, 2014. **122**: p. 13-19.

221. Huang, C.L. and C.J. Cheng, *A unifying mechanism for WNK kinase regulation of sodium-chloride cotransporter.* Pflugers Arch, 2015. **467**(11): p. 2235-41.

222. Moriguchi, T., et al., *WNK1 regulates phosphorylation of cation-chloride-coupled cotransporters via the STE20-related kinases, SPAK and OSR1.* J Biol Chem, 2005. **280**(52): p. 42685-93.

223. Davies, M.R.P., et al., *The Thiazide-Sensitive Co-Transporter Promotes the Development of Sodium Retention in Mice with Diet-Induced Obesity.* Kidney & Blood Pressure Research, 2015. **40**(5): p. 509-519.

224. Wu, J.J., et al., *Renal NKCC2 Is Dual Regulated by the Synergy of 20-HETE and High-Fat Diet in CYP4F2 Transgenic Mice.* Kidney & Blood Pressure Research, 2021. **46**(5): p. 601-612.

225. Wang, Q., et al., *Hydrogen Sulfide Prevents Advanced Glycation End-Products Induced Activation of the Epithelial Sodium Channel.* Oxid Med Cell Longev, 2015. **2015**: p. 976848.

226. Spires, D., A.D. Manis, and A. Staruschenko, *Ion channels and transporters in diabetic kidney disease.* Curr Top Membr, 2019. **83**: p. 353-396.

227. Delaloy, C., et al., *Multiple promoters in the WNK1 gene: one controls expression of a kidney-specific kinase-defective isoform.* Mol Cell Biol, 2003. **23**(24): p. 9208-21.

228. Gallolu Kankanamalage, S., et al., *Multistep regulation of autophagy by WNK1.* Proc Natl Acad Sci U S A, 2016. **113**(50): p. 14342-14347.

229. Zagorska, A., et al., *Regulation of activity and localization of the WNK1 protein kinase by hyperosmotic stress.* J Cell Biol, 2007. **176**(1): p. 89-100.

230. Kim, B.S. and M.S. Goligorsky, *Role of VEGF in kidney development, microvascular maintenance and pathophysiology of renal disease.* Korean J Intern Med, 2003. **18**(2): p. 65-75.

231. Xie, J., et al., *Endothelial-specific expression of WNK1 kinase is essential for angiogenesis and heart development in mice.* Am J Pathol, 2009. **175**(3): p. 1315-27.

232. Huang, H.C. and P.A. Preisig, *G1 kinases and transforming growth factor-beta signaling are associated with a growth pattern switch in diabetes-induced renal growth.* Kidney Int, 2000. **58**(1): p. 162-72.

233. Gallolu Kankanamalage, S., A.S. Karra, and M.H. Cobb, *WNK pathways in cancer signaling networks.* Cell Commun Signal, 2018. **16**(1): p. 72.

234. Zhang, Y.J., et al., *WNK1 is required for proliferation induced by hypotonic challenge in rat vascular smooth muscle cells.* Acta Pharmacol Sin, 2018. **39**(1): p. 35-47.

235. Morito, N., et al., *Overexpression of Mafb in podocytes protects against diabetic nephropathy.* J Am Soc Nephrol, 2014. **25**(11): p. 2546-57.

236. Grigorieva, I.V., et al., *A Novel Role for GATA3 in Mesangial Cells in Glomerular Development and Injury.* J Am Soc Nephrol, 2019. **30**(9): p. 1641-1658.

237. Al-Jaber, H., L. Al-Mansoori, and M.A. Elrayess, *GATA-3 as a Potential Therapeutic Target for Insulin Resistance and Type 2 Diabetes Mellitus.* Current Diabetes Reviews, 2021. **17**(2): p. 169-179.

238. Marumo, T., et al., *Diabetes Induces Aberrant DNA Methylation in the Proximal Tubules of the Kidney.* Journal of the American Society of Nephrology, 2015. **26**(10): p. 2388-2397.

239. Zhou, H., et al., *Loss of the podocyte glucocorticoid receptor exacerbates proteinuria after injury.* Sci Rep, 2017. **7**(1): p. 9833.

240. Srivastava, S.P., et al., *Loss of endothelial glucocorticoid receptor accelerates diabetic nephropathy.* Nature Communications, 2021. **12**(1).

241. Obojski, A. and M. Kraus-Filarska, *[Molecular mechanisms of anti-inflammatory actions of glucocorticoids and their synergy with beta2-agonists].* Pol Arch Med Wewn, 2004. **111**(6): p. 743-7.

242. Leonard, M.O., et al., *Potentiation of Glucocorticoid Activity in Hypoxia through Induction of the Glucocorticoid Receptor1.* The Journal of Immunology, 2005. **174**(4): p. 2250-2257.

243. Landry, T., D. Shookster, and H. Huang, *Circulating alpha-klotho regulates metabolism via distinct central and peripheral mechanisms.* Metabolism, 2021. **121**: p. 154819.

244. Kuroo, M., et al., *Mutation of the mouse klotho gene leads to a syndrome resembling ageing.* Nature, 1997. **390**(6655): p. 45-51.

245. Kuro, O.M., *The Klotho proteins in health and disease.* Nat Rev Nephrol, 2019. **15**(1): p. 27-44.

246. Sas, K.M., et al., *Tissue-specific metabolic reprogramming drives nutrient flux in diabetic complications.* JCI Insight, 2016. **1**(15): p. e86976.

247. Hasegawa, S., et al., *The oral hypoxia-inducible factor prolyl hydroxylase inhibitor enarodustat counteracts alterations in renal energy metabolism in the early stages of diabetic kidney disease.* Kidney International, 2020. **97**(5): p. 934-950.

248. Kolesnichenko, M. and P.K. Vogt, *Understanding PLZF: two transcriptional targets, REDD1 and smooth muscle alpha-actin, define new questions in growth control, senescence, self-renewal and tumor suppression.* Cell Cycle, 2011. **10**(5): p. 771-5.

249. Plaisier, C.L., et al., *Zbtb16 has a role in brown adipocyte bioenergetics.* Nutrition & Diabetes, 2012. **2**.

250. Schefe, J.H., et al., *A novel signal transduction cascade involving direct physical interaction of the renin/prorenin receptor with the transcription factor promyelocytic zinc finger protein.* Circ Res, 2006. **99**(12): p. 1355-66.

251. Liska, F., et al., *Downregulation of Plzf Gene Ameliorates Metabolic and Cardiac Traits in the Spontaneously Hypertensive Rat.* Hypertension, 2017. **69**(6): p. 1084-1091.

252. Chen, S., et al., *Control of hepatic gluconeogenesis by the promyelocytic leukemia zinc finger protein.* Mol Endocrinol, 2014. **28**(12): p. 1987-98.

253. Zhao, H., et al., *Tangshen formula attenuates diabetic renal injuries by upregulating autophagy via inhibition of PLZF expression.* PLoS One, 2017. **12**(2): p. e0171475.

254. Zhang, T., et al., *G-protein-coupled receptors regulate autophagy by ZBTB16-mediated ubiquitination and proteasomal degradation of Atg14L.* Elife, 2015. **4**: p. e06734.

255. Papademetriou, V., et al., *Pharmacological Management of Diabetic Nephropathy.* Curr Vasc Pharmacol, 2020. **18**(2): p. 139-147.

256. Stavropoulos, K., et al., *Sodium-glucose Cotransporter 2 Inhibitors: Nephroprotective Impact on Diabetic Kidney Disease.* Cardiovasc Hematol Disord Drug Targets, 2018. **18**(2): p. 120-126.

257. Lugner, M., et al., *Cardiorenal and other diabetes related outcomes with SGLT-2 inhibitors compared to GLP-1 receptor agonists in type 2 diabetes: nationwide observational study.* Cardiovasc Diabetol, 2021. **20**(1): p. 67.

258. Long, S.A. and C. Speake, *Combination therapy in recent-onset type 1 diabetes.* Lancet Diabetes Endocrinol, 2021. **9**(4): p. 191-193.

259. Figarola, J.L., et al., *LR-90 a new advanced glycation endproduct inhibitor prevents progression of diabetic nephropathy in streptozotocin-diabetic rats.* Diabetologia, 2003. **46**(8): p. 1140-52.

260. Peppa, M., et al., *Prevention and reversal of diabetic nephropathy in db/db mice treated with alagebrium (ALT-711).* Am J Nephrol, 2006. **26**(5): p. 430-6.

261. Sugahara, M., et al., *Prolyl Hydroxylase Domain Inhibitor Protects against Metabolic Disorders and Associated Kidney Disease in Obese Type 2 Diabetic Mice.* J Am Soc Nephrol, 2020. **31**(3): p. 560-577.

Appendix

No.	Matrix Family	p-Value	Description	Matrix similarity	Total Match	Common to seq.
1	V$AP1F	0.147323	Activator protein 1	0,929	1	1
2	V$AP2F	0.140516	Activator protein 2	0,914	12	1
3	V$VMAF	0.147262	v-Maf	0,843	14	1
4	V$EGRF	0.145266	EGR/nerve growth factor induced protein C and related factors	0,813	20	1
5	V$KLFS	0.0325929	Krueppel-like transcription factors	0,953	25	1
6	V$VEZF	0.0937505	Vascular endothelia zinc finger factor	0,886	3	1
7	V$YY1	0.106959	Transcription factor yin yang 1	0,876	2	1
8	V$CTCF	0.144353	CTCF and BORIS gene family, transcriptional regulators with 11 highly conserved zinc finger domains	0,820	11	1
9	V$HIF1	0,146242	Hypoxia inducible factor	0,937	2	1
10	V$p53F	0,139855	P53 tumor supressor	0,838	1	1

Supplemental table 1: Detailed description of transcription factors found common to L-wnk1 (Matrix family having a total match of 1 and above are presented).

No.	Matrix Family	Description	Matrix similarity
1	V$STAT5	Signal transducer and activator of transcription 5	0,882
2	V$PLZF	Promyelocytic leukemia zinc finger	0,862
3	V$VMAF	v-Maf	0,843
4	V$NFAT5	Nuclear factor of activated T-cells	0,882
5	V$KLFS	Krueppel like factors	0,953
6	V$HNF-1	Hepatic nuclear factor 1	0,830
7	V$GATA3	GATA binding factors	0,831
8	V$GRE	Glucocorticoid receptor	0,892
9	V$OCT1	Octamer-binding factor 1	0,825
10	V$p53F	P53 tumor suppressor	0,855

Supplemental table 2: Detailed description of transcription factors found common to Ks-wnk1 (Matrix family having a total match of 1 and above are presented).

L-wnk1 promoter sequence (1200 bp). Putative Transcriptions factors:

G GTACCGAGCT CTTACGCGTG CTAGCCCGGG CTCGAGCCCA -1191

CGAGGCATTA GGCTACAGCA ACCGCAAGGC ATCACGGAAG TCGTAGGCAC TTTTCTTCTA GGTCCCGTTC -1121

ATCCCCGCCA ACCCGTAAAC TATAAGTCCC AGGGTGCCTC GGGGCTAGCA CGCCTGCGCA AAAGCCCCGG -1051

AGCGAGTTGG GGGGTGGGGC TGCTCCGGGC GGCGGGGGGC GGGATCCGAG CGGGCTGTGT GGAGGCTTCA -981

KLF2 **KLF15**

GACTCCCGGC GCCATTTAGC GCGGAGAGTT TCCCGGGTGG ACGCGGCTCC TCTCTCGGCC ACTCCGCACC -911

ATF6

CCCATCTTCG GTGACAGAAG GCGCCTGGTG GGGGTGGCTG CTCTTTTCTC TCCCTGTTCC CCCTCACCCA -841

YY1

GTCCTCTAGG TCTCCTCTCC TCTTGCCTCA GAGAAGCAGC GGAGCTCGGG CCCCGCGGTG AGCGGCCCTC -771

CCCTCCCCGC CGTTCCCTCC TCCGTCAGCC CCCGGCACCG GCCCGGGAGG AGACGGGTTT GCCAGGCCTG -701

MAFB

GGGCGGGCGG GGAGGCCTCG GGGAAGGGGG GGCCCGCTCC TCAGGCGCCG AGGCTCCGAG GCTCCGGCCC -631

EGR1 **CTCF**

TTCGCCTCTG GGCGATGGGC GACCTGTGAG GCCGGTCCCC ATCGCTGGGG GCGCGTGTGG GAGGAGGCGG -561

VEZF1

CCGCCCGAGT GACCGGGAGC CGGGCCGCGG CCTTCCCTCG CCCGCCTCGG CCCCTCCCAC TCCTCTGCCC -491

CGGGGCCGCC ACCGCCCGGG CGTCGGACCT GGTCCCGTGC TCGCGGTGCC GCCGCCCTCT GGGCCTAGCC -421

CGCCCAGCTC GGCGAGCGGC GGCAGTGGGA GCCGCGTCCG CCGCATCCGC CTCGACTCGG TGCCGGCCCC -351

TGGCCCTCCC CTCATGACTG CGGCGCCTCT GCTGCCACCG CCCGCCCGGC CGCCGCTAGG ATGGATGCGG -281

ZBTB17

ACCGTGCGGC GCTAACCCCC GTGGCTCAGC TCCCGAATCG CCCGCCTTCG AGCCCTCCTC GTGAGCCGCA -211

HIF-1

GCAGCCTCGG TGCCAGCCCC CGCCGCAGCT GGGCCCAGCG GTCCGCCTGT CCCTCGTTGC GGCTTGTCGG -141

TGCTGAGTGA GGCGTCGTCC GGGTCGGCGC GAACCCGCCC GGCCGCGGTT CCCTGCAGAC CTCTGCGCGG -71

AP-1

GCGGCTCGGC CCTTCACGCC CTTTTCGTTC ACGAATCCGA GCCCGCTCGC CTCTCTCCAG CGAACCGACC -1

Supplemental figure 1. Transcription factor consensus binding sites of L-wnk1 promoter.

Ks-wnk1 promoter sequence (1191 bp). Putative transcription factors:

CCAGTACTAGG GGGCTATATCT TAGGAACATT TTGCATGATT -4427

TTCAGAAGCA TTTCATTATT CTGCTGTGAT TTAATTAAGA TTAAAGGTGG TAGCATTCCC AGTGTTTTAG -4357

TCAGAATTCC TCAAAAAAGC TGACCTTACT TACCTACCCT GAATATTGAT CTGTAATTCA CAAGGCGGTA -4287

GACTACAGAA TAAAAACAAA GGATATAGAA AGATTGTTTT CCATATTTAA ATACAGCAGT ACTGAGTTTT -4217

KLF2

CTGATATACT GTAAATAACC TAAATGCTAA AGGATTCATA TAGATACTTT GTAATTGCTA CTTTCTCTAA -4147

TGGATTGTAT GTATATATGA TTTGAGGTAT ACCCTGAAAG AAGCATAAGA CTCAGTTGAC TGAAAAAAGG -4077

GGGCAGAATA GGAAAAGTAT TCTTGTTGGT AGAAGTGTTC ACTAAAGTAT TCAGTGAACA AGTAACCAGT -4007

NFAT5 **STAT5**

TTGACTGAAC TTACTTTGGG GAGATTGGGT AAAGATGTGG GTGGAAGTTA AATTATGATT TTCACACCAC -3937

TTTTAAAAGC ACAATAACAT GGACCAGAAA TAACATTAAA CTAGATGCTG GAAAATCTGG ATTCTAGTTT -3867

TTGTTTTACC ATTGATTCGG CCCGTACTTA ACTGGAGTAT AAATTATATT TATCTTCTAG GTGGTGAAGG -3797

TGGTGCAGTG TATCTAGCAG ATTGCCTGAT AGCTGTTAGA CTAGATGAGA CACTCCATAG TCAACTAGTT -3727

GATA3

GAATTAATGG ATTAATTCTC TTTTTTTTTT TTTTTTTTTT TTTTGAGATA TAGTCTCACT CTGTCGTTAG -3657

GCTGGAGTGC AGTGGCATGA TCTTGGCTCA CTGCAACCTC CGCCTCCCAG GTTTAAGTGAT AACTCCTGAC -3587

NF-1 **GATA2**

TCAGCCTCCC GAGTAGCTGG GACTACAGGC ATGTGCCAAC ATGCCCAGCT AATGTTTGTG TTTTTAGTAG -3517

p53

AGACGGGGTT TCACCATGTT GGCTAGGATG GTCTTTCTTG ACCTCCTCGT GATCTGCCCG CTTCGGCCCT -3447

ZBTB17

CCAAAGTGTT GGGATTACAG GCGTGAGCCA CCGCGCCTGG CTGGCTAATG -70

GAGTAGGTGG AGCATTGAGC AAGTAAAAAT CCCATTTTGC TTGTCTAGGA TCTATTACTG TTGGCAGAGA -1

AGCAGAAGGAATATTAAC +18

Supplemental figure 2. Transcription factor consensus binding sites of Ks-wnk1 promoter.

List of publications

- Rinschen, M. M., Harder, J. L., Carter-Timofte, M. E., **Zanon Rodriguez, L**., Mirabell, C.,Demir, F., Kurmasheva, N., Ramakrishnan, S. K., Kunke, M., . . . Theilig, F. VPS34-dependent control of apical membrane function of proximal tubule cells and nutrient recovery by the kidney. Sci Signal. 2022 Nov 29;15(762): eabo7940. doi: 10.1126/scisignal.abo 7940. Epub 2022 Nov 29. PMID: 36445937.

- Kunke, M., Knoefler, H., **Zanon Rodriguez, L**., Böttner, M., Larionov A., Dahlke, E., Saudenova, M., … Theilig, F. (2023). Targeted deletion of von-Hippel-Lindau in the proximal tubule conditions the kidney against early diabetic kidney disease. Diabetes. (Submitted for publication).

Acknowledgements

This project is the result of my work but also of many people that have made it possible through strong accomplishment and dedication.

First, I would like to express my deep sense of gratitude and thankfulness to my supervisor Prof. Dr. Franziska Theilig for her competent supervision, trust, patience and for bringing new ideas that make possible the development of this scientific work.

I am also very grateful to Prof. Dr. Thilo Wedel, Prof. Dr. Ralph Lucius and all the Institute of Anatomy for their professionality and kindness, for the invaluable encouragement and support, guidance and resources availability that turned my PhD programme into an enjoyable experience. I sincerely thank Prof. Dr. Martina Böttner and Junior Prof. Dr. Francois Cossais for their moral support and discussions throughout my doctoral work.

A very big thank you to Madlen for her unconditional support from the very beginning, for helping me with the design programmes and for the coffee moments. Many thanks to Eileen for her scientific enthusiasm and cooperation that has always been a source of inspiration for me and for bringing new ideas and solutions to move forward.

Special thanks to Makhabbat for her valuable expertise and knowledge, for being a great friend and someone I could always count on during all my PhD years. I am also very grateful to Otfried for his friendship and technical support specially during the pandemia.

I would like to extend my sincere thanks to Inka for her dedication, good tips and help in the lab, to Miriam for optimizing my cell culture knowledge and all the great experiences, to Alyn for her amazing support and effort in the last part of my thesis and last but absolutely not least to Serab and Sandra for their helpfulness and technical support.

I wish to sincerely thank Prof. Dr. med. Markus Rinschen and Prof. Dr. Stefan Krautwald for their collaboration in this research and also thank Dr. Arohan R. Subramanya for kindly providing us with kidneys of KS-WNK1 knockout mice.

Many thanks to my best friends in Spain and in Germany for their moral support and confidence during all my studies. I would also like to express my gratitude towards my father José who always trusted me and lean on me when I most needed. To my mother Luisa and to my brothers Enrique and Pepe for their immense love, support and confidence.

Declaration

I, Luis Zanon Rodriguez, declare that the content and design of this doctoral thesis was composed by myself. The experimental work is almost entirely on my own, references have been provided on all supporting literature and resources and the collaborative contributions have been clearly indicated.

Furthermore, I confirm that this thesis has not been submitted either partially not fully as a part of a doctoral examination procedure and that part of this work has been published and submitted for publication. This thesis has been prepared subject to the Rules of Good Scientific Practice of the German Research Foundation and no academic degree has ever been withdrawn.

Kiel, 04.04.2023

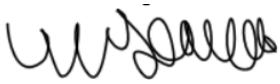

(Luis Zanon Rodriguez)